# ABSTRACT

| | |
|---|---|
| Title of Dissertation: | LOCAL AND TOP-DOWN REGULATION OF OLFACTORY BULB CIRCUITS |
| | Ruilong Hu, Doctor of Philosophy, 2020 |
| Dissertation directed by: | Ricardo C. Araneda, Associate Professor, Department of Biology |

The olfactory bulb (OB) is the first place in the brain where chemosensory processing occurs. The neurophysiological mechanisms underlying these processes are mostly driven by inhibition, which is implemented by a large population of local inhibitory neurons, and among them, the granule cell (GCs) is the most prominent type. Local inhibitory interneurons sculpt the coding of output neurons, affecting odor detection, discrimination, and learning. Therefore, the regulation of inhibitory circuits is critical to OB function and fine-tuning OB output. Specifically, inhibitory tone in the OB can be regulated by the dynamic interactions between cell-intrinsic factors affecting neuronal excitability and extrinsic top-down modulation associated with an animal's behavioral state. Here, I provide new evidence for intrinsic mechanisms governing inhibitory interneuron excitability in the OB and how modulation by noradrenaline works in concert with these intrinsic mechanisms to affect circuit function. This work highlights circuit- and cell-specific differences in noradrenergic modulation with regards to short- and long-term plasticity within OB circuits.

# LOCAL AND TOP-DOWN REGULATION OF OLFACTORY BULB CIRCUITS

by

Ruilong Hu

Dissertation submitted to the Faculty of the Graduate School of the
University of Maryland, College Park, in partial fulfillment
of the requirements for the degree of
Doctorate of Neuroscience
& Cognitive Sciences
2020

Dissertation Committee:
Dr. Ricardo Araneda, Chair
Dr. Matthew Roesch, Deans Representative
Dr. Jens Herberholz
Dr. Quentin Gaudry
Dr. Katrina Macleod

# Preface

Electrophysiological experiments and analysis were performed by Ruilong Hu. Immunohistochemistry data in Chapter 3, were obtained in collaboration with Pablo S. Villar.

One publication resulted from this work has been published so far:

Ruilong Hu, Katie A Ferguson, Christina B Whiteus, Dimphna H Meijer, Ricardo C Araneda (2016). Hyperpolarization-Activated Currents and Subthreshold Resonance in Granule Cells of the Olfactory Bulb. *eNeuro*, 3(5), ENEURO.0197-16.2016. https://doi.org/10.1523/ENEURO.0197-16.2016

Abstract: An important contribution to neural circuit oscillatory dynamics is the ongoing activation and inactivation of hyperpolarization-activated currents ($I_h$). Network synchrony dynamics play an important role in the initial processing of odor signals by the main olfactory bulb (MOB) and accessory olfactory bulb (AOB). In the mouse olfactory bulb, we show that $I_h$ is present in granule cells (GCs), the most prominent inhibitory neuron in the olfactory bulb, and that $I_h$ underlies subthreshold resonance in GCs. In accord with the properties of $I_h$, the currents exhibited sensitivity to changes in extracellular $K^+$ concentration and ZD7288 (4-ethylphenylamino-1,2-dimethyl-6-methylaminopyrimidin chloride), a blocker of $I_h$. ZD7288 also caused GCs to hyperpolarize and increase their input resistance, suggesting that $I_h$ is active at rest in GCs. The inclusion of cAMP in the intracellular solution shifted the activation of $I_h$ to less negative potentials in the MOB, but not in the AOB, suggesting that channels with different subunit composition mediate $I_h$ in these regions. Furthermore, we show that mature GCs exhibit $I_h$-dependent

subthreshold resonance in the theta frequency range (4–12 Hz). Another inhibitory subtype in the MOB, the periglomerular cells, exhibited $I_h$-dependent subthreshold resonance in the delta range (1–4 Hz), while principal neurons, the mitral cells, do not exhibit $I_h$-dependent subthreshold resonance. Importantly, $I_h$ size, as well as the strength and frequency of resonance in GCs, exhibited a postnatal developmental progression, suggesting that this development of $I_h$ in GCs may differentially contribute to their integration of sensory input and contribution to oscillatory circuit dynamics.

This work is described in Chapter 2.

Three publications are currently being prepared from data presented in Chapters 3 through 5.

Ruilong Hu, Pablo S Villar, Ricardo C Araneda (in preparation). $\alpha_2$ - adrenergic modulation of $I_h$ in adult-born granule cells and dendrodendritic inhibition in the olfactory bulb

Ruilong Hu, Ricardo C Araneda (in preparation). Differential noradrenergic modulation between the main and accessory olfactory bulbs.

Ruilong Hu, Allison L Arai, Ricardo C Araneda (in preparation). Sexual dimorphic pushedregulation of a sensory circuit by noradrenaline.

# Dedication

To my parents, Jun Fu and Yaozhong Hu, who have worked incredibly hard and made many sacrifices in their immigration to the United States of America, enabling my pursuit of higher education, and ultimately my doctorate.

# Acknowledgements

I would like to acknowledge and thank my thesis advisor and mentor, Ricardo Araneda. He imbued a steadfast passion for our projects, and fostered a collaborative lab environment for his students. I am incredibly grateful for his support. Furthermore, I would like to thank acknowledge the committee for their assistance over the years.

From the Araneda lab, I would like to thank Richard Smith for being a fantastic role model when I joined the lab, and Pablo Villar for being an amazing teammate who helped me grow as a scientist throughout my PhD experience. In addition, I would like to thank the numerous undergraduates and technicians for their support over the years.

From my undergraduate research lab at Washington University in St. Louis School of Medicine, I would like to thank Jeff Gidday and Ann Stowe for their continued support and for inspiring me to pursue a PhD. Outside the lab, I would like to thank Felix Bartsch, Andrew Borrell, Molly Hyer, Gregory Perrin, Jonathan Schenk, Kevin Schneider, Clare Sengupta, and Lauren Weiss for their camaraderie throughout graduate school.

Finally, I would like to acknowledge my family: my parents, Jun Fu and Yaozhong Hu, my uncle, Fu Bin, and my cousin Guangwei Fu, for their support, inspiration, and generosity.

# Table of Contents

# List of Figures

# Chapter 1: Introduction

## Olfactory bulb processing overview

In most mammalian species, olfaction is the most important sense guiding the search for nutrients, detecting potential threats, and engaging in social behaviors. The mammalian olfactory system consists of two parallel pathways: the main olfactory system (MOS) and the vomeronasal system (VNS). In combination, these two systems detect and process a wide range of odorant molecules, from smaller volatile environmental cues by the MOS, to large complex proteins involved in social communication by the VNS. Chemosensory neurons of these parallel pathways synapse into two anatomically distinct regions of the brain, the main olfactory bulb (MOB) and the accessory olfactory bulb (AOB). The circuits of the MOB and AOB constitute the first brain region to process odor information. Unlike other sensory modalities, which relay information through the thalamus, the olfactory bulb (OB) projects directly to cortical areas involved in odor perception and subcortical areas that orchestrate goal-directed behaviors. As the first stage of central olfactory processing, and the only preceding higher order processing, the OB circuit has a critical role in the neurophysiological mechanisms that contribute to odor sensitivity, discrimination, and learning. The neurophysiological mechanisms underlying these processes are mostly

driven by inhibition, which is implemented by a large population of local inhibitory neurons, and among them, the granule cell (GCs) is the most prominent type. Further highlighting the importance of these inhibitory circuits in olfactory processing is their regulation by feedback projections from cortical and subcortical areas targeted by the OB, as well as neuromodulatory systems from the basal forebrain and midbrain. The expression of several olfactory mediated behaviors, exhibited from early development through adulthood, requires neuromodulation of GCs by noradrenaline, a neurotransmitter involved in physiological arousal and alertness. However, despite the recent progress, the role of the noradrenergic system in the OB, both at the cellular and system levels, and its role in odor learning, is poorly understood. Moreover, while most of GC function has been studied from the perspective of top-down regulation, little is known of how the intrinsic excitability of GC contributes to olfactory processing. Thus, the central aim of my dissertation is to determine how GC function is regulated by intrinsic mechanisms and by noradrenaline.

**Organization of the main and accessory olfactory systems**

Odorants bind to an unprecedented large family of G-protein coupled receptors (GPCRs) expressed by the sensory neurons, which in the rodents corresponds to ~1,200 different odor receptors (ORs), (Buck & Axel, 1991; Firestein, 2001; Glezer & Malnic, 2019; Wilson & Mainen, 2006). Surprisingly,

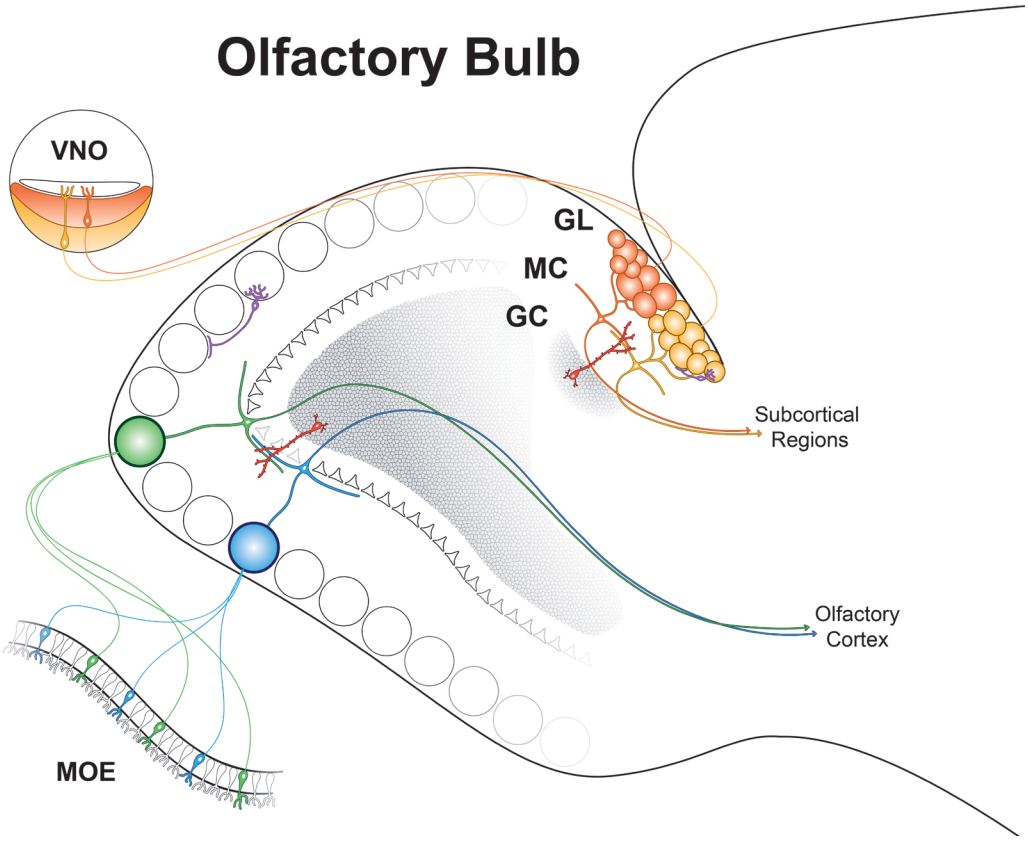


**Figure 1. Diagram of the olfactory bulb.**
Sensory neurons in the main olfactory epithelium (MOE) project their axons to the main olfactory bulb (MOB) while sensory neurons in the vomeronasal organ (VNO) project their axons to the accessory olfactory bulb. These axons synapse with the mitral/tufted cells (MCs) in the glomerular layer (GL), and MCs of the MOB project to the olfactory cortex, while the MCs of the AOB project to subcortical areas (diagram from the Araneda Lab).

each sensory neuron expresses only one type of OR from this vast genetic repertoire (Hsieh et al., 2017). In addition to the large number of ORs, variability in chemical receptive ranges amongst individual odorant receptors along with potential concurrent activation of multiple odorant receptor subtypes allow for an incredibly diverse combinatorial strategy for the downstream generation of different odor percepts (Araneda et al., 2000,

2004; Mori & Sakano, 2011). In the MOE, olfactory sensory neurons detect small volatile cues, and the electrical signals are transmitted, via the olfactory nerve, to the MOB. In the VNS, the vomeronasal sensory neurons detect nonvolatile pheromonal cues, including larger molecules and peptides found in excretions, including, but not limited to urine, saliva, tears, or feces (Chamero et al., 2012; Keverne, 1999; Liberles, 2014). Vomeronasal sensory neurons send their projections to the AOB (Fig 1).

In both the MOB and AOB, the axons of sensory neurons form excitatory, glutamatergic synapses with the apical dendrites of the principal neurons, the mitral and tufted cells (MCs herein). Sensory axon terminals and MC apical dendritic tufts form a dense spherical bundle of neuropil, called a glomerulus. In the MOS, the axons of all olfactory sensory neurons expressing the same olfactory receptor type converge onto approximately two glomeruli per OB (Lodovichi & Belluscio, 2012; Mombaerts et al., 1996). In turn, MCs in the MOB send a primary apical dendrite and innervate a single glomerulus (Gordon M Shepherd, 2004). This neuroanatomical scheme allows for any individual MOB MC to encode information from a single odorant receptor subtype, thus following a labeled-line code with the number of input channels directly proportional to the number of odorant receptor genes in an animal. In contrast, in the VNS, axons of vomeronasal sensory neurons may synapse onto over 10 glomeruli in the AOB (Rodriguez et al., 1999), while a single MC projects its apical dendrite to multiple glomeruli,

allowing for innervation of glomeruli associated with the same or different vomeronasal receptors (Brignall & Cloutier, 2015; Wagner et al., 2006). This diversity in AOB MC glomerular projections enable a combinatorial code and transformation in the representation of semiochemical information at the level of the AOB.

**Olfactory bulb processing and output**

While other sensory systems consist of multiple sequential anatomical stages that separate a sensory neuron from higher cortical areas (Kay & Sherman, 2007), the olfactory system is unique in that the OB sends information directly to higher order brain regions involved in perception and behavior. Specifically, in the MOS, the MOB projects directly to several cortical areas such as the piriform cortex (PCx), anterior olfactory nucleus (AON), olfactory tubercle (OT), cortical amgydala (ACo), and lateral entorhinal cortex (LEC), which are involved in several aspects of odor perception, such as localization, valence, and multisensory object integration (Bekkers & Suzuki, 2013; Gottfried, 2010; Sosulski et al., 2011). While the MOB exhibits a broadly loose odotopic arrangement across glomeruli, organized by general function (Ma et al., 2012; Mori & Sakano, 2011), the axonal projections from MCs show no anatomical organization in their distribution within downstream areas (Ghosh et al., 2011; Sosulski et al., 2011). With no clear odotopic organization, the representation of complex odor mixtures in the PCx occurs

across a distributed ensemble of neurons (Bekkers & Suzuki, 2013; Stettler & Axel, 2009).

With individual MOB MCs receiving input from one odorant receptor subtype, it may seem that MOB MCs act as a simple relay to downstream cortical areas. However, a large degree of information transformation and odor processing occurs in the MOB, utilizing elements of temporal coding. Importantly, the MOB inputs are driven by the respiration cycle, and the spiking of MCs relative to the timing of the sniff cycle carries crucial information relating to odor identity and concentration (Cang & Isaacson, 2003; Smear et al., 2011). Furthermore, at a population level, the synchronized activity of MCs contributes to fast network oscillations, including field potential oscillations in the gamma-frequency range (30 – 80 Hz) (Lagier et al., 2004; Lepousez & Lledo, 2013). Within a single sniff cycle, this network level synchrony is accompanied by a general decorrelation of MC spiking activity, serving as a mechanism for pattern separation that is critical for odor discrimination (Gschwend et al., 2015; Wanner & Friedrich, 2020). Downstream in the PCx, decorrelated MC spiking activity driven by temporally segregated activation of different glomeruli induces changes in the spiking of pyramidal neurons (Haddad et al., 2013). With sparse, broadly distributed activation of PCx neurons in response to odors, the precise, temporally coordinated activation of MC populations is critical to driving PCx neuron

activity (Miura et al., 2012; Uchida et al., 2013), emphasizing the importance of temporal coding in MOB MCs.

In the VNS, AOB MCs project directly to subcortical areas that have a critical function in organizing innate, social, and emotional behavior, including the medial and posteromedial cortical amygdala (MeA and MePA), the bed nucleus of stria terminalis (BNST), and the medial preoptic area (MPOA) (Dulac & Wagner, 2006; Scalia & Winans, 1975; Yoon et al., 2005). Among social behaviors, the VNS pathway in mice is involved in territorial aggression (Haga et al., 2010; Stowers et al., 2002), sex identification for courtship and mating (Kimchi et al., 2007), and pregnancy block in females (Kaba et al., 1989). Like the MOS, vomeronasal sensory neurons follow the general one-receptor per neuron rule, however, the VNS uses two different families of chemosensory receptors, coded by distinct gene families, the V1R and the V2Rs. Moreover, vomeronasal sensory neurons expressing V1Rs project to the anterior portion of the AOB, while V2R-expressing neurons project to the posterior AOB (Dulac & Wagner, 2006; Tirindelli et al., 2009). This segregated projection pattern to the AOB has suggested that the V1Rs and V2Rs are parallel pathways, that encode different type of chemosensory information in the VNS (Brignall & Cloutier, 2015; Chamero et al., 2012). However, similar to that of MOB MCs, the central projections of AOB MCs are not segregated and instead, MC axons from the anterior and posterior AOB converge in the amygdalar nuclei, BNST, and MPOA (Von Campenhausen &

Mori, 2000). Interestingly, projections from the PCx also converge in the MeA (Brennan & Keverne, 2014); therefore, as an area of convergence of the MOS and VNS, the MeA has been shown to integrate social odor cues and is critical for the initiation of social behaviors such including mating and aggression (Hong et al., 2014; Kondo & Arai, 1995; Y. Li et al., 2017; Y. Wang et al., 2013). Because AOB MCs project directly to subcortical areas that directly affect social and emotional responses, it has been proposed that like in the MOB, processing of pheromonal and social information must already occur at an early stage of sensory processing in the AOB. Accordingly, previous studies have shown that AOB MC spiking activity can encode the sex and strain of conspecifics (Ben-Shaul et al., 2010; Tolokh et al., 2013). Furthermore, several lines of evidence have suggested that the learning of mate identity in females during mating, and more recently, the learning of conspecific identity during aggression, occurs at the level of the AOB (Brennan & Keverne, 1997, 2014; Cansler et al., 2017; Kaba et al., 1989; Smith et al., 2015). However, the neurophysiological mechanisms for this transformation of information at the level of AOB are not understood. The activation of odor pathways in the VNS is significantly slower than the respiratory rhythm (Meredith, 1994), and instead it depends on autonomic control of the uptake of chemosensory stimuli by the VNO (Doving, Kjell B;Trotier, 1998; Keverne, 1999). Furthermore, direct stimulation of sensory neurons in the VNO or pheromonal investigation of conspecifics elicits a

sustained firing in MCs, on the order of seconds (Ben-Shaul et al., 2010; Luo et al., 2003). In contrast, a single respiratory cycle driving MOB MCs is on the order of 100 to 500 ms (2 – 10 Hz). Despite the existence of fast and slow network oscillations in the AOB (Binns & Brennan, 2005; Gorin et al., 2016; Pardo-Bellver et al., 2017), whether this coordination of network activity plays a role in AOB coding is not known. Given that AOB MCs show slow sustained spiking in the presence of sensory stimuli (Luo et al., 2003; Wagner et al., 2006), they are more likely to engage in a rate code, which is limited by the dynamics of stimulus uptake by the VNO (Yoles-Frenkel et al., 2018).

**Inhibition in the olfactory bulb**

Neuronal inhibition plays a crucial role in sensory processing (Isaacson & Scanziani, 2011; P. Lledo et al., 2005). In the OB, inhibitory interneurons outnumber excitatory neurons at least 100:1, indicating that inhibitory mechanisms are an important component of odor processing in the OB (Gordon M Shepherd, 2004). These inhibitory circuits are thought to produce a spatiotemporal modification of MC output, adjusting the system gain, enhancing signal to noise ratio and pattern separation (Economo et al., 2016; Gschwend et al., 2015; Isaacson & Scanziani, 2011; Miyamichi et al., 2013; Schoppa & Urban, 2003). These transformations occur in multiple layers of the OB, each with unique sets of inhibitory interneurons that contribute to specific components in odor processing. In the MOB glomerular layer,

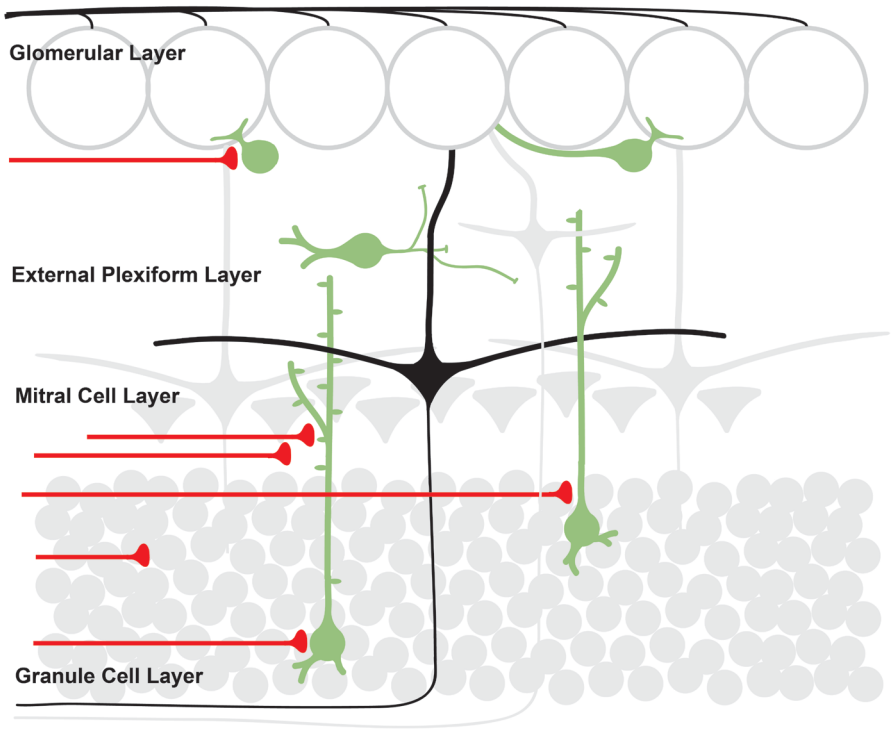


**Figure 2 Anatomical stratification of the olfactory bulb.**
A diagram of the MOB circuit showing the different layers of the MOB. Diagram contains output neurons (black) and few of the inhibitory neurons (green) across the different layers, along with afferent fibers (red) that modulate the inhibitory interneurons.

inhibitory interneurons called periglomerular cells (PGCs) receive excitation by the sensory input and mediate feedforward inhibition onto MCs that acts as a gain control mechanism (Banerjee et al., 2015; Gee et al., 2014; Nagayama et al., 2014). In the external plexiform layer of the MOB, a sparse population of interneurons that includes fast-spiking interneurons (FS), are thought to contribute to broad lateral inhibition of MCs (Kato et al., 2013; Miyamichi et al., 2013). In both MOB and AOB, the most populous interneuron population, and a primary source for inhibition of MCs, is the granule cells (GCs), which

mediate recurrent and lateral inhibition of MC through dendrodendritic synapses (Isaacson & Strowbridge, 1998; Jahr & Nicoll, 1980; Schoppa et al., 1998). Dendrodendritic inhibition is critical for odor discrimination and network oscillatory dynamics, controlling the spike-timing of MCs as well as their odor tuning (Fukunaga et al., 2014; Lepousez & Lledo, 2013; Schoppa & Westbrook, 1999; Yokoi et al., 1995). Despite the extensive work on the role of inhibitory circuits in the MOB, the contribution of inhibitory neurons to the processing of chemosensory information by the AOB is poorly understood (Larriva-Sahd, 2008; Takami & Graziadei, 1991). At a superficial level, GABAergic PGCs are also present in the glomerular layer of the AOB, but the extent of glomerular interneuron diversity in the AOB is not well understood. Furthermore, unlike the MOB, the MC layer is diffuse, and the analogous EPL of the AOB contains the MCs and a sparse population of interneurons called external granule cells (extGC). While the extGCs seemingly appear to be similar to the MOB FS in connectivity (Larriva-Sahd, 2008; Maksimova et al., 2019), they exhibit sparse responses to odors, which is opposite to what has been observed with MOB FS interneurons (Kato et al., 2013; Zhang & Meeks, 2020). As such, a detailed understanding of the function of these interneurons in the AOB circuit and their regulation remains unknown.

**Granule cells in olfactory processing**

GCs comprise approximately 90% of the inhibitory interneurons in the

OB, and they are heterogeneous with regards to morphology and physiology, suggesting that different GCs may play different computational roles in the OB (Gordon M Shepherd, 2004). A unique feature of GCs is that they are axon-less and therefore their inhibitory output occurs at their dendrites, in specialized structures, the dendritic spines. GCs have an apical dendrite that projects into the EPL, where it branches into distal segments; it is here where they make dendrodendritic synapses with secondary lateral dendrites of MCs (Egger et al., 2003; Schoppa et al., 1998). While the distal dendrites of GCs contribute to dendrodendritic inhibition of MCs, the basal and proximal dendrites integrate top-down feedback afferent from the olfactory cortices and several neuromodulatory centers associated with various olfactory behaviors and behavioral states (Boyd et al., 2012; Lepousez et al., 2013). Neuromodulatory inputs, including those from the noradrenergic system, can regulate and fine-tune the dendrodendritic inhibitory output onto MCs at their distal dendrites and spines.

Dendrodendritic synapses occur between distal dendritic spines in GCs and the secondary or lateral dendrites of MCs. Upon depolarization, MCs release glutamate from its lateral dendrites, which activates AMPA and NMDA receptors on the GC spines (Isaacson & Strowbridge, 1998; Schoppa et al., 1998). Depolarization of a GC spine in response to glutamate activates voltage-gated sodium and calcium channels which contribute to the release of GABA onto the MCs from the same GC spine (Bywalez et al., 2015; Egger et

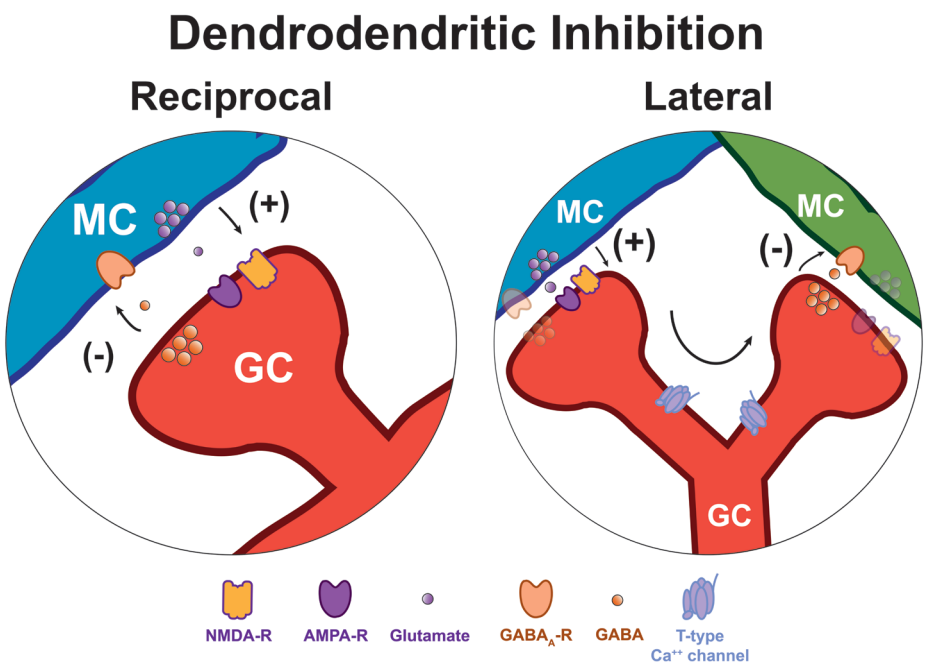


**Figure 3: Reciprocal and lateral inhibition at the dendrodendritic synapse** Glutamate released from a MC act on glutamatergic AMPA and NMDA receptors to induce release of GABA from GCs back to the MC in the form of reciprocal inhibition (left). Glutamatergic excitation of GC spines can invade the dendrite, trigger low threshold T-type calcium channels to propagate the signal to neighboring spines to mediate lateral inhibition (right).

al., 2005; Isaacson, 2001). In addition, the activation of a GC single spine by a MC can produce lateral inhibition of other MCs through propagation of low-threshold T-type calcium spikes that travel across the dendrite of the GC to invade spines synapsing onto other MCs (Egger et al., 2003). In this scheme, a somatic action potential from a GC is not necessary for recurrent and lateral inhibition of MCs to occur. However, somatic action potentials can be driven by a combination of direct axonal synapses from MCs onto GCs, cortical feedback excitation, and neuromodulation, which can lead to feedforward

inhibition of MCs.

In the AOB, GCs are also the most abundant cells, exhibit similar morphological and physiological properties, and make dendrodendritic synapses with MCs (Jia et al., 1999; Larriva-Sahd, 2008). Only a few studies have characterized GC-MC dendrodendritic interactions in the AOB, suggesting that the synaptic mechanisms are different. For example, activation of type 1 metabotropic glutamate receptors (mGluR1) is partially necessary for recurrent inhibition in the AOB, but is not required in the MOB (Castro et al., 2007). As the odor signaling in the AOB may use a different coding scheme, how GC-MC dendrodendritic interactions sculpt MC activity to affect coding and regional output is still not well-understood.

**Postnatal integration of granule cells**

The OB and the hippocampus are the only two regions known to undergo prominent adult neurogenesis in the mammalian brain. While the number of MCs are fixed by the time of birth, the number of inhibitory interneurons in the OB, as well as the overall size of the OB, increase throughout life (Platel et al., 2019; Gordon M Shepherd, 2004). GCs originate from neuronal precursors in the subventricular zone of the lateral ventricles, and migrate to the OB through the rostral migratory stream (RMS) (Carleton et al., 2003; P.-M. Lledo et al., 2008). Migrating GCs arrive within 1 – 2 weeks in the granule cell layer (GCL), and as they mature, they exhibit a wide

diversity in the expression of molecular markers, proteins, and morphology (Batista-Brito et al., 2008; Imamura & Greer, 2015; P.-M. Lledo et al., 2006). Throughout the maturation process, GCs interact functionally with the existing OB circuit. They form functional synapses shortly upon arriving in the OB after 1 week, receiving both glutamatergic and GABAergic inputs, as well as forming dendrodendritic synapses with MCs (P.-M. Lledo et al., 2006; Zhao et al., 2008). Because GCs undergo physiological changes throughout their maturation, current models posit that GCs at different stages of integration play different functional roles in the circuit, with younger GCs being more excitable and broadly tuned to odors while older GCs are less excitable and narrowly tuned to odors (Lepousez et al., 2013; Sahay et al., 2011; Wallace et al., 2017). In addition, GCs undergo a critical period 1-2 weeks after arriving to the OB, in which their integration is regulated by the presence of odor stimuli. Interestingly, most postnatally-born GCs become fully integrated after arriving in the OB, while approximately half of adult-born GCs undergo apoptosis by the time the cells reach 6 weeks of age (Petreanu & Alvarez-Buylla, 2002; Winner et al., 2002a). Because the GC survival is highly activity-dependent, the role of top-down neuromodulatory feedback, including noradrenergic modulation, can play a critical role in their integration. Accordingly several studies suggest that GC integration is strictly regulated, activity-dependent, and at the same time sensitive to external modulatory processes (Bauer et al., 2003; Gao & Strowbridge, 2009; Kuhn, 2016; Moreno

et al., 2012; Petreanu & Alvarez-Buylla, 2002).

**Noradrenergic modulation of MOS and VNS in social behavior**

The noradrenergic system has extensive projections through the entire neuraxis, including the OB, and plays an important role in neuronal excitability in physiological states such as attention, anxiety and emotions (Berridge & Waterhouse, 2003; Gu, 2002). Noradrenergic fibers originate from the brain stem in the locus coeruleus (LC), and three general classes of receptors mediate adrenergic responses in the brain; $\alpha_1$, $\alpha_2$ and β, each of which is further divided in subtypes (Hein, 2006; Khvotchev & Kavalali, 2008; Small et al., 2003). Amongst these receptors, $\alpha_2$-ARs exhibit a higher sensitivity to noradrenaline (NA) than $\alpha_1$-ARs (Kunisawa et al., 1985), while β-ARs exhibit the lowest sensitivity to NA (Molinoff, 1984; Rang, 2012). Each of these receptors exerts distinct cellular effects through the activation of different transduction mechanisms involving a subset of GTP-binding proteins. For example, $\alpha_1$-AR couple to $G_q$ mediated pathways, which through activation of phospholipase C (PLC) which can result in production of inositol triphosphate (IP3) and elicit calcium release from intracellular stores (Marzo et al., 2009; Rang, 2012), while β adrenergic receptors generally activate adenylyl cyclase though Gs. Gq activation can also lead to reduction of leak $K^+$ currents (McCormick & Wang, 1991), causing an increase in membrane resistance and neuronal excitability. The $\alpha_2$- and β-ARs signal through opposing

mechanisms via the Gi and Gs proteins, respectively, by inhibiting or activating adenylyl cyclase and in turn increasing or decreasing production of cyclic adenosine monophosphate (cAMP). These changes in intracellular cAMP modulate the voltage gating and activation kinetics of hyperpolarization cyclic-nucleotide-gated (HCN) channels, which in turn affect neuronal excitability (Benarroch, 2013; Zagotta et al., 2003). Furthermore, Gi-activation by $\alpha_2$-ARs can suppress voltage-gated calcium currents as well as enhance leak K+ conductances to suppress neuronal excitability (Y. W. Li et al., 1995; Timmons et al., 2004), whereas Gs activation by β-ARs can inhibit K+ conductances and lower sodium channel thresholds to increase cell excitability (Haas & Rose, 1987; Matsuda et al., 1992). In GCs of AOB and MOB, activation of $\alpha_1$-ARs not only depolarizes the neurons, but stimulus-elicited spiking also produces a calcium-mediated slow after-depolarization that increases spike probability and cell excitability (Smith et al., 2009; Zimnik et al., 2013). Despite the cell-specific expression of $\alpha_2$- and β-ARs in the OB, how the activation of these receptors affects neuronal physiology is poorly understood.

NA levels correlates strongly with wakefulness, alertness, and physiological arousal in mammals (Aston-Jones & Cohen, 2005; Florin-Lechner et al., 1996; Foote et al., 1980; Salgado et al., 2016). LC neurons can increase their activity in a task-dependent manner, and can respond to task-relevant sensory stimuli (Bouret & Sara, 2004; Clayton et al., 2004). In

the MOB, NA has been implicated in long-term plasticity mechanisms involving odor learning (Doucette et al., 2007; Sullivan et al., 1992), structural plasticity and survival of adult-born neurons (Moreno et al., 2012; Veyrac et al., 2009), as well as short-term effects in affecting signal-to-noise ratio adjustments and network oscillatory dynamics (Manella et al., 2017; Ramirez-Gordillo et al., 2018). In the AOB, noradrenergic modulation is critical for circuit plasticity involved in social learning, including the learning of stud pheromonal identity after mating in females (Brennan et al., 1995; Brennan & Keverne, 1997), and the recruitment of noradrenergic modulation is critical in triggering aggressive behaviors in males (Marino et al., 2005; R. J. Nelson & Trainor, 2007). At the circuit level, noradrenergic modulation has been shown to generally increase inhibitory tone onto AOB MCs (Araneda & Firestein, 2006; Doyle & Meeks, 2017). However, how short-term effects of NA at the circuit level result in long-term plasticity, leading to odor learning is unknown.

While noradrenergic modulation is involved in both MOB and AOB processing of social odors, how both the MOS and VNS are utilized in social behaviors is not well understood. Because both MOS and VNS respond to social odor cues (Spehr, 2006), both systems can be recruited in parallel to affect social behavior, and both are affected by noradrenergic modulation. The recognition of offspring after parturition in sheep, has been shown to depend on elevated concentrations of NA in the MOB (Brennan & Kendrick, 2006). Similarly, the recognition of the stud after mating is also dependent on

a surge in NA concentration in the AOB of females (Brennan et al., 1998). As noradrenergic modulation is implicated and recruited during social behavior in both systems, defining the cellular and circuit effects of NA is critical to the understanding adrenergic modulation of social odor processing and learning.

**Specific aims**

Noradrenergic actions on MOB and AOB inhibitory circuits rely on a complex combination of cell-type specific activation of G-protein coupled noradrenergic receptors. While the initial downstream signaling pathways of these ARs are known, how these secondary messenger pathways affect GC excitability or plasticity at dendrodendritic synapses is not well understood. While GC function has been primarily studied from the perspective of extrinsic regulation by local circuitry or top-down afferents, little is known about the intrinsic mechanisms that regulate GCs function, and how these are regulated by the noradrenergic system. Furthermore, At the level of the circuit, NA can target multiple inhibitory cell types, but little is known about the regulation of other inhibitory types by NA. The overall goal of the experiments in this thesis is to define how GC function is regulated by intrinsic mechanisms and by noradrenaline in the OB.

*Specific aim 1: Hyperpolarization-activated currents in GCs of the olfactory bulb*

HCN channels play an essential role in neuronal function and network

oscillatory dynamics, including the control of membrane excitability and integration of synaptic inputs, the generation of membrane potential oscillations, and subthreshold resonance of neurons (Fan et al., 2005; George et al., 2009; Hu et al., 2009; Magee, 1998; McCormick & Pape, 1990). GCs are critical to OB network oscillations, however the presence and function of $I_h$ in these inhibitory neurons is unknown. In this first aim, I characterized $I_h$ in both MOB and AOB GCs born postnatally and its role in their physiology.

*Specific aim 2: Adrenergic modulation of $I_h$ in adult-born GCs and its role in dendrodendritic inhibition in the MOB*

Changes in intracellular cAMP concentration in response to neuronal metabolic state or to the action of neuromodulators, including NA, can affect $I_h$, and, in turn, alter membrane excitability of diverse cell types (Pape & McCormick, 1989; Valsecchi et al., 2013), as well as regulate dendritic excitability (Barth et al., 2008; Carr et al., 2007; M. Wang et al., 2007). Here, I show that adult-born GCs, like postnatal born GCs, exhibit $I_h$ and that this current is modulated by NA through the activation of $\alpha_2$-ARs. Given the prevalence of $I_h$ in GCs I examined the role of $\alpha_2$-AR modulation of $I_h$ on reciprocal and lateral inhibition of MCs.

*Specific aim 3: Differential modulation by noradrenaline of the AOB and MOB circuits*

NA is postulated to play a critical role in in social behavior mediated through the MOB and AOB circuits. Despite the neuroanatomical similarities of these circuits, the neurophysiological correlates of chemosensory processing appear to be different and how NA regulates these circuits is not completely understood. In this aim, I examined how NA affects MC excitability in the AOB and MOB. In addition, I examined the properties of the inhibition onto MCs recruited by NA, and the types of inhibitory neurons besides GCs that contribute to the inhibition of MCs.

*Specific aim 4: Long-term plasticity elicited by NA in MCs of the MOB and AOB*

Noradrenergic modulation serves as a gate for multiple plasticity mechanisms in the central nervous system, and is critical for social odor learning in both MOB and AOB (Brennan & Keverne, 1997; Pawlak et al., 2010; Sara, 2009). Therefore, in this last and preliminary aim, I began to explore mechanisms by which NA can induce long-term changes in MC excitability.

# Chapter 2: Hyperpolarization-activated currents in granule cells of the olfactory bulb

## Introduction

Hyperpolarization-activated cyclic nucleotide gated (HCN) channels play an essential role in neuronal function and network oscillatory dynamics, including control of membrane excitability and integration of synaptic inputs, the generation of membrane potential oscillations and subthreshold resonance of neurons (Fan et al., 2005; George, Abbott, & Siegelbaum, 2009; Hu, Vervaeke, Graham, & Storm, 2009; Magee, 1998; McCormick & Pape, 1990). Moreover, the voltage sensitivity and kinetic properties of the HCN mediated current ($I_h$), is dependent on the subunit composition of the channels (HCN1-4), which confers differing sensitivities to cyclic nucleotides, providing a rich heterogeneity to the contribution of these channels to network function (Kaupp & Seifert, 2001; Wainger et al., 2001). Thus, changes in intracellular cAMP concentration in response to neuronal metabolic state or to the action of neuromodulators can affect $I_h$ and in turn alter membrane potential oscillations of pacemakers cells in the brain and in the heart (Pape & McCormick, 1989; Valsecchi et al., 2013).

In olfaction, initial processing of odor signals occurs through two parallel, albeit complementary, pathways in the olfactory bulb (OB). In general, the main olfactory bulb (MOB) receives input from the nasal epithelium and is largely tuned to environmental odors, whereas the

accessory olfactory bulb (AOB) receives input from the Vomeronasal organ and is largely responsible for the detection of semiochemicals (Keverne, 1999; Lledo, Gheusi, & Vincent, 2005; Shepherd, 1972). In the MOB network synchrony is a substrate to important aspects of olfactory coding such as sparsening and feature binding of odor representations (Binns & Brennan, 2005; Brody, 2003; Osinski & Kay, 2016) and network synchrony may also play a role on pheromonal processing by the AOB (Binns & Brennan, 2005; Leszkowicz et al., 2012). This network synchrony arises from the activity of dendrodendritic synapses between a large number of intrinsic inhibitory neurons, including the granule and periglomerular cells (GCs and PGCs) and the output neurons, the mitral and tufted cells (MCs and TCs) (Gschwend et al., 2015; Kay, 2014; Lagier et al., 2004; Lepousez & Lledo, 2013). In the MOB, network oscillations in the theta frequency (4-12 Hz), entrained by the respiratory cycle are in part mediated by periglomerular cells (PGCs) (Fukunaga et al., 2014), while gamma oscillations (40-80 Hz), are mediated by GCs (Fukunaga et al., 2014; Kay, 2014; Lagier et al., 2004).

Surprisingly, despite the influence of inhibitory neurons in promoting network oscillations in the OB, the presence and contribution of $I_h$ to GC excitability has not been addressed. Here, using whole-cell patch clamp recordings, we show that most GCs of the OB exhibit $I_h$. Targeted recording of postnatally labeled neurons indicated that the contribution of $I_h$ to GC physiology increases throughout postnatal development, leveling between 4

and 6 weeks post-birth. In the presence of ZD7288, an $I_h$ blocker, GCs hyperpolarized and their input resistance increased, suggesting that at rest $I_h$ contributes to the excitability and passive properties of GCs. Importantly, mature MOB GCs and PGCs exhibited an $I_h$-dependent subthreshold resonance with resonant frequencies in the delta and theta range (1-12 Hz). These results suggest that the expression of $I_h$ and subthreshold resonance in inhibitory neurons may impart unique features to odor processing in the OB and facilitate oscillatory network activity in both the main olfactory and Vomeronasal systems.

**Materials and methods**

*Animals*: All experiments were conducted following the guidelines of the IACUC of the Author's University. Experiments were performed on wild-type (C57/BL6) mice of either sex ranging in age from postnatal day 15 to 60 days old.

*Electroporation*: To label postnatally born neurons with the green fluorescent protein (GFP), mice (P1-P4) were anesthetized by hypothermia and 2 µL (4 µg/µL) of pCAG-GFP plasmid (Addgene) was injected into the lateral ventricle. Immediately after the injection, twizzer-type electrodes (BTX) were placed on the sides of the head for electroporation (5 x 100 V pulses of 50 ms) using an ECM830 Electro square pulser (BTX). Recordings of GCs were conducted at least one week post electroporation, and onwards, in cells identified by the expression of GFP under a fluorescent microscope.

*Slice Preparation*: Experiments were performed in OB slices using methods previously described (Smith et al, 2015). Briefly, brain slices were prepared in an oxygenated ice-cold artificial cerebrospinal fluid (ACSF) containing low Ca2+ (0.5 mM) and high Mg2+ (6 mM). Sagittal sections of the OB (250 µm) were then transferred to an incubation chamber containing normal ACSF (see below) and left to recuperate for at least 30 minutes at 35°C until the recordings. In all experiments, unless otherwise stated, the extracellular solution is ACSF of the following composition (in mM): 125 NaCl, 26 NaHCO3, 1.25 NaH2PO4, 2.5 KCl, 2 CaCl2, 1 MgCl2, 1 myo-inositol, 0.4

ascorbic acid, 2 Na-pyruvate, and 15 glucose, continuously oxygenated (95% O2-5% CO2) to give a pH 7.4 and an osmolarity of 305 mOsm.

*Electrophysiological Recordings*: Neurons were visualized using an Olympus BX51W1 microscope and recorded using a dual EPC10 amplifier (HEKA, Union City, NY) in voltage and current clamp modes. In a subset of the experiments, to visualize and confirm GCs identity and morphology, the fluorophore Alexa 594 (red) was included in the recording pipette solution (20 μM). Electrical stimulations and recordings were performed using the PatchMaster software. Experiments were performed at room temperature, or at 32 ± 2°C, using the TC-342B Automatic Temperature Controller (Warner Instruments, Hamden, CT) with a perfusion speed of 2-3 mL/min. Cells were patched using standard patch pipettes (4-8 MΩ resistance). The membrane potential was not corrected for junction potential. Although our experiments in whole cell recordings precluded an accurate measurement of Vm, right after rupturing the seal, the Vm in GCs of the MOB was –71.9 ± 1.5 mV (n = 26) and –64.4 ± 1.5 mV (n = 5) in the AOB. These measurements are in agreement with previous studies indicating that GCs maintain a hyperpolarized Vm in the slice preparation (Cang & Isaacson, 2003; Egger, Svoboda, & Mainen, 2005). Therefore, unless otherwise indicated, voltage and current-clamp experiments in GCs were conducted at –60 or –70 mV.

*Solutions and pharmacological agents*: In whole-cell recordings the internal solution had the following composition (in mM): 120 K-gluconate, 10 Na-

Gluconate, 4 NaCl, 10 HEPES-K, 10 Na phosphocreatine, 2 Na-ATP, 4 Mg-ATP, and 0.3 GTP adjusted to pH 7.3 with KOH. This internal solution, which contains Na, was used in order to compare the physiology of GCs with previous work published from our lab (Smith et al., 2015). In some experiments, 0.5 mM cAMP was added to the internal solution. The osmolarity of the internal solutions was adjusted to 290–305 mOsm. For experiments using high extracellular K+, the ACSF contained 25 mM KCl and 102.5 mM NaCl. Drugs were prepared freshly from stocks and diluted into the external solution; ZD7288 (4-Ethylphenylamino-1,2-dimethyl-6-methylaminopyrimidin chloride) was purchased from Tocris Cookson (UK) and it was applied at 30 μM.

*Data Analysis*: All electrophysiological recordings were analyzed in MATLAB (Mathworks). In order to isolate $I_h$, leak currents were subtracted from the voltage-current relationships using multiples of a small voltage step (–60 to –65 mV) elicited at the end of each voltage clamp trace. Recorded GCs exhibited heterogeneity in physiological properties, such as input resistance and capacitance, presumably due to the presence of a heterogeneous population that included mature and immature cells. To compensate for these differences, in some instances (i.e. high $K^+$ or ZD288) $I_h$ was normalized to the current elicited by a voltage step from –60 mV to –130 mV.

Voltage dependency was calculated by fitting the tail-current maximum values to a Boltzmann function of the following form (Dibattista et al., 2008;

Ludwig et al., 1998), $I = I_{max}/\{1 + \exp[(V-V_{half})/k_s]\}$ where $I_{max}$ is the maximal current, V is the prepulse potential, $V_{half}$ is the half activation potential of the current, and $k_s$ is the slope factor. The current (I) values were measured as the peak current obtained with a step to –130 mV from the prepulse potential (Fig 2A inset), and were then normalized to the fitted $I_{max}$ value for each cell. The activation time constant ($\tau$) for $I_h$ was determined by fitting a single exponential function to the raw voltage trace when stepping from –60 mV to –130 mV.

The sag potential was calculated from the voltage deflection elicited by a negative current pulse and corresponds to the difference between the peak minimum voltage and the membrane potential (Vm) upon reaching a steady state (after 1 s). The change in membrane potential ($\Delta V$) in response to ZD7288 was measured as the difference between the baseline Vm (before the drug) and at the Vm at peak of the response, which under our perfusion speed occurred within ~ 6-10 min. Subthreshold resonance was measured using a standard impedance amplitude protocol (ZAP), in which a stimulus of sinusoidal current of constant amplitude and exponentially increasing frequency (0.2 to 20 Hz) is injected into the cell. The ZAP protocol was obtained at different negative potentials (–60 mV to –100 mV), which are correspondingly indicated throughout the text. The impedance profile was calculated as the magnitude of the ratio of the fast Fourier transforms of the

voltage response and current input (Gutfreund et al., 1995; Hutcheon & Yarom, 2000; Vera et al., 2014):

$Z(f) = |FFT[V(t)]/FFT[I(t)]|$

The exponential ZAP protocol we employed works best on cells with lower resonant frequencies; therefore we also confirmed our findings in mature cells using a linear ZAP protocol (Hu, Vervaeke, & Storm, 2002; Narayanan & Johnston, 2007) allowing us to better sample higher frequencies (data not shown). The impedance profile is smoothed and the resonant frequency ($f_{res}$) is the frequency at which the maximal impedance value occurs. If the peak value is not clear, the impedance profile is fit with a quadratic function to provide an estimate. The strength of resonance (Q factor) is calculated as the ratio between the maximal impedance ($|Z(f_{res})|$) and the lowest frequency impedance values ($|Z(f_{low})|$; 0.5 Hz). The cell is considered resonant if $f_{res} > f_{low}$ and $Q > 1$. Statistical significance was determined by a student's t-test, Mann-Whitney U test, one-way ANOVA, logistic regression, or linear regression.

## Results

### $I_h$ is present in GCs of the AOB and MOB

We conducted whole-cell patch clamp recordings in GCs of the MOB and AOB. In both regions GCs are located in easily identified layers and exhibit characteristic morphology, including the presence of basal dendrites and a single apical dendrite, which bifurcates into several branches, populated by prominent dendritic spines (Fig 1A) (Larriva-Sahd, 2008; Price & Powell, 1970). In voltage clamp (Fig 1B), hyperpolarizing steps from –60 mV to –130 mV revealed a slowly developing inward current, with characteristics of $I_h$, that occurred in the majority of GCs; ~96% in the AOB (80/83) and ~90% in the MOB (106/118). In agreement with the properties of $I_h$, the peak amplitude of the inward current was enhanced ~3-fold by increasing the external K+ concentration from 2.5 mM to 25 mM (Fig 1C). Thus, the normalized mean currents in high K+ were 3.7 ± 0.9 (n = 5, Mann-Whitney U test, $p < 0.01$) in the AOB and 3.5 ± 1.1 in the MOB (n = 4, Mann-Whitney U test, $p < 0.01$). Importantly, in the presence of the selective $I_h$ blocker, ZD7288 (30 μM, see methods), the inward current was reduced by over 60% (Fig 1C). The normalized mean current in the presence of ZD7288 was 0.4 ± 0.1 in the AOB (n = 4, Mann-Whitney U test, $p < 0.03$) and 0.36 ± 0.16 in the MOB (n = 7, Mann-Whitney U test, $p < 0.001$).

Different subunit composition in the tetrameric HCN channels confers distinct cyclic nucleotide sensitivity to $I_h$, which in turn influences the voltage

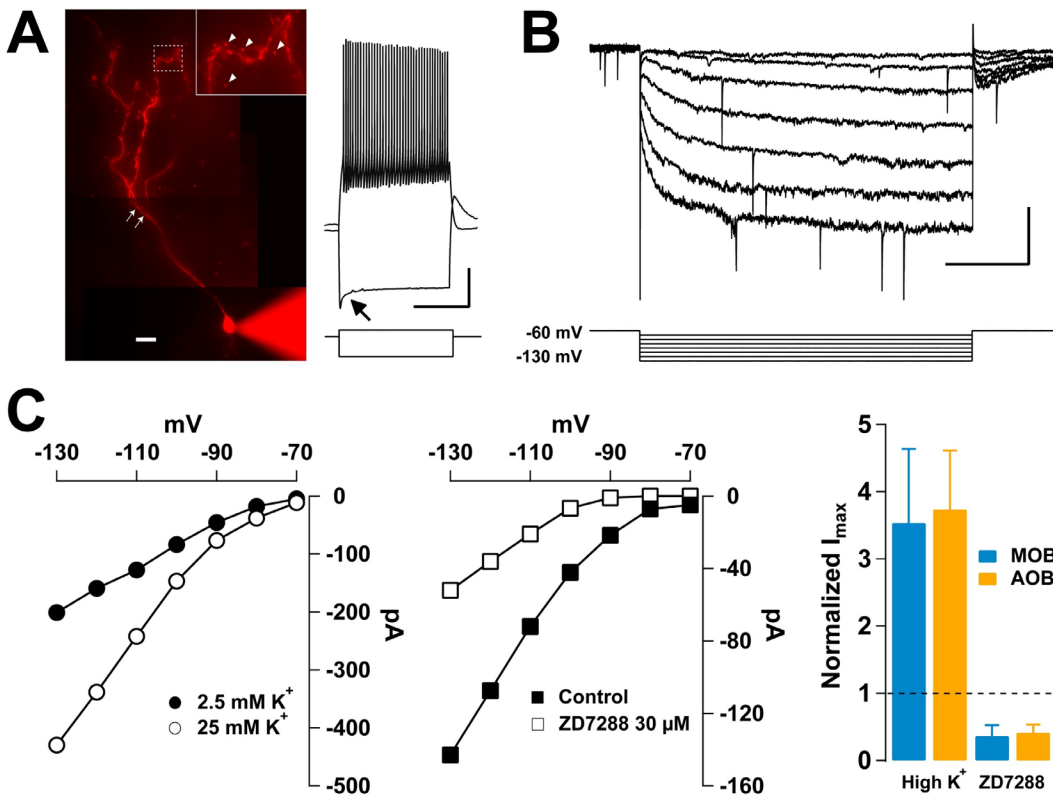


**Figure 1: Properties of hyperpolarization-activated cation currents in GCs of the OB.**
A: Left, image of a GC recorded in the AOB, with Alexa 594 in the pipette. Mature GCs are characterized by the presence of branches in the apical dendrite (white arrows), and prominent dendritic spines (inset, arrow heads). The scale bar is 20 µm. Right, current clamp response of the GC shown on the left. A hyperpolarizing current step (–60 pA) produces a sag in the membrane potential ($V_m$, arrow), while a depolarizing current step (20 pA) elicits a train of action potentials. The resting $V_m$ in this cell is –60 mV; scale bars are 20 mV and 1s. B: Hyperpolarizing voltage steps from –60 mV to –130 mV (10 mV steps) elicited a slowly developing hyperpolarization-activated inward current (scale bars is 500 ms and 50 pA). C: Left, current-voltage (IV) relationship for $I_h$ in an AOB GC. Raising the external $K^+$ concentration from 2.5 (filled circles) to 25 mM (empty circles) increased the inward current at each potential. Middle, IV relationship of an AOB GC in control (filled squares) and in the presence of the $I_h$ blocker ZD7288 (30 µM, empty squares); at all potentials ZD7288 reduced $I_h$. Right, summary plot showing the effect of high $K^+$ and ZD7288 on the normalized mean $I_h$ at –130 mV. In the MOB (blue) and AOB (orange), high $K^+$ produced at least 3-fold increase in the current. Similarly, ZD7288 produced over a 60% decrease in $I_h$ in both regions.

sensitivity and kinetics of the channels (Benarroch, 2013; Craven & Zagotta,

2006). Therefore, we compared the properties of $I_h$ by recording GCs with and without cAMP (0.5 mM) in the internal solution, determining the kinetics of $I_h$ activation and maximal current elicited in voltage clamp (Fig 2A). Analysis of the voltage dependency using a Boltzmann fit (see methods) and the kinetics of a ctivation of $I_h$ revealed significant differences between GCs in the AOB and MOB. In the absence of cAMP, activation of $I_h$ occurred at more positive potentials in the AOB than in the MOB; $V_{half}$ of activation of $I_h$ in AOB was –94.8 ± 4 mV (n = 15) while in the MOB $V_{half}$ was –103 ± 6 mV (n = 10) (AOB vs. MOB, Student's t-test, $p < 0.03$). Furthermore, in the absence of cAMP the activation of $I_h$ was slower in the AOB than in the MOB (Fig 2B; $\tau$ = 123 ± 14 ms vs. $\tau$ = 58.8 ± 12.9 ms, respectively, Student's t-test, $p < 0.007$). Interestingly, adding cAMP to the internal solution shifted $V_{half}$ by ~10 mV in the MOB (–94 ± 5 mV, n = 11, Student's t-test, $p < 0.04$), while it produced no significant effect in the AOB (–94.5 ± 3 mV, n = 12, Student's t-test, $p > 0.4$). In contrast, $\tau$ decreased by ~half in both regions (AOB, 55.3 ± 8.7 ms, Student's t-test, $p < 0.001$; MOB, 30 ± 6.8 ms, Student's t-test, $p < 0.03$). Together, these findings indicate that the sensitivity to cAMP is region specific

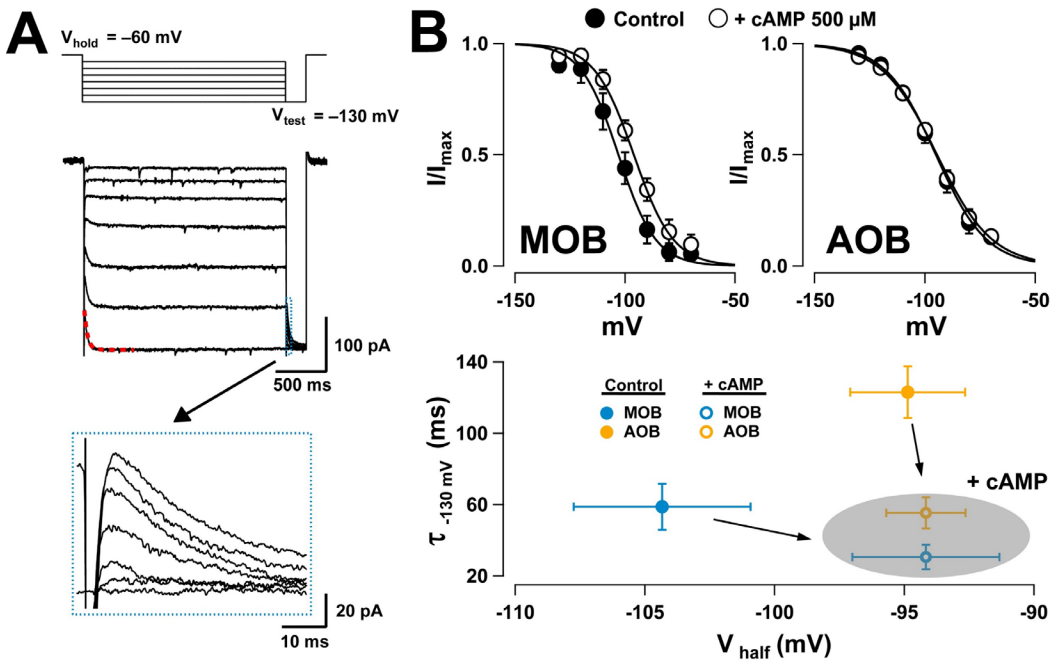


**Figure 2. Voltage Dependency of $I_h$ and sensitivity to intracellular cAMP.** A: Voltage clamp responses in an MOB GC with added cAMP in the internal solution showing $I_h$ elicited by 10 mV hyperpolarizing steps from –60 mV to –130 mV. At the end of each step, a test pulse to –130 mV ($V_{test}$) was elicited to measure the maximal current at each potential (traces shown in the bottom box inset). The current amplitudes measured at the peak were normalized to $I_{max}$ and fitted to a Boltzmann function (see methods). The time constant of activation (τ) was estimated by fitting the current elicited by stepping from –60 to –130 mV (red dotted line, 25.5 ms for this trace). B: Top, Boltzmann fits for $I_h$ in GCs of the MOB (left) and AOB (right) in recordings conducted with internal solutions without (filled circles) or containing cAMP (0.5 mM, empty circles). Bottom, summary plot comparing the cAMP sensitivity of $V_{half}$ and τ in AOB (orange) and MOB GCs (blue). In the presence of cAMP, the $V_{half}$ was shifted to more positive potentials in MOB CGs, while in the AOB τ was reduced (shaded oval).

and suggest that GCs may express HCN channels with different subunit composition in these regions.

The voltage-dependency of $I_h$ in GCs suggests it could be active at resting membrane potential ($V_m$, see methods). In agreement with this possibility, in current clamp experiments bath perfusion of ZD7288 invariably

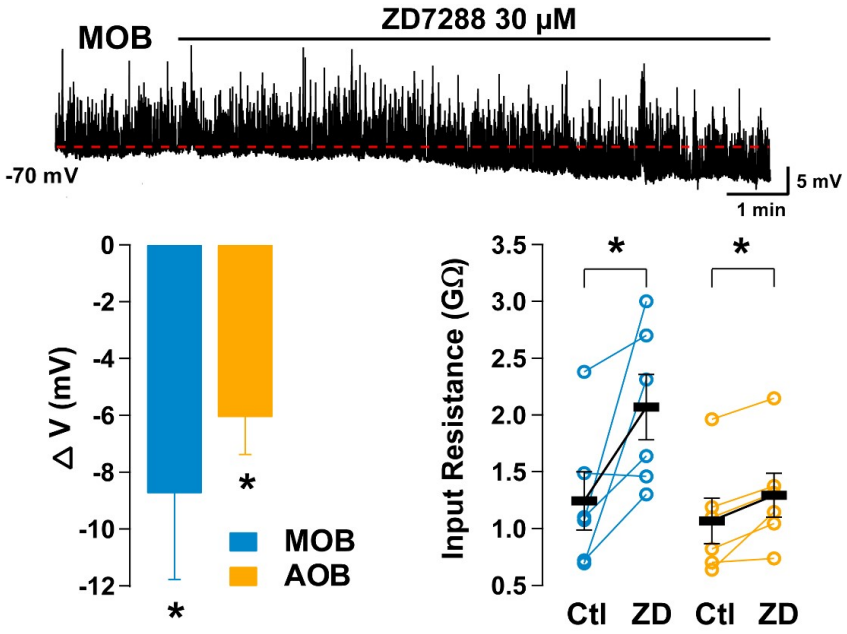


**Figure 3. $I_h$ contributes to the intrinsic properties of GCs.**
Top trace, current clamp responses in an MOB GC. Bath perfusion of ZD7288 produces a hyperpolarization (red dotted line). Spontaneous postsynaptic potentials appear as upward spikes. Bottom left, summary of the effects of ZD7288 on $V_m$, application of ZD7288 reduces the membrane potential of GCs of the MOB and AOB. Right, pharmacological block of $I_h$ significantly increases GCs input resistance measured from a holding potential of –60 mV with a negative current step.

produced a hyperpolarization in GCs (Fig 3). Blocking $I_h$ reduced the membrane potential by 6 ± 1.3 mV in the AOB (orange, n = 6, student's t-test, $p < 0.005$) and by 8.8 ± 3.7 mV in the MOB (blue, n = 5, Student's t-test, $p < 0.04$). This effect of ZD7288 was still present in the presence of blockers of fast synaptic transmission (APV, 100 µM; CNQX, 10 µM; and Gabazine, 10 µM), suggesting a direct effect on GCs. Application of ZD7288 reduced the membrane potential by 3.7 ± 1 mV in AOB GCs (n = 4, Student's t-test, $p < .007$) and 6.9 ± 3.3 mV in MOB GCs (n = 4, Student's t-test, $p < .05$). In

addition, ZD7288 produced a significant increase in GCs input resistance ($R_i$) in both regions (Fig 3, AOB; 1.04 ± 0.20 vs. 1.27 ± 0.19 GΩ; Student's t-test, $p < 0.01$; MOB 1.24 ± 0.25 vs. 2.06 ± 0.28 GΩ; Student's t-test, $p < 0.05$).

**GCs exhibit subthreshold resonance that depends on $I_h$**

In other brain regions, $I_h$ plays a critical role in generating subthreshold resonance of neurons, which in turn contributes to network oscillatory properties (Hu et al., 2002; Narayanan & Johnston, 2007; van Brederode & Berger, 2011; Vera et al., 2014). Therefore, we examined subthreshold resonance in GCs that exhibited $I_h$, using a sinusoidal current stimulus of increasing frequency (ZAP stimulus, see methods) in animals older than P30. Surprisingly, we observed a significant heterogeneity in responses to the ZAP stimulus amongst GCs, with a mixed population of resonant and non-resonant cells (Fig 4A). The percentage of resonant cells in the AOB was ~71% (15/21), and ~52% (10/19) in the MOB. In addition, among all resonant cells (AOB plus MOB), the response to the ZAP stimulus revealed heterogeneity in the resonant frequency ($f_{res}$), with cells distributed along the delta and theta range (data not shown). Importantly, this subthreshold resonance could affect the global excitability of GCs. Accordingly, when we adjusted the ZAP protocol to elicit action potentials in a subset of resonant MOB and AOB GCs, these action potentials occurred at a frequency within the range of $f_{res}$ for each cell, with 79% of the action potentials falling within ± 3 Hz relative to the cell's resonant frequency (Fig 4B).

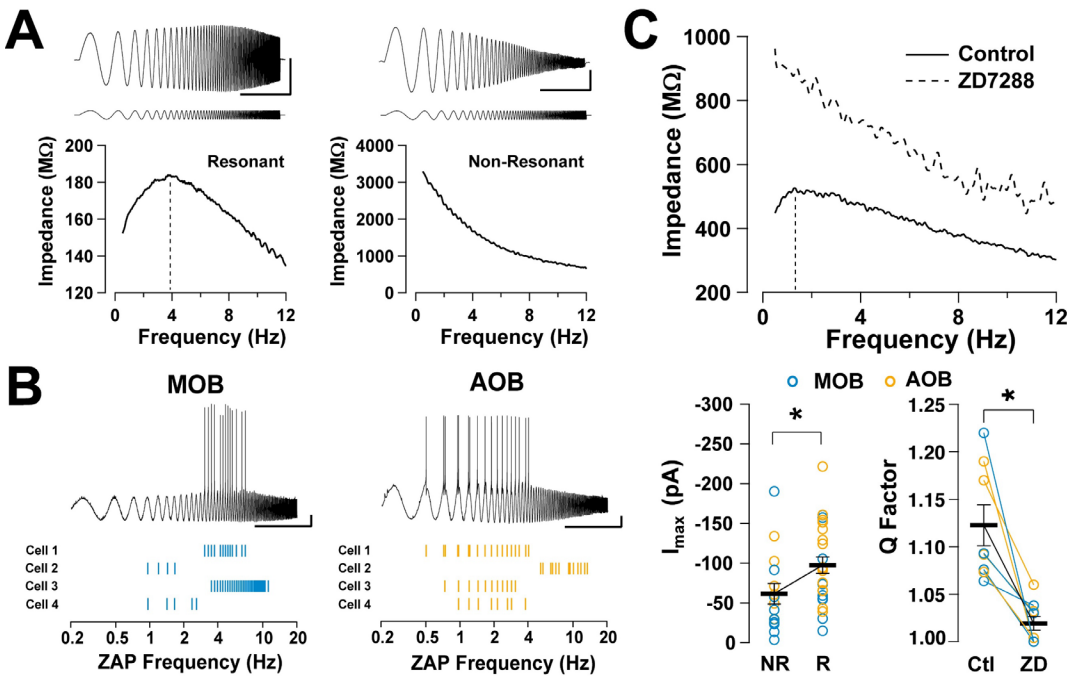


**Figure 4. Contribution of $I_h$ to subthreshold resonance in GCs.**
A: Top, voltage responses (upper traces) to a ZAP current stimulus (lower traces) in MOB GCs in a resonant (left) and, a non-resonant (right) cell. Bottom, impedance profiles for the cells shown above. In the resonant cell (left), resonance strength (Q) is 1.20 and the peak frequency ($f_{res}$) 3.88 Hz, whereas for the non-resonant cell (right), $f_{res} = f_{low}$ and the Q factor is 1. The scale bars are 5 s and 10 mV, with a 50 pA (left) and 5 pA (right) ZAP stimulus amplitude. The $V_m$ for both cells is –80 mV. B: ZAP stimulus applied to resonant GCs in the MOB (top) and AOB (bottom); the current amplitude was adjusted to elicit action potentials, which occurred around the cell's resonant frequency. C: Top, the impedance profile of an AOB GC that exhibits subthreshold resonance in control and, in the presence of ZD7288. In control conditions, Q is 1.21 and the $f_{res}$ is 1.3 Hz (black line). In the presence of ZD7288, the resistance of the GC increases, the resonance is abolished and, the impedance profile resembles that of a non-resonant cell (Q = 1). Bottom left, summary plot showing the distribution of values for maximal $I_h$ (measured at –130 mV) for MOB (blue, n= 19) and AOB (orange, n= 21) GCs; resonant cells have larger $I_h$. Bottom right, the Q factor significantly decreases after perfusion of ZD7288 in the AOB (n = 4) and MOB (n = 4).

The heterogeneity of subthreshold resonance we observed prompted us to examined whether the size of $I_h$ in GCs could contribute to these differences. Across the total population of GC studied (AOB and MOB)

resonant cells had larger $I_h$ than non-resonant cells, suggesting that $I_h$ amplitude is a predictor of resonance (Fig 4C; resonant cells, $I_{max}$ = –97.5 ± 10.3 pA, n= 25; non-resonant cells, $I_{max}$ = –61 ± 13.0 pA, n= 15; logistic regression, $p < 0.02$). Similarly, $I_h$ amplitude is predictive of resonance strength ($I_{max}$ vs. Q, in a linear regression model, $p < 0.02$). In agreement with a larger $I_h$, $R_i$ was significantly lower in resonant cells than in non-resonant cells (1.14 ± 0.01 GΩ vs. 1.61 ± 0.17 GΩ; logistic regression, $p < 0.01$). Notably, the subthreshold resonance was abolished in the presence of ZD7288, (Fig 4C); the strength of resonance or Q factor (see methods) was reduced from 1.12 ± 0.02 to 1.02 ± 0.01 in the presence of ZD7288 (n = 8, Student's t-test, $p < 0.0005$). Together, these results suggest that $I_h$ is a major contributor to the expression of subthreshold resonance in AOB and MOB GCs.

To further characterize subthreshold resonance in AOB and MOB GCs, we performed targeted recordings of postnatally labeled neurons (see methods). After 4 weeks, GCs are fully integrated, with intermediate stages of development that exhibit characteristic physiological and morphological properties (Carleton et al., 2003; P.-M. Lledo et al., 2006; Petreanu & Alvarez-Buylla, 2002; Winner et al., 2002b). At this age (Fig 5A), analysis of voltage dependency indicated that $f_{res}$ in the AOB did not vary with voltage (–70 mV, 3.47 ± 0.37 Hz; –90 mV, 3.24± 0.21 Hz; n=3; one-way ANOVA, $p > 0.6$). However, $f_{res}$ was larger at more negative potentials in the MOB (–70 mV, $f_{res}$

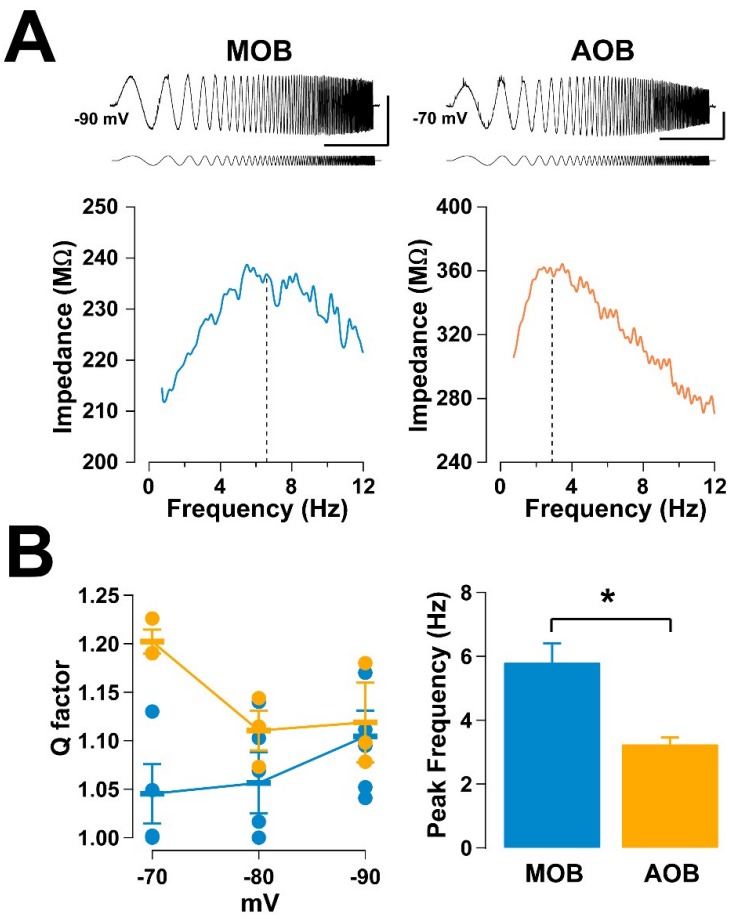


**Figure 5. The subthreshold resonance in AOB and MOB GCs exhibits different voltage dependency.**
A: Top, ZAP protocol applied to 4-week old mature GCs labeled with GFP, in the MOB (left) and AOB (right), along with their respective impedance profiles (bottom). For the MOB GC, Q is 1.17 and $f_{res}$ is 6.77 Hz, indicated by the vertical black dashed line; for the AOB GC, Q is 1.19 and $f_{res}$ is 2.89 Hz (dashed line). The scale bars are 10 mV and 5 s; the ZAP stimulus amplitude is 20 pA for the MOB and a 30 pA for the AOB. Bottom, summary plots for voltage dependency of Q and peak frequencies in MOB (blue) and AOB (orange) GCs (n = 5 and 3, respectively). B: Left, in MOB GCs, Q is strongest at more negative potentials, while in AOB GCs Q is larger at more positive potentials. Right, at –90 mV the average peak frequency in MOB GCs is significantly higher than in the AOB (see results).

= 1.09 ± 0.45 Hz; –90 mV, $f_{res}$ = 5.80± 0.60 Hz; n=5; one-way ANOVA, $p < 0.001$). Thus, at –90 mV the average peak frequency in MOB GCs is significantly higher than in AOB GCs (Fig 5B; Student's t-test, $p < 0.03$).

Furthermore, although the values did not reach significance there was a tendency for the strength of resonance to increase at more negative potential in MOB GCs (Fig 5B. –70 mV, Q = 1.04 ± 0.03; –90 mV, Q = 1.10 ± 0.02; n= 5; one-way ANOVA, $p < 0.1$), while we observed the opposite in the AOB (–70 mV, Q = 1.20 ± 0.01; –90 mV, Q = 1.12± 0.04; n= 4; one-way ANOVA, $p < 0.03$).

**Developmentally timed expression of $I_h$ and subthreshold resonance in GCs in the MOB**

GCs undergo a critical period and exhibit varied physiological properties over the course of development (Lepousez et al., 2013; P.-M. Lledo et al., 2006; Yamaguchi & Mori, 2005), therefore, we compared $I_h$ and subthreshold resonance expression in GCs at two and 6 weeks post birth in the MOB. As shown in Fig 6A, we found that $I_h$-mediated sag amplitude in GCs significantly increased between 2 (n = 5) and 6 weeks (n = 5) post birth, (–1.9 ± 0.4 vs. –4.6 ± 0.7 mV, Student's t-test, $p < 0.006$). Similarly, the $I_h$ amplitude nearly doubled between 2 and 6 weeks, albeit it was not significant within our sampled population of cells (–121.1 ± 31.1 pA vs. –215.9 ± 37.0 pA, Student t-test, $p < .09$). Nevertheless, and in agreement with the developmental increase in $I_h$-mediated sag amplitude, resonance in GCs increased as a function of cell age (Fig 6B). Between 2 and 6 weeks, resonance strength increased from 1.05 ± 0.01 to 1.10 ± 0.01 (Student t-test, $p < 0.02$). Interestingly, we also observed a developmental increase in $f_{res}$. At

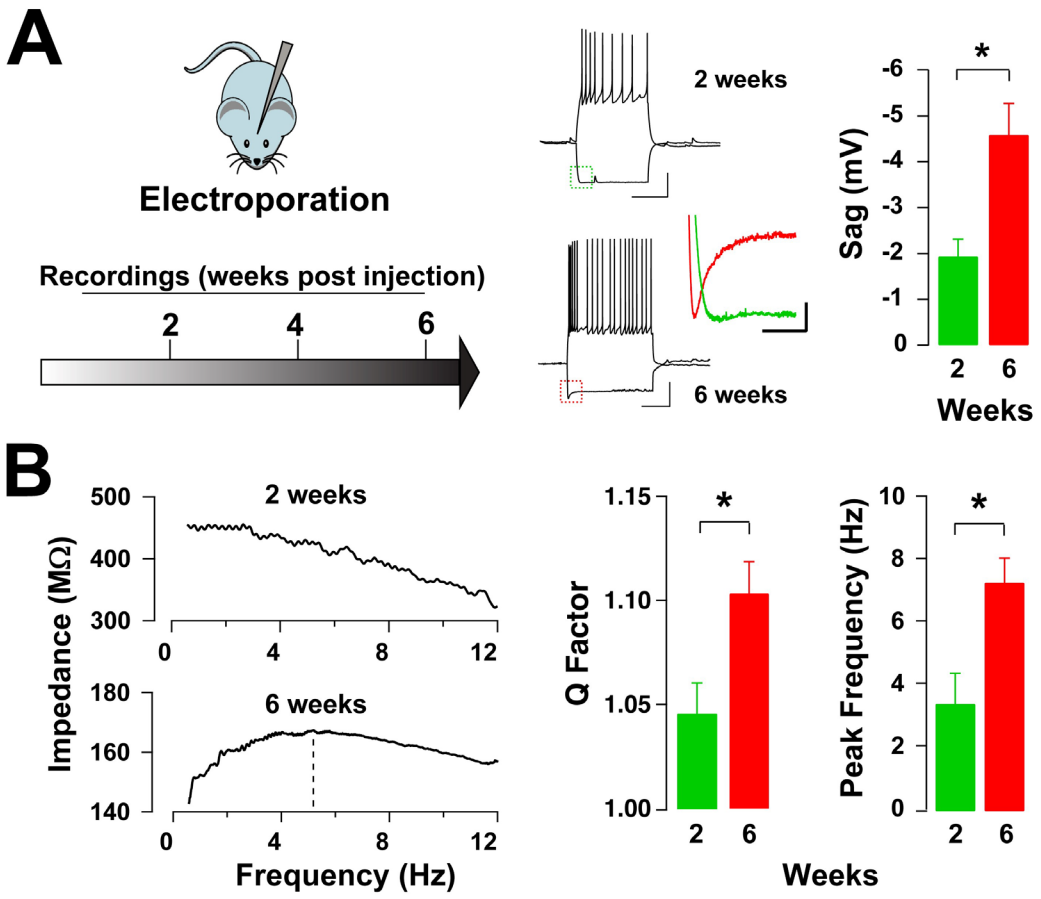


**Figure 6. Postnatal development and subthreshold resonance in MOB GCs.**

A: Left; diagram of the time course used for labeling and recording from GCs at different stages of development. Mice were electroporated at P1 and recordings were conducted at different postnatal weeks. Right, sample current clamp traces from labeled GCs at 2 and 6 weeks; recorded cells exhibit robust action potentials. At both ages, a hyperpolarizing current step elicits an $I_h$-mediated sag upon hyperpolarization (see inset). Scale bars at 500 ms and 20 mV. The colored inset compares the sag amplitudes of the cells shown at 2 (green) and 6 (red) weeks. Scale bar at 100 ms and 2 mV. The bar graph summarizes the change in sag amplitude between 2 and 6 weeks post-labeling. B: Left, example plots of impedance profile at 2 and 6 weeks post-electroporation obtained using a ZAP protocol, corresponding to the cells above in (A). At 2 weeks, Q is 1.02 while at 6 weeks Q is 1.14 and $f_{res}$ 5.18 Hz (dotted line). Right, bar graphs showing the increase in Q factors and peak frequencies between 2 and 6 weeks.

2 weeks, $f_{res}$ was 3.44 ± 0.98 Hz and at 6 weeks, 7.32 ± 0.79 Hz (Student t-test, $p < 0.02$). Altogether, these results indicate that as GCs mature, their $f_{res}$

becomes tuned towards the physiological breathing rates of mice (1-12 Hz).

**Subthreshold resonance in other OB subtypes**

We next examined whether other neurons in the OB circuit exhibit subthreshold resonance. In particular, we examined another inhibitory neuron, the PGC, which contributes to network oscillations entrained by the respiratory cycle (Fukunaga et al., 2014). Therefore we examined the presence of subthreshold resonance in PGCs sampled from animals older than P30. MOB PGCs exhibited a prominent $I_h$, with a sag potential of 5.2 ± 1.5 mV (n = 9). In recordings, conducted with cAMP in the pipette, the $V_{half}$ for $I_h$ in PGCs was more positive than in MOB GCs (Fig 7A; –82.6 ± 3.4 mV, n = 9; Student's t-test, $p < 0.03$), while τ was significantly slower (81.1 ± 22.5, n = 9, Student's t-test, $p < 0.01$), indicating differences in $I_h$ between these inhibitory subtypes. Importantly, the majority of MOB PGCs (9/11) exhibited subthreshold resonance with a mean resonant frequency of 2.02 ± 0.16 Hz and a Q factor of 1.15 ± 0.03. Moreover, application of ZD7288 completely abolished the subthreshold resonance (Fig 7A, n = 3), indicating that subthreshold resonance in PGCs, like in GCs, depends on the expression of $I_h$.

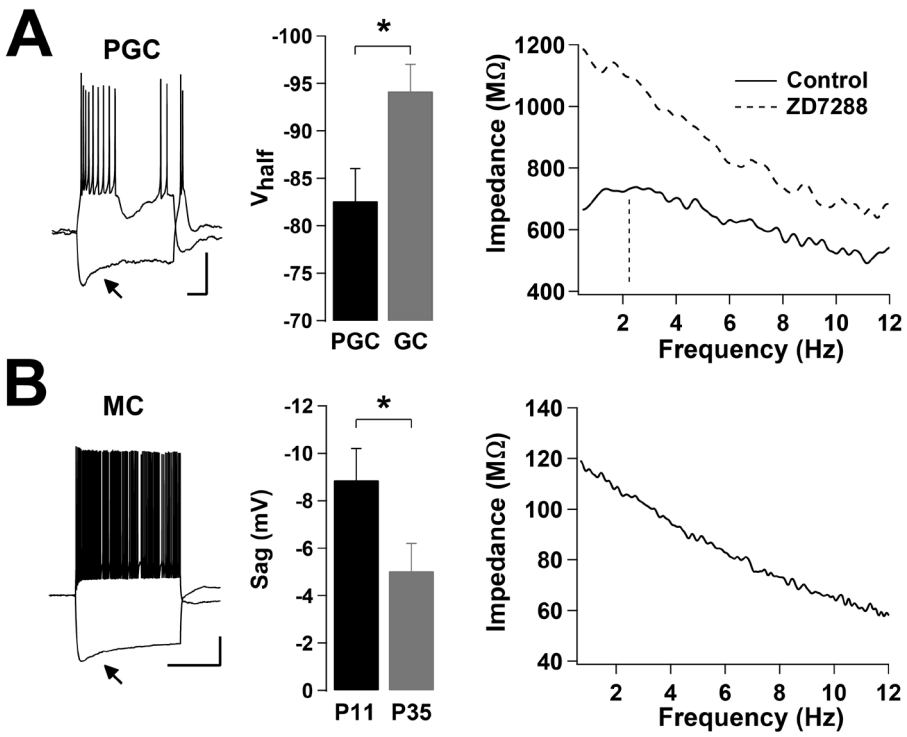


**Figure 7. PGCs, but not MCs exhibit $I_h$-mediated subthreshold resonance in the MOB.**
A: Left, current clamp responses of an MOB PGC; a hyperpolarizing current step (–10 pA) produces a sag in $V_m$ (arrow), while a depolarizing current step (5 pA) elicits a burst of action potentials characteristic to PGCs. The resting $V_m$ in this cell is –70 mV and the scale bars at 20 mV and 200 ms. Middle, summary bar graph showing that PGCs (n = 9) exhibit a more depolarized $V_{half}$ than GCs (n = 11). Right, impedance profile of a different PGC obtained using a ZAP protocol while holding at –70 mV. The subthreshold resonance is abolished in the presence of ZD7288 (control: black line, $f_{res}$ = 2.24 Hz, indicated by the vertical dashed line, and Q = 1.10; ZD7288, dashed line, $f_{res} = f_{low}$, and Q = 1). B: Left, a current clamp response of an MC at P11; a hyperpolarizing current step (–350 pA) produces a sag in $V_m$ (arrow), while a depolarizing current step (350 pA) elicits a train of action potentials. The resting $V_m$ in this cell is –60 mV and the scale bars are 20 mV and 1 s. Middle, summary bar graph showing the decrease in sag potential in MCs between P11 and P35 (P11, n = 8; P35, n = 6). Right, impedance profile of the MC shown on the left, obtained using a ZAP protocol while held at –90 mV, despite exhibiting $I_h$, the cell is non-resonant ($f_{res} = f_{low}$, and Q = 1).

In addition, we examined subthreshold resonance in MOB MCs, which have been previously shown to have $I_h$, with its expression decreasing with

age (Angelo & Margrie, 2011; Yu et al., 2015). To this extent, we recorded from two age groups of MCs, young (P11; n = 8) and old (P35; n = 6). In both age groups, MCs exhibited $I_h$, and in agreement with previous work, $I_h$ was more prominent in the younger group, with sag values of 8.9 ± 1.3 mV (young) vs. 5.0 ± 1.2 mV (old) (Fig 7B, Student's t-test, $p < 0.02$). In these recordings, which we conducted with cAMP in the pipette, the $V_{half}$ for $I_h$ was –97 ± 2.8 mV and τ was 500 ± 84 ms at P11 (MC τ vs PGC τ, Student's t-test, $p < .0001$). Intriguingly, despite the expression of $I_h$, none of the recorded MCs, in either group, exhibited subthreshold resonance. Furthermore, while $I_h$ has also been observed in AOB MCs (data not shown, and see Gorin et al., 2016), we did not observe subthreshold resonance in recorded AOB MCs (n = 5), nor in AOB PGCs (n = 4).

## Discussion

Throughout the brain, regulation of membrane excitability by $I_h$ plays an important role in neuronal function and network dynamics (Benarroch, 2013; George et al., 2009; Luethi & McCormick, 1998; Narayanan & Johnston, 2007). Network synchrony dynamics are an important component of the initial processing of odor signals in the OB. GCs comprise the largest population of inhibitory neurons in the OB, where they integrate local and afferent top-down signals to convey inhibition to output neurons, the MCs. Here, we show that $I_h$ is present in GCs and that its expression follows the postnatal development of GCs, increasing with age. In addition, we show that GCs and MOB PGCs exhibit an $I_h$-dependent subthreshold resonance in the 1-12 Hz frequency range. These results suggest that regulation of $I_h$ can play a role on circuit dynamics in the OB entrained by respiration.

GCs are a heterogeneous group of neurons, and they exhibit distinct characteristics in the AOB and MOB, including synaptic properties and regulation by neuromodulatory transmitters (Burton & Urban, 2015; Castro et al., 2007; Smith et al., 2015; Zimnik et al., 2013). Accordingly, we found that the voltage sensitivity of $I_h$ was modulated by cAMP in the MOB but not in the AOB; nevertheless, $I_h$ activation was faster in the AOB in the presence of cAMP. Among HCN subunits, HCN1 exhibit the fastest kinetics, but the weakest cAMP sensitivity (Accili et al., 2002; Kaupp & Seifert, 2001), while HCN2 and 4 exhibit slower kinetics but are more cAMP-sensitive (Kaupp &

Seifert, 2001; Wainger et al., 2001). On the other hand, the HCN3 subunit exhibits slow kinetics but is not cAMP-sensitive (Mistrik et al., 2005). Therefore, the kinetic parameters we determined suggest that MOB GCs may express a combination HCN1, 2, and 4 subunits, while HCN3 subunits predominantly contribute to $I_h$ in AOB GCs. In agreement with this possibility, all four HCN subunits are expressed in the OB, with HCN1 present in PGCs and GCs (Fried et al., 2010; Holderith et al., 2003), whereas HCN2-4 are more strongly expressed in inner layers of the MOB (Notomi & Shigemoto, 2004). In the AOB, HCN1, 2, and 4 are moderately expressed while HCN3 exhibits the strongest expression (Notomi & Shigemoto, 2004). Interestingly, despite exhibiting different kinetics and voltage sensitivity, our data with ZD7288 suggests that $I_h$ in GCs of both regions is active at rest. In other neurons, $I_h$ has been shown to contribute to baseline membrane excitability as well as dendritic integration (Benarroch, 2013; Fan et al., 2005; Magee, 1999); we propose a similar function of $I_h$ in GCs. In fact, as they lack axons, the integration of synaptic inputs and the output occurs solely in dendritic processes in GCs. Interestingly, GCs receive most afferent excitatory input in basal and proximal dendrites (Boyd et al., 2012; Markopoulos et al., 2012); therefore, the extent of regulation, by these inputs, of dendrodendritic synapses in distal regions of GC's apical dendrites, could also be modulated by the tonic influence of $I_h$.

Mature AOB and MOB GCs exhibited subthreshold resonance but there was a stark contrast in the membrane potential at which the resonance was strongest, as well as the peak frequency. In AOB GCs, subthreshold resonance was stronger at more depolarized potentials, and GCs were resonant in the delta range (1 - 4 Hz), whereas in MOB GCs resonance was strongest at more negative potentials and resonance frequencies were in the theta range (4 - 12 Hz). These differences in GCs could underlie different circuit dynamics to accommodate their specific sensory inputs, which could be arriving at these specific frequency bands. In the MOB, inputs from the main olfactory epithelium are driven by breathing and arrive in the theta range (Manabe & Mori, 2013; Smear et al., 2011). Thus, in the theta range, subthreshold resonance for GCs may act as a band-pass filter for inputs at this frequency. In the AOB however, the Vomeronasal organ (VNO) is driven constriction and dilation of large blood vessels acting as a pump (Keverne, 1999), and therefore activity in the AOB may not be directly driven by breathing, but instead by the autonomic nervous system. Interestingly, previous studies have shown the presence of $I_h$ in VNO sensory neurons, however at this time is unknown whether these cells exhibit subthreshold resonance (Cichy et al., 2015; Dibattista et al., 2008). The lower frequency in AOB GCs suggests that the information processing and timing of inputs can work on a different timescale compared to the MOB. For example, the delta range resonance we found in the AOB matches the lower frequency baseline

activity of AOB MCs near ~4 Hz (Luo et al., 2003), as well as VNO activity near ~ 1 Hz (Meredith, 1994). We note that differences in resonant frequency could be due to the contribution of other currents to the subthreshold resonance, for example, $I_m$ (Hu et al., 2009; Hutcheon & Yarom, 2000); however, our data indicates that in the MOB, the subthreshold resonance arises from $I_h$ and passive properties of GCs. Further studies should examine the possibilities of other contributing currents known to play a role in subthreshold resonance, such as $I_m$, or $I_{NaP}$, and corroborated with a computational model.

In several brain regions, $I_h$ underlies the expression of subthreshold resonance in principal neurons, as well as interneurons (Hu et al., 2009; Hutcheon & Yarom, 2000; Ulrich, 2002, 2014; Vera et al., 2014; Zemankovics, Káli, Paulsen, Freund, & Hájos, 2010). Our data indicates that inhibitory neurons in the MOB, the GC and PGCs, exhibit subthreshold resonance and that this property is dependent on the presence of $I_h$ in both subtypes, however in the AOB, $I_h$-mediated subthresold resonance may be present only in GCs. In fact, we found that subthreshold resonance in GCs strongly correlated with the presence of $I_h$. This was particularly evident when we compared $I_h$ expression and the presence of resonance during postnatal development. In two weeks old GCs $I_h$ was smaller and the resonance strength was low, while they were significantly larger at 6 weeks. Although we did not perform a developmental analysis in MOB PGCs, we hypothesize

they exhibit a similar developmental progression of $I_h$ size and the expression of subthreshold resonance. However, this was not the case for principal neurons, the MCs. In agreement with a previous report we observed a developmental decrease in $I_h$ (Yu et al., 2015), yet even when $I_h$ was present, MCs did not exhibit $I_h$-mediated subthreshold resonance. However, it has been suggested that MOB MCs exhibit gamma-frequency subthreshold resonance due to a persistent Na+ current (Brea, Kay, & Kopell, 2009), which was not addressed in our studies. Even in the AOB, $I_h$ has been described in MCs, but blocking it had no effect on the intrinsic oscillations MCs (Gorin et al., 2016). In agreement with these findings we found no $I_h$-mediated subthreshold resonance in AOB MCs.

In summary, we provide evidence that the two predominant subtypes of inhibitory neurons in the MOB, the GCs and PGCs, exhibit subthreshold resonance mediated by $I_h$, but the primary output neurons, the MCs, do not. Various studies indicate that top-down neuromodulatory projections and cortical feedback target principally PGCs and GCs. Therefore, it is possible that subthreshold resonance and underlying $I_h$ contribute to the integration of this top-down information. In addition, activation of cAMP dependent pathways by neuromodulators could lead to changes in $I_h$ kinetics, affecting the resonant frequency and oscillations at the network level. Future *in vivo* studies will address how these properties of inhibitory neurons may contribute to OB circuit dynamics and odor processing.

# Chapter 3: Adrenergic modulation of $I_h$ in adult-born GCs and its role in dendrodendritic inhibition in the MOB

## Introduction

The regulation of inhibitory circuits is crucial for sensory processing (Griffen & Maffei, 2014; Isaacson & Scanziani, 2011; P. Lledo et al., 2005). In the olfactory bulb (OB), the first stage of central olfactory processing, granule cells (GCs), a type of inhibitory neuron, comprise the largest population and their activity is finely tuned by several top-down inputs and intrinsic cellular mechanisms (R. Hu et al., 2016; Lepousez et al., 2013; P.-M. Lledo et al., 2006). A major functional role of GCs is the reciprocal and lateral inhibition of output neurons, the mitral and tufted cells (MCs, herein) via dendrodendritic synapses (Isaacson & Strowbridge, 1998; Jahr & Nicoll, 1980). Through these inhibitory mechanisms, GCs are thought to participate in network oscillations and decorrelation of principal neurons allowing for discrimination of similar odor patterns (Fukunaga et al., 2014; Gschwend et al., 2015; Lepousez & Lledo, 2013; Wanner & Friedrich, 2020). In agreement with their important role in the modulation of MC output, and odor processing, their activity is regulated by intrinsic mechanisms, feedback afferents from regions targeted by the MCs, and several neuromodulatory centers (Boyd et al., 2012; Fletcher & Chen, 2010; Schoppa & Urban, 2003; Schoppa & Westbrook, 1999; Stroh et al., 2012).

Notably, GCs are continuously born throughout life in a process known as adult neurogenesis (Altman, 1962; Altman & Das, 1965). Thus, the dendrodendritic synapses in the OB undergo constant remodeling (Lois & Alvarez-Buylla, 1994; Petreanu & Alvarez-Buylla, 2002). Although the molecular mechanisms underlying the functional integration of adult-born GCs (abGCs) in the OB remain unknown, this process appears to be highly regulated by both local and afferent influences. During their integration abGCs arborize and form functional synaptic contacts with the local circuit, and undergo an activity-dependent critical period that affects synaptic connectivity and cell survival (Carleton et al., 2003; P.-M. Lledo et al., 2006; Petreanu & Alvarez-Buylla, 2002). These changes are accompanied by time dependent expression ion channels which ensure a timely and organized integration in the OB circuit (Belluzzi et al., 2003; Carleton et al., 2003; P.-M. Lledo et al., 2006). Interestingly, studies have suggested that integrating and fully-mature abGCs have different circuit functions, with odor learning tasks preferentially recruiting the activity of younger abGCs, those in their critical period (Forest et al., 2020; Magavi et al., 2005). Furthermore, during their critical period, abGCs responses show a broader odor tuning compared to fully-integrated abGCs (Wallace et al., 2017).

A key regulator of both dendrodendritic inhibition and the functional integration of abGCs is noradrenergic modulation from the locus coeruleus (Fletcher & Chen, 2010; Jahr & Nicoll, 1982; Moreno et al., 2012; Veyrac et

al., 2009). Pharmacological blockade of adrenergic receptors in the OB has been shown to impair task-dependent cell survival (Moreno et al., 2012; Veyrac et al., 2009), suggesting noradrenaline (NA) may affect abGC physiology as early as their critical period, however, the mechanisms underlying this regulation have not been characterized. NA has been shown to regulate cell excitability and network dynamics through a cAMP-dependent hyperpolarization-activated current, $I_h$ (Berridge & Waterhouse, 2003; Luethi & McCormick, 1998; Sara, 2009), through the alteration of intracellular cAMP levels via $\alpha_2$- or β-adrenergic receptors (ARs). In previous work, we showed that GCs born postnatally express $I_h$, and that this current could influence intrinsic excitability of GCs (R. Hu et al., 2016). However, the presence of $I_h$ in abGCs and its regulation by NA in the MOB has not been studied.

Here, using whole-cell patch clamp electrophysiology, we show that in abGCs, basic physiological parameters affecting neuronal excitability exhibit a gradual change that extend beyond their critical period. Importantly, $I_h$ is present in abGCs and the size of this current increases throughout their functional integration. In addition, we show that activation of $\alpha_2$-ARs suppresses $I_h$ via cAMP-dependent mechanisms. This suppression of $I_h$ increases dendritic excitability, thereby enhancing lateral inhibition onto MCs through interactions with low threshold T-type calcium channels. Therefore, the $\alpha_2$-AR modulation of $I_h$ in abGCs may impart unique features towards dendrodendritic interactions with MCs in a state-dependent manner.

**Materials and methods**

*Animals*: All experiments were conducted following the guidelines of the IACUC of the University of Maryland. Experiments were performed on both adult male and female wild-type (C57/BL6) or Thy1-ChR2 (Jackson Laboratory: #007612) mice 2 to 6 months of age.

*AAV Injections:* To label adult born GCs, mice (P40 – P50) were injected with 200 nL of AAV5-Syn-GFP in the rostral migratory stream (Addgene). Anesthetized C57/BL6 mice (2% isoflurane) were head-fixed (model 900, Kopf Instruments) and a 33-gauge needle (5 uL syringe, Hamilton) was inserted through a 1 mm craniotomy window. The speed of virus injection (200 nl/min) was controlled using a syringe pump (Micro4 Microsyringe pump, World Precision Instruments).

*Electrophysiology slice preparation:* Experiments were performed in OB slices using methods previously described (Hu et al, 2016). Briefly, sagittal or horizontal OB slices were prepared in an oxygenated ice-cold artificial cerebrospinal fluid (ACSF) containing low Ca2+ (0.5 mM) and high Mg2+ (6 mM). Sections (250 μm) were then transferred to an incubation chamber containing normal ACSF (see below) and left to recuperate for at least 30 min at 35°C, before the recordings. In all experiments the extracellular solution is ACSF of the following composition (in mM): 125 NaCl, 26 NaHCO3, 1.25 NaH2PO4, 2.5 KCl, 2 CaCl2, 1 MgCl2, 1 myo-inositol, 0.4 ascorbic acid, 2 Na-pyruvate, and 15 glucose, continuously oxygenated (95% O2-5% CO2).

Electrophysiological recordings and analysis: Neurons were visualized using an Olympus BX51W1 microscope and recorded using a dual EPC10 amplifier interfaced with the PatchMaster software (HEKA, Harvard Bioscience). Whole-cell recordings (voltage and current clamp) were performed at RT (~22° C), using standard patch pipettes (2-8 MΩ resistance) with an internal solution of the following composition (in mM): 130 K-gluconate, 4 KCl, 10 HEPES-K, 10 Na phosphocreatine, 2 Na-ATP, 4 Mg-ATP, and 0.3 GTP adjusted to pH 7.3 with KOH (~290–305 mOsm). For MC voltage clamp recordings, the K-gluconate was substituted with Cs-gluconate. Alexa Fluor 594 (20 μM) was included in the internal recording solution for validation and reconstruction of labeled neurons. All electrophysiological recordings were analyzed in MATLAB (Mathworks). Although the whole-cell configuration precludes an accurate measurement of the resting membrane potential ($V_m$), we estimated $V_m$ right after rupturing the seal. Properties of $I_h$ were measured as previously described (Hu et al, 2016). Activation kinetics (τ) were determined by fitting a single exponential function to the current trace when stepping from -60 to -130 mV. Voltage dependency was calculated by fitting the tail-current values to a Boltzmann function of the following form: $I = I_{max}/\{1 + \exp[(V - V_{half})/k_s]\}$, where $I_{max}$ is the maximal current, $V$ is the prepulse potential, $V_{half}$ is the half-activation potential of the current, and $k_s$ is the slope factor. Statistical significance was determined by student's t-test, Kolmogorov–Smirnov test, or one-way ANOVA.

*Pharmacological agents:* The following drugs were included in the bathing solution and perfused at a speed of ~3 mL/min: 4-(N-ethyl-N-phenylamino)-1, 2-dimethyl-6-(methylamino) pyrimidinium chloride (ZD7288), 8-(4-chloro-phenylthio)-2-O-methyladenosine-3,5-cyclic monophosphate (8-CPT-cAMP), N-(2,6-dichlorophenyl)-4,5-dihydro-1H-imidazol-2-amine;hydrochloride (clonidine, Clon), (1S,2S)-2-[2-[[3-(1H-Benzimidazol-2yl)propyl]methylamino]ethyl]-6-fluoro-1,2,3,4-tetrahydro-1-(1-methylethyl)-2-naphthalenyl methoxyacetoacetate dihydrochloride (mibefradil, Mib), 6-cyano-7-nitroquinoxaline-2,3-dione disodium,6-Imino-3-(4-methoxyphenyl)-1(6H)-pyridazinebutanoic acid hydrobromide (gabazine, GBZ), tetrodotoxin (TTX). All drugs were purchased from Tocris (Bio-Techne), except for 8-CPT-cAMP (Abcam).

## Results

### Changes in intrinsic electrophysiology and $I_h$ in adult-born granule cells

To investigate the neurophysiological properties of abGCs during the time window of their functional integration in adult mice, we expressed GFP to label abGCs, using viral injections in the RMS (see methods). We recorded labelled abGCs at two time points: 2- and 6- weeks post-injection. Previous studies have shown that during this time, abGCs are functionally interacting with the pre-existing circuit, however at 2 weeks GCs are undergoing a critical period of synaptic remodeling, whereas cells at 6 weeks are considered to be fully integrated (Lepousez et al., 2013; P.-M. Lledo et al., 2006; Petreanu & Alvarez-Buylla, 2002). At 2 weeks post-injection, abGCs exhibit already mature morphological characteristics, including a primary apical dendrite, along with distal branches and prominent spines, with 53% corresponding to class V, 37% as class IV, and 10% as class III as previously described (Fig 1A; class V, 41/78; class IV, 29/78; class III, 8/78; n = 3 animals) (Carleton et al., 2003; Petreanu & Alvarez-Buylla, 2002). Interestingly, despite the degree of maturation exhibited by abGCs at 2 weeks, we observed significant changes in the general excitability as they matured. Specifically, the resting membrane potential and input resistance were significantly different between these two age groups (Fig 1B. 2 wk: n = 16, 6 wk, n = 18). At 2 wk, abGCs had a more depolarized resting membrane potential than at 6 wk (–67.9 ± 1.2 mV vs. –73.1 ± 1.1 mV, p = 0.003), and had a higher input resistance (1.64 ±

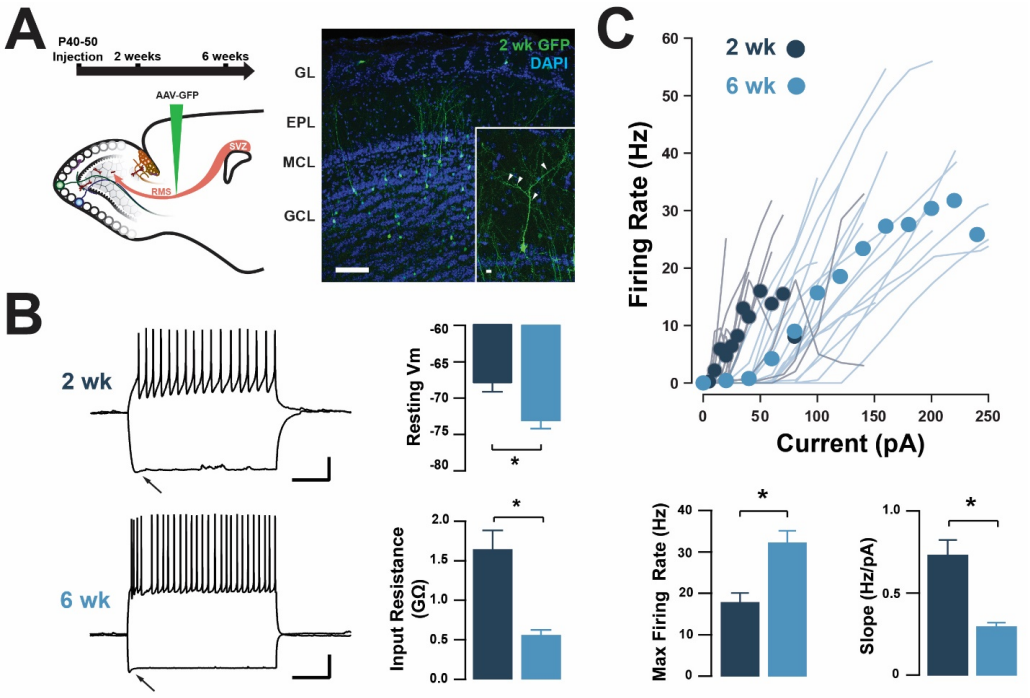


**Figure 1. Intrinsic physiological properties of adult-born GCs**
A. Left, Diagram of the strategy used for labeling adult-born GCs. Adult born neurons were transduced with an AAV-GFP virus injected in the RMS at postnatal days 40-50 (p40-50). GC were recorded at 2- and 6-weeks post injection. Right, confocal images of a horizontal section of the MOB showing abundant GFP-labeled adult-born neurons (green), 2-weeks post injection. The inset shows a mature GC with a primary apical dendritic branch and abundant dendritic spines (arrow heads). MOB cell layers, indicated on the left, were determined using DAPI (blue), showing the glomerular layer (GL), external plexiform layer (EPL), mitral cell layer (MCL), and granule cell layer (GCL). Calibration:100 µm and 10 µm. B. Left, representative current-clamp recordings from cells at 2- and 6-weeks post injection showing responses to depolarizing and hyperpolarizing current pulses (2 wk: -35 pA and 15 pA; 6 wk: -100 and 80 pA). At both ages, the cells displayed sustained firing with depolarization and a small sag in the voltage trace at negative potentials (arrows). The resting membrane potentials is –63 mV and –78 mV, respectively. Calibration: 20 mV, 500 ms. Right: bar graphs summarizing changes in GC excitability at the two stages of cell maturation recorded post-injection (2-week, dark blue, n = 16; 6-week, light blue, n = 18). From 2- to 6-weeks adult born GCs show a significant decrease in the resting membrane potential (Vm) (upper, p = 0.003), and a decrease in the input resistance (lower, p = 0.0001). C. Top, input-output curves for firing rates elicited by increasing currents (2 s, 0-250 pA). Bottom, bar graphs summarizing the responses, GCs at 6-weeks exhibited a higher maximal firing rate (left, p = 0.0005), and a shallower slope in the input output function (right, p = 0.00003).

0.24 GΩ vs. 0.56 ± 0.06 GΩ, p = 0.0001). In contrast, we did not find

differences in cell capacitance (2 wk, 35.7 ± 3.7 pF; 6 wk, 36.2 ± 2.8 pF, p = 0.91). However, in response to current stimuli, abGCs at 6 wk exhibited a significantly higher maximum frequency of firing (2 wk = 17.8 ± 2.3 Hz, 6 wk = 32.3 ± 2.8 Hz, p = 0.0005), with the fitting of input-output functions exhibiting a shallower slope (2 wk = 0.73 ± 0.09 Hz/pA, 6 wk = 0.29 ± 0.03 Hz/pA, p = 0.00003), suggesting a change in the gain function as abGCs became more mature. In addition to changes in excitability due to intrinsic membrane properties, there was a significant increase in the spontaneous excitatory postsynaptic currents (sEPSCs) as the cells matured (Fig 1 SI 1A. 2 wk: n = 12; 6 wk: n = 13). At –70 mV, the frequency of sEPSCs increased by two-fold with cell age (Fig 1 SI 1B. 2 wk = 2.8 ± 0.7 Hz, 6 wk = 6.8 ± 1.5 Hz, p = 0.03). In addition, the average amplitude of the sEPSCs increased with the maturation of the aGCs (Fig 1 SI 1B. 2 wk = 10.1 ± 0.5 pA, 6 wk = 13.9 ± 1.3 pA, p = 0.02). Lastly, the rise and decay times both decreased with cell-age (Fig 1 SI 1B. rise time: 2 wk = 1.7 ± 0.1 ms, 6 wk = 1.1 ± 0.08 ms, p = 0.0001; decay: 2 wk = 6.8 ± 0.3 ms, 6 wk = 5.1 ± 0.4 ms, p = 0.003). Together, these results indicate that despite the apparent decrease in abGC excitability as the cells functionally integrate, between 2 and 6 weeks of cell age, there is a dramatic increase in the number of excitatory inputs, which exhibit distinct kinetic properties.

Previously, we described the presence of $I_h$ in GCs born just after birth, and found that this current increased during their postnatal maturation (R. Hu

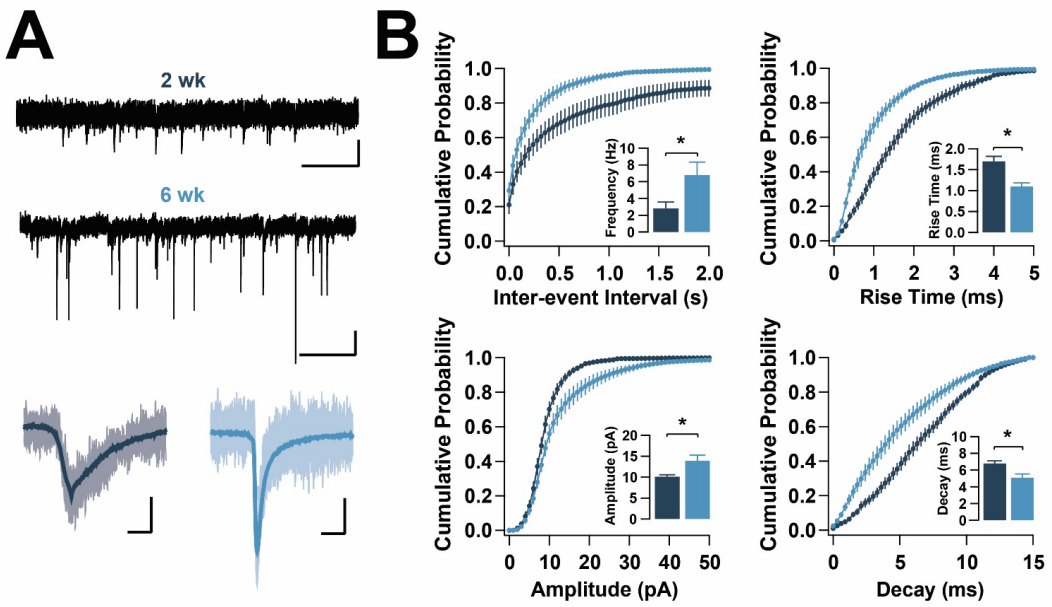


**Figure 1 Supplement 1. Changes in kinetic properties of excitatory synapses in adult-born GCs**
A. Top: Representative voltage clamp recordings at −70 mV showing spontaneous excitatory post-synaptic currents (sEPSCs) in GCs at 2-weeks (upper) and 6-weeks (lower) post injection (2 wk: n = 12; 6 wk: n = 13). GCs at 6 wk exhibit a higher frequency of events. Calibration: 10 pA, 500 ms. Bottom: Average sEPSC waveforms from GCs at 2- wk (dark blue) and 6-wk (light blue). At 2-wk, the sEPSC exhibit slower rise time and decay time and smaller amplitude. Calibration: 5 pA, 5 ms. B. Average cumulative probability distributions for show shifts in for shorter inter-event intervals (KS, $p = 1.6 * 10^{-156}$), larger amplitude (KS, $p = 1.7 * 10^{-106}$), faster rise and decay times for the sEPSCs (rise time, KS, $p = 1.6 * 10^{-249}$; decay time, KS, $p = 1.1 * 10^{-230}$). Insets for the averaged frequency (p = 0.03), amplitude (p = 0.02), rise time (p = 0.0001), and decay time (p= 0.003) of the sEPSCs were significantly different at these two ages.

et al., 2016). As shown in Fig 2A, stepping to negative potentials (–60 to –130 mV), revealed a characteristic inward current at both 2 and 6 weeks; however, at –130 mV the $I_h$ current was ~40% greater at 6 wk compared to 2-wk (2 wk = –72.9 ± 9.6 pA, n = 17; 6 wk = –101.4 ± 9.4, n = 18, p = 0.03). Because HCN subunit composition determines kinetic properties and voltage dependency of the currents (Shah, 2014; Zagotta et al., 2003), we examined

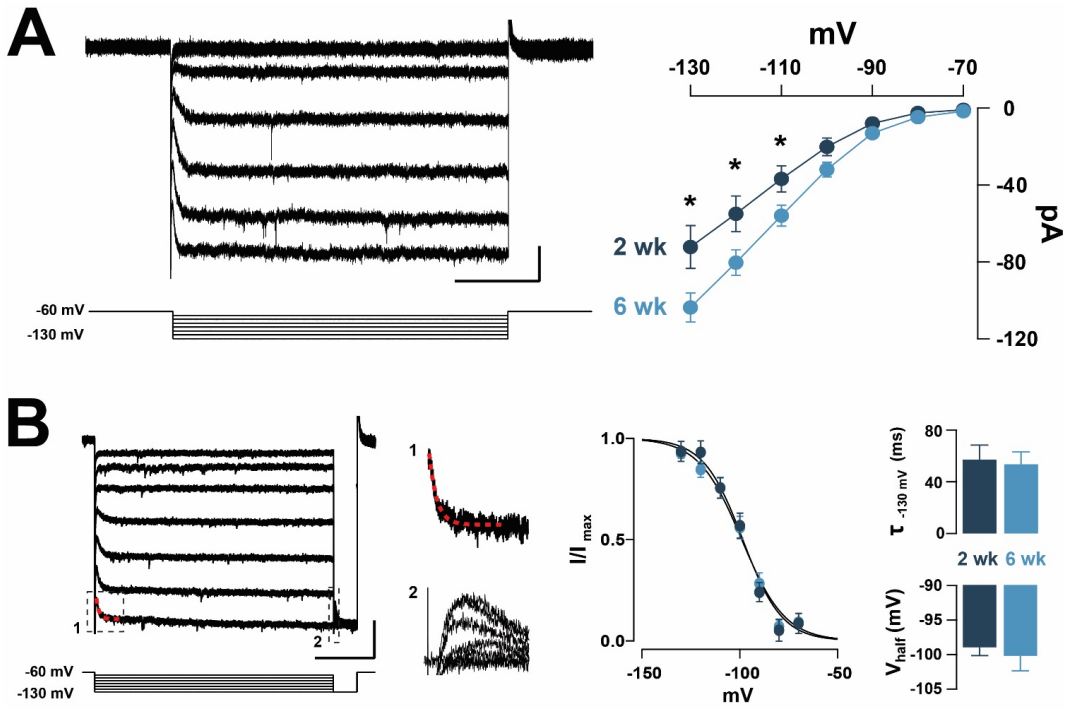


**Figure 2. Functional properties of $I_h$ in adult-born GCs**
A. Left: Representative voltage-clamp recording in a GC 2-weeks post injection. Hyperpolarizing voltage steps from −60 to −130 mV (10 mV steps) elicited a hyperpolarization-activated inward current (Ih). Calibration: 20 pA, 500 ms. Right: The current–voltage (I–V) relationship for $I_h$ in adult born GCs at 2- and 6-weeks. There are a significant increases in $I_h$ amplitude from –110 mV to –130 mV with cell age (2 wk, n = 17; 6 wk, n = 18; –110 mV, p = 0.04; –120 mV, p = 0.04; –130 mV, p = 0.03). B. Left: Hyperpolarizing steps from −60 to−130 mV with a test pulse to −130 mV to elicit a tail current. Calibration: 50 pA, 500 ms. The activation of the current (box 1) at −130 mV was fitted to a single exponential to determine the activation kinetics (τ = 43 ms). The tail current amplitude (box 2) was used to determine the voltage dependency of $I_h$. Right: The Boltzmann fits for $I_h$ at 2- and 6-weeks show no difference in the activation curve. The summary bar graphs show that the average activation rate (upper graph, $\tau_{130mV}$, p = 0.8) and the half activation potential (lower graph, $V_{half}$, p = 0.6) were not different at these ages.

the activation speed and the voltage-dependency at $I_h$ at both ages. The rate of activation of $I_h$ and the voltage-dependency were not different at these two time points (Fig 3B. τ: 2 wk = 57.3 ± 11.1 ms, 6 wk = 53.7 ± 9.6 ms, p = 0.8; $V_{half}$: 2 wk = –98.8 ± 1.2 mV, 6 wk = –100.2 ± 2.2 mV, p = 0.6). These results

indicate that abGCs, like postnatal born GCs, exhibit an age-dependent increase in $I_h$ (R. Hu et al., 2016).

**Adrenergic modulation of $I_h$ in adult-born GCs**

Previous studies have shown that NA can regulate $I_h$ thought the activation of $\alpha_2$-AR, which through a Gi-coupled pathway reduce cAMP, leading to a reduction in $I_h$ (Barth et al., 2008; Umemura et al., 1986). To examine the possibility that NA can directly regulate Ih in abGCs, we conducted experiments in the presence of blockers of synaptic transmission and TTX (10 μM CNQX, 50 μM APV, 10 μM GBZ, 0.5 μM TTX). Under these conditions, NA reduced the $I_h$ current by approximately 20% in both 2 and 6 wk old abGCs (Fig 3A. normalized current: 2 wk = 0.77 ± 0.06, n = 5, p = 0.07; 6 wk = 0.82 ± 0.03, n = 4, p = 0.02). Importantly, application of the selective $\alpha_2$-AR agonist, clonidine (Clon, 10 μM), similarly reduced the $I_h$ current at these two ages (Fig 3A. normalized current: 2 wk = 0.79 ± 0.06, n = 6, p = 0.03; 6 wk = 0.77 ± 0.04, n = 7, p = 0.001). To examine the possibility that the reduction in $I_h$ by $\alpha_2$-AR activation is due to changes in intracellular cAMP, we conducted additional pharmacological experiments in 6 wk-old abGCs. Application of the membrane-permeable cAMP analogue, 8-CTP-cAMP (8-CPT, 100 μM), increased $I_h$ by 15% (Fig 3A. normalized current: 1.15 ± 0.03, n = 5, p = 0.01), while pre-application of 8-CPT occluded the clonidine-mediated suppression of $I_h$ (Fig 3A. normalized current: 0.93 ± 0.09, n = 5, p = 0.45). In agreement with a regulation of the HCN by cAMP,

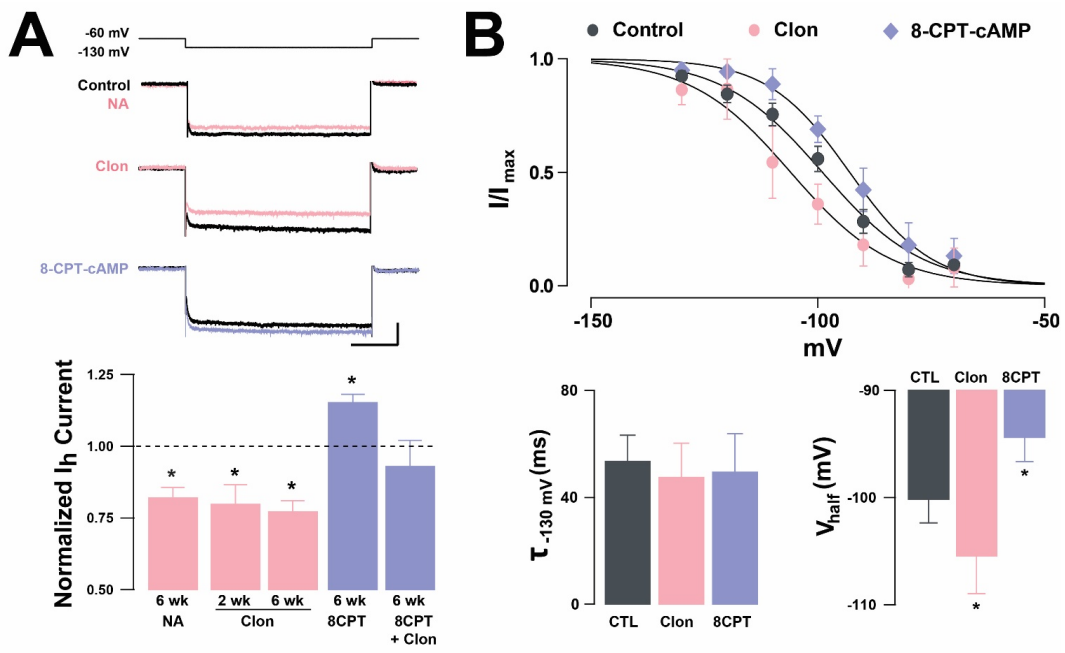


**Figure 3. Activation of α2-ARs by NA reduces $I_h$ in adult-born GCs**
A. Top, example traces of $I_h$ elicited with a hyperpolarizing step from −60 to −130 mV. NA (10 μM) reduced the $I_h$ in a 6-wk GC (control, black; NA, pink). A similar reduction is elicited by the selective α2-AR agonist, clonidine (Clon, 10 μM, pink). In contrast, application of a membrane-permeable cAMP analog, 8-CPT-cAMP (100 μM, purple) produced an increase in $I_h$. Calibration: 50 pA, 500 ms. Bottom, summary bar graphs showing the effects of the pharmacological treatments on the normalized $I_h$ amplitude (at −130 mV), with respect to control. NA and Clon reduced the $I_h$ amplitude in GCs at 2- and 6-weeks post injection (NA, 6 wk, n = 4, p = 0.02; Clon, 2 wk, n = 6, p = 0.03; 6 wk, n = 7, p = 0.001), while $I_h$ amplitude is increased by the addition of 8-CPT-cAMP (n = 5, p = 0.01). In the presence of 8-CPT-cAMP, the $I_h$ amplitude was not significantly different from control (n = 5, p = 0.45). B. Top: Boltzmann fits for the voltage-dependency of activation of $I_h$ in GCs 6-weeks post injection showing that activation of α2-ARs by Clon and application of 8-CPT-cAMP shifts the voltage-dependency of $I_h$ in opposite directions. Bottom: Summary bar graphs showing that application of Clon or 8-CPT-cAMP does not alter the activation kinetics of $I_h$ (Left, Clon, p = 0.16; 8CPT, p=0.54). Right, α2-AR activation by Clon shifts the half-activation potential ($V_{half}$) to more negative potentials (p = 0.04), whereas 8-CPT-cAMP shifts the $V_{half}$ to more positive potentials (p = 0.02).

clonidine shifted the voltage dependency of $I_h$ to more negative potentials (Fig 3B, $V_{half}$: Control = –98 ± 3.4 mV; Clon = –105.5 ± 3.4 mV, p = 0.04), while the addition of 8-CTP shifted the $V_{half}$ to more positive potentials (–94.4 ± 3.0 ms,

p = 0.02). In contrast, the activation speed of $I_h$ did not change with $\alpha_2$-AR activation or by the addition of 8-CPT (Fig 3B. τ: Control = 53.7 ± 9.5 ms; Clon = 47.7 ± 12.5 ms, p = 0.16; 8-CPT = 49.7 ± 14.2 ms, p = 0.54). However, pre-application of the cAMP analog occluded the change in voltage dependency elicited by clonidine (8CPT + Clon = –99.1 ± 4.2 mV, p = 0.58). Lastly, in agreement, with the decrease in $I_h$ elicited by $\alpha_2$-AR activation, clonidine also produced an apparent increase in input resistance at both time points, albeit the effect was only significant at 6 wk (fold-increase: 2 wk = 1.29 ± 0.1, p = 0.08; 6 wk = 1.37 ± 0.08, p = 0.01). Together, these results indicate that the regulation of intrinsic excitability in abGCs by $I_h$ can be modulated by NA, through the activation of $\alpha_2$-ARs, and that this regulation is present as early as the critical period of their functional integration.

**$\alpha_2$-AR modulation of dendritic excitability in abGCs and reciprocal dendrodendritic inhibition**

The most important function of GCs is the inhibition of output neurons, the MCs, which is mediated through dendrodendritic synapses in their apical dendrites, their primary output (Price & Powell, 1970). The previous section and our published work indicates that expression of $I_h$ is prevalent across developmentally and adult born GCs (R. Hu et al., 2016). Thus, we hypothesized that $I_h$ by modulating dendritic excitability in GCs can be a regulatory mechanism for dendrodendritic inhibition of MCs. To this extent we recorded from MOB MCs in symmetric chloride conditions and elicited

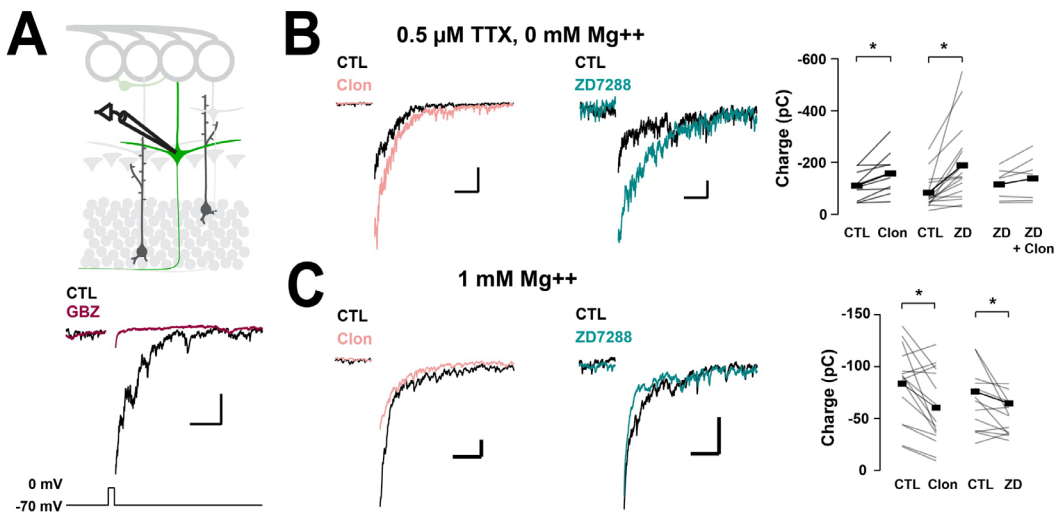


**Figure 4. α2-AR modulation of Ih on reciprocal inhibition and GC dendritic excitability**

A. Top, diagram of recording scheme for eliciting reciprocal dendritic inhibition in MCs. The sample traces below show dendrodendritic inhibition elicited by a depolarizing step from –70 to 0 mV, which is abolished by GABAA antagonist GBZ (10 µM, red). B. In TTX (0.5 µM) and $Mg^{++}$-free ACSF, representative averaged traces (left) and summary plots (right) show activation of α2-ARs by Clon (10 µM; pink, n = 10, p = 0.01) and blockade of Ih with ZD7288 (10 µM; teal, n = 16, p = 0.003) increased the recruited inhibition. With pre-application of ZD7288, Clon failed to increase the recruited inhibition (n = 7, p = 0.14). Calibration 100 pA, 500 ms. C. In physiological ACSF (no TTX, and 1 mM Mg++), α2-AR activation and Ih blockade failed to increase reciprocal inhibition onto MOB MCs, with a small reduction observed instead (Clon, n = 15, p = 0.006; ZD, n = 13, p = 0.03). Calibration: 50 pA, 200 ms.

dendrodendritic reciprocal inhibition by depolarizing steps (–70 to 0 mV). To isolate the dendritic output from GCs, we performed these experiments in the presence of TTX (0.5 µM) and in 0 $Mg^{++}$, to block somatically driven action potentials in GCs, and to enable GABA release solely by the activation of both AMPA and NMDA receptors. Under these conditions, a depolarizing step (50 ms) elicited a large inward current, with a slow decay (369 ± 43 ms, n = 26), which correspond to dendrodendritic reciprocal inhibition (Isaacson &

Strowbridge, 1998; Schoppa et al., 1998), and as previously shown, this current was abolished by the $GABA_A$ receptor antagonist, GABAzine (Fig 5A. GBZ, 10 μM, n = 4). Quantification of the transferred charge indicated that clonidine produced a significant increase in this inhibitory current (Fig 5B. Control = –110.7 ± 17.5 pC, Clon = –157.6 ± 25.6 pC, n = 10, p = 0.01), without a significant change in the rate of decay of the current (Control = 315 ± 57 ms, Clon = 479 ± 53, p = 0.08). Importantly, the selective $I_h$ blocker, ZD7288 (ZD, 10 μM) also increased dendrodendritic inhibition onto MCs (Fig 4B. Control = –83.1 ± 15.8 pC, ZD = –189.2 ± 37.7 pC, n = 16, p = 0.003). Furthermore, pre-application of ZD occluded the increase in dendrodendritic inhibition by $\alpha_2$-AR activation (Fig 4B. ZD, control = –115.3 ± 22.6 pC, ZD + clonidine = –138.4 ± 32.4 pC, n = 7, p = 0.14), suggesting that the $\alpha_2$-mediated increase in dendrodendritic inhibition occurs via a suppression of $I_h$. Surprisingly, however, when we used a physiological concentration of external $Mg^{++}$ (1 mM), $\alpha_2$-AR activation resulted in a decrease in DDI (Fig 4C. Control = –83.4 ± 9.4 pC, clonidine = –60.2 ± 9.4, n = 15, p = 0.006), similarly, application of the $I_h$ blocker also resulted in a small reduction in DDI (Fig 4C. Control = –66.4 ± 8.2 pC, ZD = –51.3 ± 5.0 pC, n = 13, p = 0.03). It is possible that under physiological blockade of NMDA receptors by $Mg^{++}$ suppression of $I_h$ by $\alpha_2$-AR activation would also hyperpolarize these compartments, as pharmacological blockade of $I_h$ hyperpolarizes GCs (R. Hu et al., 2016).

**$\alpha_2$-AR suppression of $I_h$ enhances lateral inhibition in the MOB**

In addition to directly modulating reciprocal inhibition, changes in GC dendritic excitability by $I_h$ could alter dendrodendritic interactions via lateral

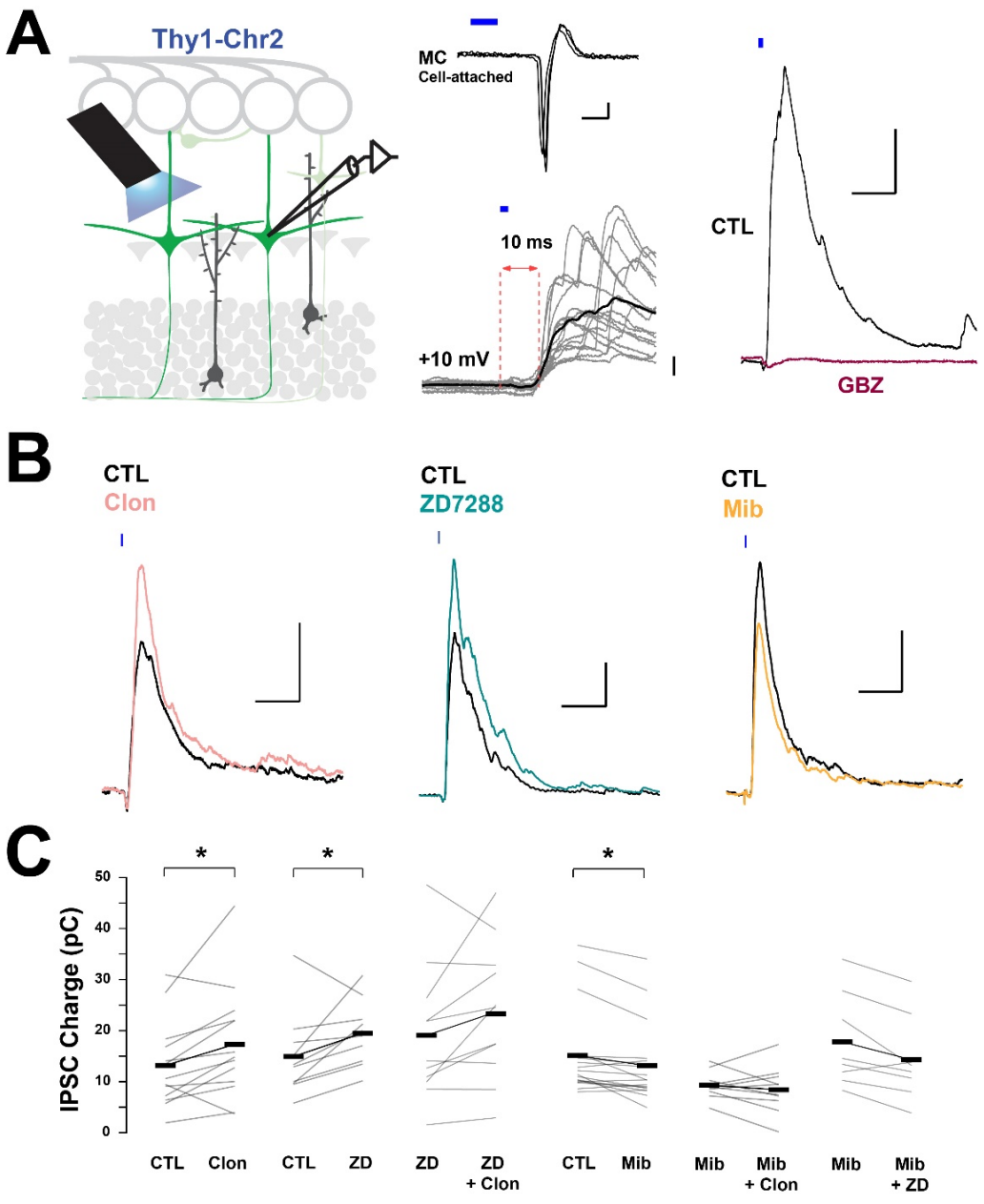

**Figure 5. Suppression of $I_h$ by α2-AR increases lateral inhibition onto MCs via interactions with low-threshold calcium channels**
A. Left: Diagram of the strategy used to elicit lateral inhibition in MCs in voltage-clamp. We recorded currents in MCs expressing ChR2 (Thy1-ChR2 mouse) stimulated by blue light (blue bars). Right: example of a cell-attached recording showing that light stimulation (2 ms) elicits reliable action potentials in the recorded MC. In the whole-cell configuration, at +10 mV, light stimulation evokes a di-synaptic inhibitory current (10 ms delay), which is completely abolished by the $GABA_A$ receptor antagonist GABAzine (GBZ, 10 μM, red). Calibration: cell-attached, 20 pA, 2 ms; whole-cell, 50 pA, 50 ms. B. Representative averaged traces (top) and summary plots (bottom) showing the effects of the pharmacological treatments on lateral inhibition. Both Clon and the $I_h$ blocker increased the light-evoked inhibitory current (Clon, n = 10, p = 0.04; ZD, n = 13, p = 0.02). In the presence of ZD, Clon failed to increase the light-evoked inhibitory currents (n = 11, p = 0.09). Furthermore, application of low-threshold T-type channel antagonist mibefradil (Mib,10 μM) attenuates lateral inhibition (n = 18, p = 0.003). Pre-application of Mib occludes the increases in elicited lateral inhibition by α2-AR activation and $I_h$ blockade (Mib+Clon, n = 10, p = 0.42; Mib+ZD, n = 8, p = 0.01). Calibration: 50 pA, 50 ms.

inhibition. To reliably and selectively elicit lateral inhibition from GCs, we used a Thy1-ChR2 mouse that expresses ChR2-YFP in MCs. In cell-attached configuration, we adjusted the light intensity so that a 2 ms light pulse reliably produced a single action potential in the MCs, with a short latency (under 5 ms, Fig 5A). We then recorded in the whole-cell configuration using a Cs-gluconate based internal solution to isolate di-synaptic lateral inhibition in the recorded MC. At –70 mV light activation elicited an immediate inward current (not shown), however, at +10 mV, light stimulation elicited a large outward current (249 ± 28 pA, n = 41), that occurred with a longer delay (9.5 ± 0.2 ms). In physiological Mg++, the outward current had a faster decay (90.8 ± 12.9 ms) and was completely abolished by the $GABA_A$ antagonist, GABAzine (GBZ, 10 μM; n = 3) consistent with the activation of dendrodendritic

synapses from neighboring MCs. We note that at this depolarized potential (+10 mV), voltage-gated sodium and calcium channels are likely in an inactive state and therefore the outward current elicited by light stimulation is unlikely to result from recurrent inhibition from the recorded MC. Therefore, this di-synaptic inhibition would be appropriately described as lateral inhibition.

Using this protocol, we found that clonidine produced an increase in the peak of the outward current (Fig 5B. peak current: control = 212.1 ± 57.2 pA, clonidine = 244.2 ± 61.5 pA, n = 10, p = 0.002), and the charge (Control = 14.9 ± 2.6 pC, Clon = 19.5 ± 1.9 pC, p= 0.04), without affecting the rate of decay of the outward current (Control = 141± 47 ms, vs Clon = 99 ± 24 ms, p = 0.44). Similarly, blockade of $I_h$ by ZD increased both the peak current and the transferred charge (Fig 5B. Control = 245.2 ± 39.7 pA, ZD = 304.6 ± 53.3 pA; p = 0.002; Control = 13.2 ± 2.3 pC, ZD = 17.3 ± 3.1 pC, p = 0.02; n = 13. As with the recurrent inhibition in 0 external Mg, pre-application of ZD occluded the increase in lateral inhibition by $\alpha_2$-AR activation Fig 5B. ZD = 313.7 ± 64.7 pA, ZD + Clon = 297.7 ± 64.4 pA, p = 0.30; ZD = 19.2 ± 4.0 pC, ZD + Clon = 23.7 ± 4.0 pC, p = 0.09, n = 11). These results suggest that suppression of $I_h$ by $\alpha_2$-AR activation can increase lateral inhibition and agree with our previously observed increase in GC dendritic output from the TTX and $Mg^{++}$-free condition.

The increase in lateral inhibition in MCs by $\alpha_2$-AR activation likely results from an increase in inhibition from GC to MC rather than an increase

in excitatory transmission from the MC to GC as clonidine did not affect the evoked EPSC on GCs, recorded at –70 mV (Fig 5 SI. peak current: Control = –33.1 ± 7.7 pA, Clon = –25.7 ± 6.1 pA, p = 0.39; control = –1.12 ± 0.20 pC, Clon = –0.91 ± 0.28 pC; p = 0.39, n = 5); a similar result was obtained with ZD (peak current: Control = –50.6 ± 14.6 pA, ZD = –56.9 ± 20.2 pA, p = 0.59;

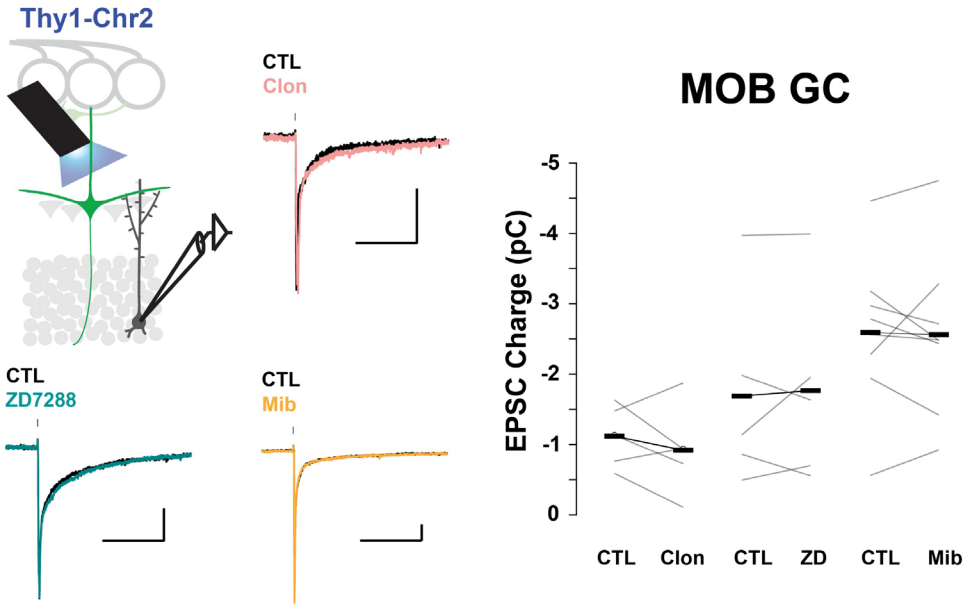


**Figure 5 Supplement 1.**
**The excitatory input from MC to GCs is not affected by $\alpha_2$-AR activation, $I_h$ blockade, or T-type $Ca^{++}$ channel blockade**
Top left: Diagram of the recording scheme used for these experiments. We recorded from GCs while optogenetically activating MCs expressing ChR2. Sample traces of light-elicited EPSCs onto MOB GCs control and in the presence Clon (pink), ZD (teal), and Mib (yellow) The EPSC waveform elicited by light stimulation shows no difference in in the presence of these pharmacological agents. Right, summary plot of EPSC charge transfer showing no significant change under these experimental conditions (Clon, n = 5, p = 0.39; ZD, n = 5, p = 0.73; Mib, n = 8, p = 0.88). Calibration: 10 pA, 200 ms.

control = –1.69 ± 0.62 pC, ZD = –1.76 ± 0.62 pC , p =0.73 n = 5). In

summary, these results suggest that modulation of $I_h$ by $\alpha_2$-AR modulation results from an increase in GABAergic transmission from the GCs to the MCs.

The $\alpha_2$-AR mediated increase in lateral inhibition may rely indirectly on the modulation of other active conductances on GC dendrites. Prior studies have indicated dendritic low-threshold T-type calcium channels in GCs play a major role in lateral inhibition (Egger et al., 2003, 2005). We have previously shown that blockade of $I_h$ hyperpolarizes GCs of the MOB and increase their input resistance (R. Hu et al., 2016). Therefore, it is possible that at a more hyperpolarized Vm, due to a reduction on $I_h$ by $\alpha_2$-AR activation, low-threshold T-type calcium channels on the dendritic arbors could enter a more readily activatable state, and produce larger calcium transients across dendritic arbors to facilitate lateral inhibition in GCs. To test this possibility, we measured lateral inhibition in the presence of a T-type calcium antagonist mibifredil (Mib, 10 μM). As expected, lateral inhibition in MCs was attenuated in the presence of Mib (Fig 5C. peak current: Control = 272.2 ± 47.8 pA, Mib = 232.12 ± 41.8 pA, p = 0.002; charge: Control = 14.9 ± 2.0 pC, Mib = 12.9 ± 1.8 pC; p = 0.003; n = 18 Furthermore, there was no change in the charge carried by the EPSC in the GCs in the presence of Mib application (Fig 5 SI. peak current: Control = –125.6 ± 50.3 pA, + Mib = –137.6 ± 53.6 pA, p = 0.45; control = –2.60 ± 0.39 pC, Mib = –4.11 ± 0.41 pC; p = 0.88, n = 8), suggesting that the reduction in lateral inhibition produced by Mib does not result from a decrease in the excitation at MC-GC synapses. Importantly, pre-

application of Mib occluded the increase in lateral inhibition produced by $\alpha_2$-AR activation (Fig 5C. peak current: Mib= 167.4 ± 157.4 pA, Mib + Clon = 157.4 ± 27.9 pA, p = 0.57; Mib = 9.2 ± 0.8 pC, Mib + Clon = 8.3 ± 1.5 pC; p = 0.42 n = 10). Furthermore, application of ZD together with Mib further suppressed the elicited lateral inhibition (Fig 5C. peak current: Mib = 312.9 ± 81.2 pA, Mib + ZD= 253.4 ± 71.3 pA, p = 0.02; Mib= 17.6 ± 3.3 pC, Mib + ZD= 14.1 ± 2.9 pC; p = 0.01; n = 8). These results suggest that activation of low-threshold T-type calcium channels are necessary for the $\alpha_2$-mediated enhancement in lateral inhibition.

## Discussion

The control of dendritic excitability on GCs is crucial for regulating dendrodendritic interactions with MCs in the MOB, with both reciprocal and lateral inhibition affecting the spatiotemporal de-correlation of MC spiking activity (Gschwend et al., 2015; Wanner & Friedrich, 2020; Wiechert et al., 2010). These inhibitory mechanisms are regulated by state-dependent noradrenergic modulation from the LC, but the mechanisms of this regulation are poorly understood (Jahr & Nicoll, 1982; Nai et al., 2009; Shipley et al., 1985; Trombley & Shepherd, 1992; Zimnik et al., 2013). Furthermore, inhibitory microcircuits within the MOB undergo an exceptional remodeling throughout life due to the neurogenesis of abGCs. While the functional role of these neurons is still debated, it is clear that the integration of abGCs is a highly regulated process (Gheusi & Lledo, 2014; Lepousez et al., 2013; P.-M. Lledo & Saghatelyan, 2005). Here, we showed that abGCs show dramatic changes in their intrinsic physiology, which extend beyond their critical period. In particular, $I_h$ is present at both 2- and 6-weeks post-labeling, and its size becomes larger with cell age. Nevertheless, regardless of cell age, $I_h$ was suppressed by noradrenaline via activation of $\alpha_2$-ARs, suggesting this adrenergic effect to be ubiquitous across abGCs. Finally, we showed that $\alpha_2$-modulation of $I_h$ increases GC dendritic excitability, as well as lateral inhibition onto MOB MCs using stimulus paradigms that dissociate reciprocal and

lateral inhibition. These results suggest that the regulation of $I_h$ by $\alpha_2$-ARs in abGCs can play distinctive roles in circuit inhibition in the MOB.

While prior studies have examined the progression of electrophysiological properties of abGCs in the MOB as they matured, the primary focus was on earlier developmental time points leading up to 2 to 3 weeks of cell age (Belluzzi et al., 2003; Carleton et al., 2003). Our data illustrate that abGCs undergo further electrophysiological changes past this critical period. Interestingly, the changes in intrinsic excitability, in particular the expression of $I_h$, mirrored those of postnatally born neurons, suggesting that regarding the expression of $I_h$, adult neurogenesis recapitulates developmental or postnatal neurogenesis.

Previous studies have shown that odor tuning and response profiles in abGCs change as a function of maturation (Magavi et al., 2005; Wallace et al., 2017); fully mature abGCs show more sparseness in odorant responses compared to abGC during their critical period. These maturation-dependent changes in the function of abGCs could arise from a combination of intrinsic and extrinsic mechanisms. Interestingly, despite the activity-dependent remodeling and refinement of synaptic connections, which are a hallmark of functional integration of abGCs, the differences in spine remodeling dynamics (Breton-Provencher et al., 2016; Sailor et al., 2016), and the density of spines and branches between critical period and fully integrated abGCs is negligible (Kelsch et al., 2008, 2009; Livneh & Mizrahi, 2011). Thus, most of the

changes observed in the function of abGCs may rely in intrinsic mechanisms. Here, our results show changes in basic electrophysiological parameters associated with general decreases in intrinsic excitability that can serve as mechanisms for the changing of odor responses profiles with maturation. Furthermore, because $I_h$ has been shown to attenuate and filter dendritic inputs (Magee, 1998, 1999), an increase in $I_h$, specifically at the level of the dendritic arbors, could also serve as a mechanism to attenuate the dendritic calcium responses observed in abGCs *in vivo*.

Because HCN channel voltage dependency and activation kinetics are modulated by intracellular levels of cAMP, $I_h$ has been implicated in critical regulation of state-dependent network activity by neuromodulators, including noradrenaline (C. He et al., 2014; Luethi & McCormick, 1998; McCormick et al., 1991; Surges et al., 2006). Our studies indicate the presence of $\alpha_2$-ARs in abGCs and that their activation produced modulation of $I_h$, as early as 2 weeks post-labeling. Furthermore, abGCs at both functional stages of integration exhibit an $\alpha_2$-mediated reduction of Ih, by shifting the voltage dependency to lower membrane potentials. We have previously shown that adding cAMP to the intracellular recording solution shifts the $V_{half}$ of $I_h$ to more positive potentials (R. Hu et al., 2016). Here, a similar effect is observed with bath application of a membrane-permeable cAMP analog (8-CPT-cAMP), and its pre-application occludes the $\alpha_2$-mediated suppression of elicited $I_h$ current relative to control conditions, as well as its voltage-dependency in abGCs.

Dendrodendritic inhibition of MCs is action-potential independent and can be subdivided into two distinct mechanisms: reciprocal and lateral inhibition (Isaacson & Strowbridge, 1998; Jahr & Nicoll, 1980; Schoppa et al., 1998). Reciprocal inhibition functions as a form of gain control and self-regulates the temporal spiking patterns of MCs (Halabisky & Strowbridge, 2003; Phillips et al., 2012), while lateral inhibition serves to spatially modulate and decorrelate MC population activity (McTavis et al., 2012; Schoppa, 2006). Our novel experimental paradigm allowed us to examine the neuromodulation by NA of reciprocal and lateral inhibition in isolation. Previous studies of dendrodendritic inhibition have often used MC depolarization to elicit reciprocal inhibition (Isaacson, 2001; Isaacson & Strowbridge, 1998), or glomerular stimulation (Pressler et al., 2007; Schoppa, 2006; Schoppa et al., 1998), which fails to distinguish the contribution of reciprocal and lateral inhibition.

Surprisingly, the neuromodulatory effect of NA in reciprocal inhibition was $Mg^{++}$-sensitive. In the absence of $Mg^{++}$ $\alpha_2$-AR activation and blockade of $I_h$ increased the GABAergic output from GCs. However, in normal $Mg^{++}$, we observed the opposite effect. We hypothesize that the $\alpha_2$-AR suppression of $I_h$ would not only increase spine or dendrite resistance, but could also hyperpolarize these compartments (R. Hu et al., 2016). In agreement, a similar effect has been observed in pre-synaptic compartments such as the calyx of Held (Huang & Trussell, 2014). At the level of the GC dendritic arbors

or a dendritic spine, the increased resistance from the suppression of $I_h$ allows for larger changes in voltage with glutamate receptor activation. This is in agreement with prior studies showing an increase in dendritic excitability with $\alpha_2$-AR suppression of $I_h$ in pyramidal neurons (Barth et al., 2007, 2008; Labarrera et al., 2018; M. Wang et al., 2007). However, in GCs, the concurrent hyperpolarization induced by suppression of $I_h$ would also shift the membrane potential farther from the voltage threshold for NMDA receptors to release its $Mg^{++}$ block, as the $\alpha_2$-mediated increase in reciprocal inhibition was observed only in the absence of $Mg^{++}$.

We hypothesize that an increase in resistance and a hyperpolarization of dendritic compartments may boost lateral inhibition by enhancing the activity of low voltage-activated T-type calcium channels. In support of this possibility, hyperpolarization of GCs followed by their excitation by glomerular stimulation elicits greater calcium responses in GC dendrites and spines, and that this increase is occluded with T-type calcium channel blockade (Egger et al., 2003, 2005). Hyperpolarization favors the activation of dendritic low-threshold T-type calcium as their activation and inactivation occurs at more negative voltages (Jones, 1998). Accordingly, the T-type calcium channel antagonist mibefradil attenuated lateral inhibition and occluded the increase in lateral inhibition produced by $\alpha_2$-AR activation and $I_h$ blockade. In addition, the changes in cable properties of the dendritic compartment by the increase in resistance would enhance the propagation of calcium transients across the

dendrites. While previous research has shown interactions with $I_h$ and T-type calcium currents in regulating spike-timing and oscillatory dynamics (Aizenman & Linden, 1999; Engbers et al., 2011; Luethi & McCormick, 1998; Marder & Goaillard, 2006), our results suggest a novel mechanism by which NA could regulate olfactory processing though the modulation of these two conductances.

Taken together, our results show that NA can differentially modulate two inhibitory functions of GCs via the interaction of $I_h$ and other conductances. At a circuit level, the enhancement of lateral, but not reciprocal inhibition, by $\alpha_2$-ARs may coordinate MC output to enhance separation of MC activity to allow for the narrowing of odor tuning curves in MCs (Yokoi et al., 1995). Due to the observed physiological differences between young and old abGCs, future studies will address the neuromodulation of dendritic computation in an age-dependent manner.

# Chapter 4: Differential modulation by noradrenaline of the AOB and MOB circuits

## Introduction

State dependent regulation of olfactory signaling is an integral component of social behaviors. In most mammals, olfactory signaling occurs through two parallel streams of information. Chemosensory neurons in the main olfactory system bind volatile odor cues, and this information is transmitted to the main olfactory bulb (MOB), and subsequently sent to higher olfactory areas, including the olfactory cortex. In parallel, pheromonal cues are detected by sensory neurons in the Vomeronasal organ that project to the accessory olfactory bulb (AOB), from which semiochemical information reaches the medial and cortical amygdala, among others. Chemosensory information conveyed by these two parallel streams is dynamically modulated by context and internal state, before being integrated to produce social recognition and other complex behavioral responses such as mating and aggression.

Noradrenaline (NA) released by neurons in the locus coeruleus (LC) of the brainstem, plays an important role in olfactory processing (McLean & Shipley, 1991; Mclean, Shipley, Nickell, Aston-Jones, & Reyher, 1989; Shipley, Halloran, & de la Torre, 1985). Noradrenergic axons target both local inhibitory and output neurons in the MOB and AOB (Fallon & Moore, 1978; Mclean et al., 1989), and the regulation of these neurons by NA has been

proposed to facilitate odor discrimination and odor learning in the MOB (Doucette et al., 2007; Shea et al., 2008; Sullivan et al., 1989, 1992; Vinera et al., 2015), and the modulation of social behaviors, such as kin recognition, mating, and aggression in both the AOB and MOB (Brennan et al., 1995; Gervais et al., 1988; Griffiths & Brennan, 2015; R. J. Nelson & Trainor, 2007; Rosser & Keverne, 1985).

In the AOB, NA increases GABAergic inhibition onto principal neurons, the mitral/tufted cells (MCs herein) (Araneda & Firestein, 2006; Smith et al., 2009); while in the MOB, both excitatory and inhibitory effects on MCs have been described (Ciombor et al., 1999; Shea et al., 2008; Zimnik et al., 2013). However, how these excitatory and inhibitory effects at the circuit level shape AOB and MOB output remain unclear. Here, we used whole-cell recordings to show that NA produces a differential regulation of the output neurons of the MOB and AOB. In MCs of the MOB, NA has a direct excitatory action through two different mechanisms, activation of $\alpha_1$- and β- adrenergic receptors. In contrast, in the AOB, NA inhibits MCs via a disynaptic mechanism that is dependent on the activation of distinct local inhibitory interneurons. At the circuit level, opposing effects on excitation-inhibition balance in MCs may result in differential network responses: NA elicited high frequency subthreshold membrane potential fluctuations in MOB MCs but not in AOB. These differences could be partially explained by a difference inhibitory input recruited by NA in these regions. The difference in the regulation of MC

output by NA could support the distinct mechanisms by which AOB and MOB receive and relay information.

**Materials and methods**

*Animals*: All experiments were conducted following the IACUC guidelines at the University of Maryland in College Park. Experiments were performed on male and female wild-type (C57/BL6) or GAD2-cre mice at 3 weeks of age or older.

*AAV Injections:* Anesthetized GAD2-cre mice (1.5% isoflurane) were head-fixed (model 900, Kopf Instruments) and a 33-gauge needle (5 uL syringe, Hamilton) was inserted through a 1 mm craniotomy window. The speed of virus injection (100 nl/min) was achieved by using a syringe pump (Micro4 Microsyringe pump, World Precision Instruments). Mice were injected with 250 nL of AAV8-CAG-FLEX-GFP in the OB and were recorded from at least 10 days post-injection.

*Slice preparation:* Experiments were performed in OB slices using methods previously described (Zimnik et al., 2013). Briefly, slices were prepared in an oxygenated ice-cold artificial cerebrospinal fluid (ACSF) containing low $Ca^{2+}$ (0.5 mM) and high $Mg^{2+}$ (6 mM). Sagittal and horizontal sections of the OB (250 μm) were then transferred to an incubation chamber containing normal ACSF (see below) and left to recuperate for at least 30 minutes at 37°C, before the recordings. In all experiments, unless otherwise stated, the extracellular solution is ACSF of the following composition (in mM): 125 NaCl, 26 NaHCO3, 1.25 NaH2PO4, 2.5 KCl, 2 CaCl2, 1 MgCl2, 1 myo-inositol, 0.4

ascorbic acid, 2 Na-pyruvate, and 15 glucose, continuously oxygenated (95% O2-5% CO2) to give a pH 7.4 and an osmolarity of ~305 mOsm.

*Electrophysiological recordings:* Neurons were visualized using an Olympus BX51W1 microscope and recorded in voltage and current clamp modes using a dual EPC10 amplifier controlled by the PatchMaster software (HEKA, Holliston, MA). Experiments were performed at room temperature (~22° C) and cells were recorded using standard patch pipettes (2-6 MΩ resistance). The internal solution had the following composition (in mM): 130 K-gluconate, 4 KCl, 10 HEPES-K, 10 Na phosphocreatine, 2 Na-ATP, 4 Mg-ATP, and 0.3 GTP adjusted to pH 7.3 with KOH. In a subset of experiments, CsCl was used instead of K-gluconate. The osmolarity of the internal solutions was adjusted to 290–305 mOsm.

*Data analysis:* Data was analyzed using custom programs written in MATLAB (Mathworks). Changes in membrane potential (∆Vm) in the presence of drugs were measured as the difference between the baseline, calculated as the mode Vm over 1 min and the maximal effect. Under the conditions of perfusion used here the max effect occurred within 2 to 3 min of the agonist application. The power of subthreshold oscillations present in Vm was determined using the MATLAB fast Fourier transform function (‘fft’), comparing 1 min intervals of Vm recordings obtained from the baseline and during the drug application, and then normalized to the baseline values. For this analysis, action potentials were removed. Spectrograms from

subthreshold Vm oscillations were generated using the Chronux toolbox (http://www.chronux.org) using a multitaper spectral estimation (Bokil et al., 2010).

For detection of post-synaptic currents, traces were baseline subtracted, low-pass filtered ($2^{nd}$-order Butterworth, 500 Hz) and passed through a peak-finding function ('findpeaks'). Once synaptic events were detected, original waveforms were used to calculate the current amplitude and kinetic parameters of the currents. The rise time of the events was calculated as 10-90% of the peak amplitude, and the decay time was determined from the weighted average of a double exponential fit. The peak-scaled nonstationary fluctuation analysis for estimating single channel conductances of $GABA_A$ receptors underlying the miniature postsynaptic inhibitory currents (mIPSCs) was carried out as described in De Koninck and Mody (1994), in which the individual mIPSCs waveforms were scaled to the averaged mIPSC and binned. The variance was then calculated for each bin, averaged across mIPSCs, and then plotted against the mean current. The mean-variance plot was fitted with the following equation: $\sigma^2(I) = -i * I + 1/N * I^2 + b$, where $\sigma^2$ is the variance, I is the mean current, $i$ is the single channel current, N is the number of channels, and b is the background variance (De Koninck & Mody, 1994). The single channel conductance, γ, is calculated as $\gamma = i/V_D$, where $V_D$ is the driving force, which corresponded to 71 mV in our experimental conditions.

To simulate sensory inputs onto MCs, we simulated synaptic currents (20 Hz, $\tau$ = 10 ms) that were overlaid on a 4 Hz respiration-like Gaussian process, with varied intensity over a 2 s current stimulus, thus each trial consisted of 8 simulated synaptic inputs. We conducted 40 trails for each control and in NA. During the NA application, changes in Vm elicited by NA were prevented by resetting Vm to the baseline value (control) by direct current injection. Spike jitter was calculated as the standard deviation of the times when spikes occurred across a given simulated respiration event; an increase in spike precision corresponds to a decrease in spike jitter (Gutkin & Ermentrout, 2003; Mainen & Sejnowski, 1995). Statistical significance was determined by generalized linear models, student's t-test, or one-way ANOVA.

*Pharmacological agents:* The following drugs, made for stock solutions, were applied in the external bath solution at a perfusion speed of 2-3 mL/min: L-(–)-norepinphrine (+)-bitartrate salt monohydrate (NA), (R)-(–)-1-(3-hydroxy-phenyl)-2-methylaminoethanol hydrochloride (phenylephrine, PE), N-[5-(4,5-dihydro-1H-imidazol-2-yl)-2- hydroxy-5, 6, 7, 8-tetrahydronaphthalen-1-yl] methanesul phonamide hydrobromide (A 61603), 4-[1-hydroxy-2-[(1-methylethyl) amino]ethyl]-1,2-benzenediol hydrochloride (isoproterenol, ISO), 4-[2-[[3-(4-Hydroxyphenyl)-1-methylpropyl]aminoethyl-1,2-benzenediol hydrochloride (dobutamine, DOB), (RS)-1-[(1-Methylethyl)amino]-3-(1-naphthalenyloxy)-2-propanol hydrochloride (propranolol, Prop), 1-(4-Amino-

6,7-dimethoxy-2-quinazolinyl)-4-(2-furanylcarbonyl)piperazine hydrochloride (prazosin, Praz), 17α-Hydroxyyohimban-16α-carboxylic acid methyl ester hydrochloride (yohimbine, Yoh), 6-cyano-7-nitroquinoxaline-2,3-dione disodium,6-Imino-3-(4-methoxyphenyl)-1(6H)-pyridazinebu tanoic acid hydrobromide (gabazine, GBZ), 6-Cyano-7-nitroquinoxaline-2,3-dione disodium (CNQX), D-2-amino-5-phos- phonopentanoic acid (APV), octahydro- 12-(hydroxymethyl)-2-imino-5,9:7,10a-dimethano-10aH - [1,3]dioxocino[6,5-d]pyrimidine-4,7,10,11,12-pentol citrate (tetrodotoxin, TTX). Drugs were purchased from Tocris Cookson (UK).

## Results

### NA produces divergent responses in MOB and AOB MCs

Excitation of GCs, mediated by $\alpha_{1A}$-adrenergic receptors, produces a robust increase in inhibitory currents in MCs of both MOB and AOB (Araneda & Firestein, 2006; Smith et al., 2009; Zimnik et al., 2013), suggesting that NA produces a similar shift in the excitation-inhibition balance in the output neurons in these two regions. Surprisingly, despite the increase in inhibitory activity in MCs, application of NA (10 μM) produced a small but consistent depolarization of MCs in the MOB (Fig. 1A; ΔV: 3.3 ± 1.0 mV, n = 20, p = 0.007). In contrast, and in agreement with its excitatory effect in GCs, MCs in the AOB were inhibited by NA (Fig. 1A; ΔV: –3.4 ± 0.5 mV, n = 15, p = 0.0009). The depolarization of MCs persisted through pharmacological isolation with blockers of fast excitatory and inhibitory synaptic transmission (APV 100 μM, CNQX 10 μM and GBZ 10 μM), indicating that NA has a direct excitatory effect on MCs of the MOB. In contrast, the inhibition of MCs in the AOB was completely abolished by the same blockers treatment (Fig. 1B, MOB, ΔV: 3.0 ± 0.5 mV, n = 7, p = 0.001; AOB, ΔV: -0.4 ± .4 mV, n = 10, p = 0.33). These results indicate that NA produces an overall opposite action in the excitability of the output neurons of the bulb: an intrinsic excitation of MCs in the MOB and an extrinsic inhibition of MCs in the AOB.

Further pharmacological characterization of the excitatory response in MOB MCs indicated that the NA effect is mediated by activation of two

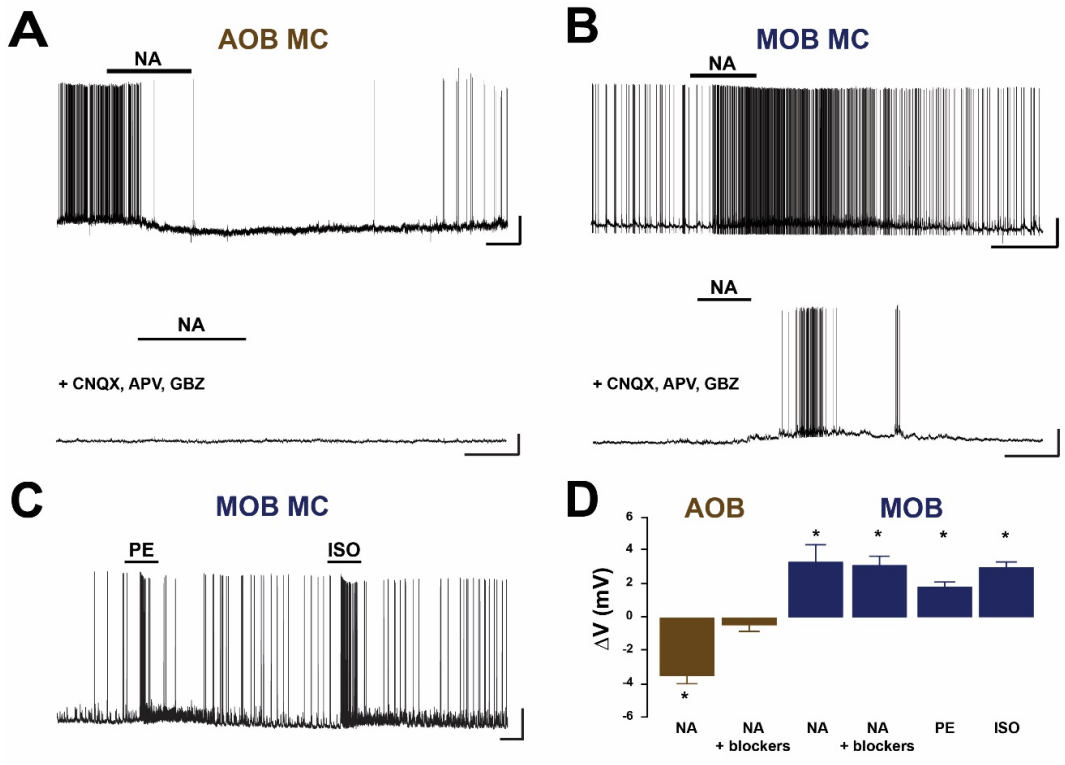


**Figure 1. Noradrenaline elicits opposing effects in MC excitability in the MOB and AOB**

A. MCs in the MOB or AOB were recorded in current-clamp. Top, noradrenaline (NA, 10 μM) hyperpolarizes MCs in the AOB, however, the hyperpolarization is abolished in the presence of pharmacological isolation with blockers of fast synaptic transmission (bottom; CNQX 10 μM; APV, 50 μM; GBZ 10 μM). The resting membrane potential is –50 mV and –61 mV, respectively. B. In contrast, NA excites MCs of the MOB (top) and the depolarization persisted after pharmacological isolation (bottom). The resting membrane potential is –51 and –58 mV, respectively. C. The depolarization of MCs is mimicked by both the $\alpha_1$ and β AR agonists, phenylephrine (PE) and isoproterenol (ISO; 10 μM each). The resting membrane potential is –62 mV. The calibration for all the traces is 20 mV and 2 min. D. Summary bar graph showing changes in membrane potential in response to NA and selective agonists in the AOB (NA, n = 13, p = 0.0009; NA + blockers, n = 10, p = 0.33), and the MOB (MOB: NA, n = 20, p = 0.007; NA + blockers, n = 7, p = 0.001; PE, n = 14, p = 0.002; ISO, n = 22, p = 0.00005).

different adrenergic receptors (ARs). As shown in Fig 1C, MCs were depolarized by both phenylephrine (PE) and isoproterenol (ISO; 10 μM each), agonists at $\alpha_1$ and β ARs, respectively (PE: ΔV: 1.8 ± 0.3 mV, n = 14, p =

0.00005; ISO: ΔV: 2.9 ± 0.3 mV, n = 22, p = 0.003). In a subset of 9 cells tested, both ISO and PE produced a depolarization, when they were applied consecutively. Furthermore, the depolarization elicited by NA was mimicked by the selective $\alpha_{1A}$-AR agonist A61603 (Fig. 1C; A61, 1 μM; ΔV: 1.1 ± 0.3 mV, n = 10, p = 0.002) and by the $\beta_1$-AR agonist dobutamine (Fig. 1C; DOB, 3 μM; ΔV: 1.2 ± 0.3 mV, n = 9, p = 0.003). As with NA, the depolarization elicited by the selective agonists was insensitive to blockers of fast excitatory and inhibitory synaptic transmission (Fig. 1C; A61603 with blockers: ΔV: 1.6 ± 0.4 mV, n = 7, p = 0.008; DOB with blockers: ΔV: 1.3 ± 0.2 mV, n = 5, p = 0.003). Together, these results indicate that NA depolarizes MOB MCs by two different mechanisms that involve activation of $\alpha_{1A}$- and $\beta_1$-ARs.

**NA increases subthreshold synaptic noise in MOB MCs**

The depolarization elicited by NA in MOB MCs was accompanied by a 2-fold increase in membrane potential variance (Fig 2A; Vm variance: 3.26 ± 1.43 $mV^2$ vs. 8.13 ± 4.15 $mV^2$, p = 0.04; n = 15, not shown) resulting in subthreshold fluctuations in the membrane potential of MCs. In the MOB, this synaptic noise may arise from dendrodendritic interactions between MCs and GCs, which can generate fast field potential oscillations between 15 to 100 Hz (usually characterized as beta and gamma oscillations) in the presence of odor stimulation (Fukunaga, Herb, Kollo, Boyden, & Schaefer, 2014; Kay, 2014; Lagier, Carleton, & Lledo, 2004; Manabe & Mori, 2013). Therefore, we used spectral analysis (see methods) to examine the effect of NA on fast field

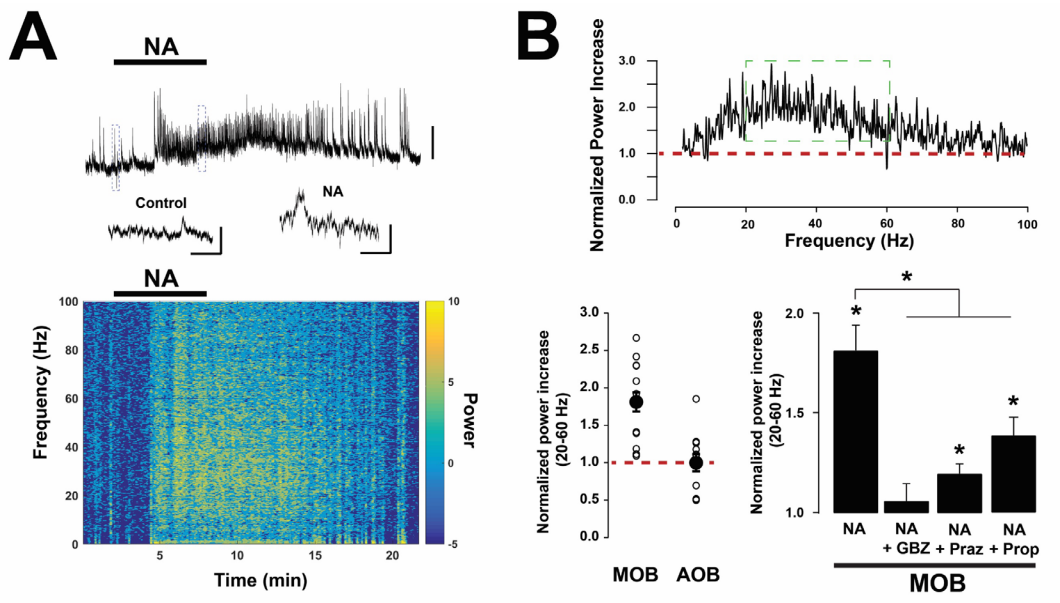


**Figure 2. NA increases subthreshold membrane potential fluctuations in MOB MCs**

A. Top, the depolarization by NA in MOB MCs was accompanied by an increase in synaptic noise, which is highlighted in the lower traces shown in an expanded time scale. The resting membrane potential is –59 mV. Calibration: upper trace: 5 mV; lower insets: 1 mV, 1 s. Bottom, spectrogram for the membrane potential in the cell shown above. NA increased the power of frequencies in the 20 to 80 Hz range. B. Top, fast Fourier transform line plot for the recording shown in A, normalized to baseline, highlighting the increase in frequency power in the gamma-frequency range (20-60 Hz, green box) produced by NA. Bottom left, summary plots showing that the enhancement of gamma-frequency synaptic noise occurs in the MOB but not in the AOB. Right, the effect of NA on the power in the gamma-frequency range is abolished with the $GABA_A$ receptor antagonist gabazine (GBZ, 10 μM; n = 10; vs. NA, p = 0.00006), and significantly reduced by the α1- AR blocker prazosin (Praz, 1 μM; n = 8; vs. NA, p = 0.004) and β-AR blocker propranolol (Prop, 10 μM; n = 8; vs. NA, p = 0.04).

potential oscillations. Bath application of NA produced a near 2-fold increase in the power of membrane potential oscillations in the gamma range (20 – 60 Hz) (Fig 2; 1.88 ± 0.15 fold-change, n = 15, p = 0.003). This increase in gamma power was completely abolished by pre-application of the $GABA_A$ receptor antagonist gabazine (Fig 2B; GBZ, 10 μM, 1.03 ± 0.07 fold-change,

n = 10, p = 0.6), suggesting that the increase in membrane potential fluctuations in MCs require GABAergic transmission. However, NA failed to increase the power of subthreshold fluctuations in the AOB (Fig 2B; 1.01 ± .12 fold-change, n = 12, p = 0.2; MOB vs. AOB, p = 0.00006), despite the robust increase GABAergic synaptic currents on to MCs (Araneda & Firestein, 2006; Smith et al., 2009). Because $\alpha_1$-AR activation in the MOB mediates both the intrinsic depolarization of MCs and the enhancement of inhibition resulting from GC activation (Zimnik et al., 2013), we reasoned that the additional excitation by $\alpha_1$-AR activation also contributed to the subthreshold membrane fluctuations elicited by NA. Accordingly, pre-application of the $\alpha_1$ antagonist prazosin (Praz, 1 μM) also produced a significant reduction on the NA-enhanced gamma power (Fig 2B; NA + Praz = 1.22 ± 0.06 fold-change, n = 8, p = 0.003). Interestingly, while β-AR activation by NA produces only an excitatory effect in MC, the enhancement of gamma power was also reduced by the β- AR antagonist propranolol (10 μM; NA + Prop = 1.39 ± 0.09 fold-change, n = 8, p = 0.04), suggesting that this intrinsic excitatory effect also contributes to the modulation of membrane potential dynamics by NA. Together, these results suggest that NA can modulate the power of network oscillations that are associated with odor processing in the MOB.

**Kinetic differences in IPSCs between AOB and MOB MCs**

In addition to the intrinsic excitatory effect on the MOB MCs, differences in the kinetics of GABAergic currents in MCs could also contribute

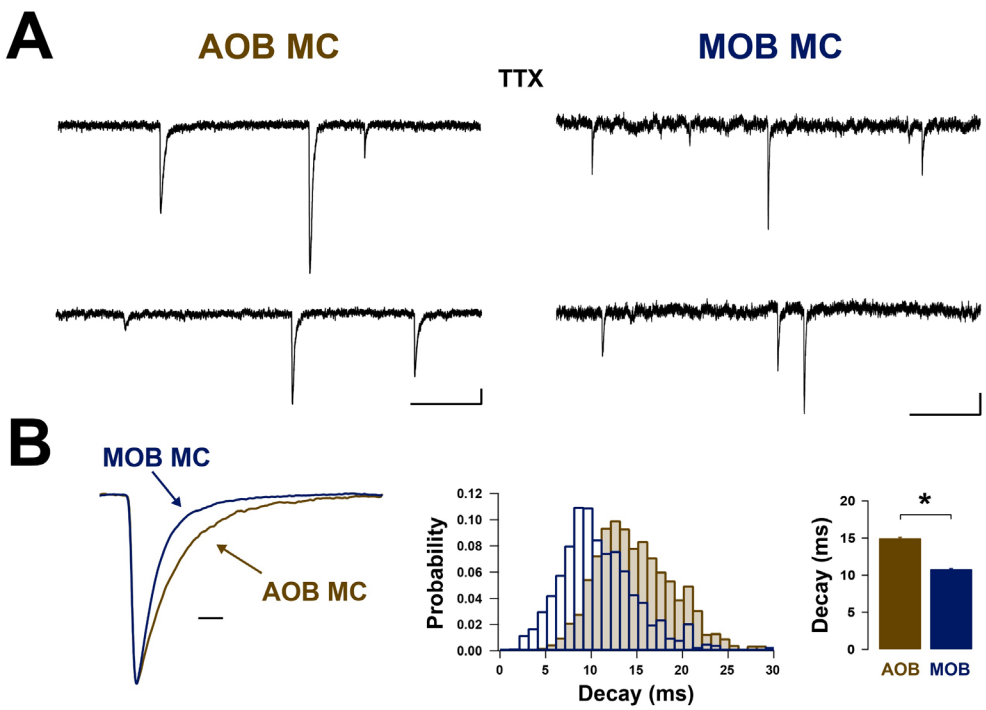


**Figure 3. Differences in the kinetics of the miniature inhibitory postsynaptic currents in MCs of the AOB and MOB.**
A. Sample recordings of miniature inhibitory postsynaptic currents (mIPSCs) in the presence of TTX (0.5 μM) in MCs of AOB and MOB MCs, with a holding potential of –70 mV. Calibration: 20 pA, 500 ms. B, left, superimposed averaged and scaled mIPSCs in MCs from the AOB (brown) and MOB (blue); the mIPSCs in the AOB exhibit a slower decay (left). Calibration 10 ms. Middle, histogram of decay distributions in the AOB and MOB. Right, the decay time is significantly faster in mIPSCs recorded in the MOB ($p = 0.000006$).

to the differential effect of membrane potential fluctuations by NA. To examine this possibility, we recorded miniature inhibitory postsynaptic currents IPSCs (mIPSCs) in AOB and MOB MCs in the presence of TTX (0.5 μM, AOB, n = 8; MOB, n = 8). While the amplitudes and rise times of the inhibitory currents were not significantly different, the decay (τ, see methods) of the mIPSCs is ~40% faster in MCs of the MOB (Fig 3 SI 1 A; MOB: 10.8 ± 0.1 ms; AOB: 15.0 ± 0.1 ms; $p = 0.000006$), suggesting differences in the properties of

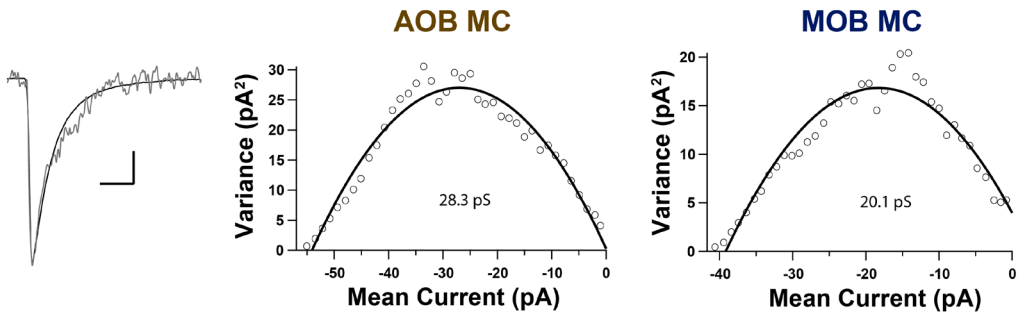


**Figure 3 Supplemental. Nonstationary fluctuation analysis of mIPSCs in AOB and MOB MCs**
Non-stationary fluctuation analysis of the mIPSCS reveals different underlying conductances. Left, sample of a peak-scaled synaptic current (grey) against the average mIPSC (black) in MCs of the AOB. The holding potential is –70 mV. Calibration: 10 pA, 20 ms. Right, plots of the variance against the mean mIPSC amplitude in sample MCs from the AOB and MOB; the estimated channel conductance is larger in the AOB.

$GABA_A$ receptors in MCs of these two regions. Accordingly, peak-scaled nonstationary fluctuation analysis of the mIPSCs in MCs revealed that $GABA_A$ receptors in the AOB had a single channel conductance of 27.3 ± 0.9 pS, while in the MOB the conductance was 21.5 ± 2.0 pS (Fig 3 SI 1 B; AOB vs. MOB: $p = 0.03$). Together, these results suggest that the inhibitory currents in MC of the AOB are mediated by $GABA_A$ receptors of larger conductance and slower kinetics; these in turn can also contribute to the differences in fast field potential oscillations observed in the presence of NA in the AOB and MOB.

**NA produces differential changes in inhibitory postsynaptic currents in MOB and AOB MCs**

To further examine the differences in the properties of the inhibitory inputs onto MC recruited by by NA, we examined the effect of NA on

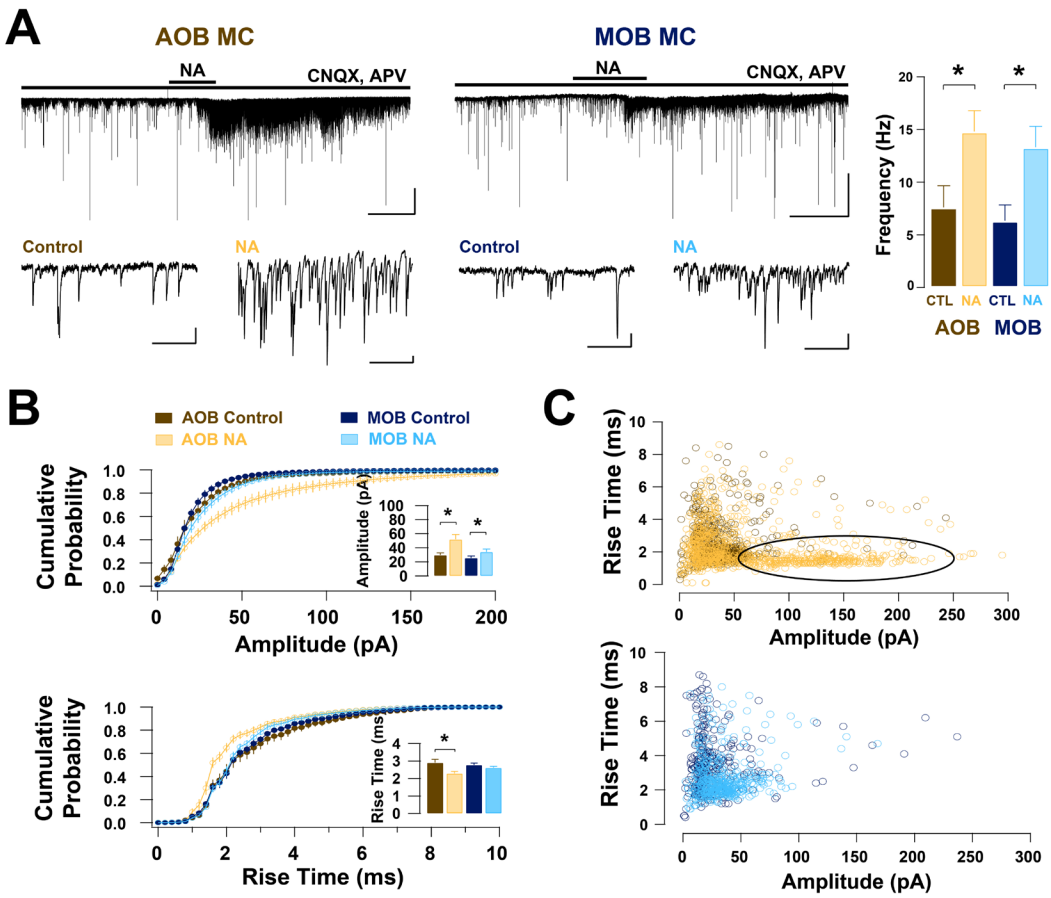


**Figure 4. NA increases synaptic inhibition in MCs of the AOB and MOB**
A. Left top, NA (10 μM) produces a significant increase in spontaneous inhibitory synaptic current (sIPSCs) in MCs of the AOB and MOB, recorded in voltage-clamp at –70 mV, and in the presence of fast-glutamatergic antagonists (CNQX, APV). Calibration: 200 pA, 2 min. Bottom, selected traces from the cells in the top, shown in an expanded time scale, highlighting the increase of sIPSCs of larger amplitude in the AOB. Calibration: 20 pA, 500 ms. Right, summary bar graphs showing the increase in frequency of sIPSCs in AOB and MOB MCs (AOB, n = 10, p = 0.00002; MOB, n = 10, p = 0.0001). B. The cumulative probability distributions and bar graphs (insets) show an increase in the amplitude (top) and speed of rise time (bottom) of the sIPSC AOB MCs (amplitude, p = 0.01; rise time, p = 0.01), with a lesser change in the MOB MCs (amplitude, p = 0.04; rise time, p = 0.21). C. Scatter plots of sIPSC amplitudes and corresponding rise times from AOB and MOB MCs. In the presence of NA, a newer population of high amplitude and fast rise time sIPSCs were recruited in AOB (top, circled), but not MOB MCs (bottom).

spontaneous IPSCs (sIPSCs) kinetics in MCs of the MOB and AOB in the

presence of blockers of excitatory synaptic transmission (n = 10, each; CNQX

10 μM, APV 50 μM). Similar to the mIPSCs, the sIPSCs had a similar amplitude and rise time in MOB and AOB MCs (Fig 4. 23.8 ± 1.6 vs 29.3 ± 3.4 pA, p = 0.18, and 2.8 ± 0.1 vs. 2.2 ± 0.1 ms, p = 0.69, respectively), however, the decay time of the sIPSC in the MOB, 13.2 ± 0.3 ms, was significantly faster than in the AOB MCs (19.4 ± 0.8 ms; p = 0.05). In agreement with our previous studies (Araneda & Firestein, 2006; Zimnik et al., 2013), NA produced a robust increase in sIPSC frequency in both MOB and AOB MCs (Fig 4A. MOB: 6.4 ± 1.5 Hz vs. 13.3 ± 1.9 Hz, p = 0.0001; AOB: 4.5 ± 1.2 Hz vs. 14.8 ± 1.9 Hz, p = 0.00002). However, while the fold-increase in frequency was similar in both regions (2 to 3-fold change), analysis of the sIPSC kinetics revealed that NA produced a differential effect on these currents. In the presence of NA, there was a significant increase in the mean amplitude and a decrease in the rise time of the sIPSCs in the AOB (Fig 4B; 29.3 ± 3.4 vs. 52.1 ± 6.9 pA, p = 0.01; 2.9 ± 0.1 vs. 2.2 ± 0.1 ms, p = 0.01), while the MOB MCs only saw a smaller increase in sIPSC amplitude (23.8 ± 1.6 vs. 33.2 ± 3.9 pA, p = 0.04; 2.8 ± 0.1 vs. 2.7 ± 0.08 ms, p = 0.21). Interestingly, the decay kinetics were not affected by NA (AOB decay: 18.7 ± 1.3 ms vs. 19.4 ± 0.8 ms, p = 0.89; MOB decay: 12.5 ± 0.4 ms vs. 13.2 ± 0.3 ms, p = 0.94).

A plot of the distribution of sIPSC amplitude vs. rise time indicated that in AOB MCs, NA recruited a population of sIPSC characterized by a higher amplitude and faster rise time (Fig 4C). Furthermore, a generalized linear

model for the different sIPSCs kinetic parameters, with and without NA, shows a significant interaction between amplitude and rise time with no significant interactions between amplitude and decay (amplitude:rise time, p = .007; amplitude:decay, p = .07, rise time:decay, p = .12), in agreement with the recruitment by NA of a sIPSC population with a larger amplitude and fast rise time in the AOB. The increase in frequency of an additional distinct population of GABAergic sIPSCs in AOB MCs suggest that in addition to GCs, NA activates a distinct inhibitory interneuron subtype that differs in its synaptic properties.

**Cell-specific noradrenergic modulation of infraglomerular and glomerular interneurons**

In addition to GCs, a diverse group of inhibitory cell types also directly synapses onto MCs in both MOB and AOB. The AOB contains a sparse population of external granule cells (extGC) in the MC layer of the AOB (Larriva-Sahd, 2008; Maksimova et al., 2019). These cells may be similar to the parvalbumin-expressing fast-spiking interneurons (FS) found in the external plexiform layer (EPL) of the MOB that form spatially extensive and dense connections with MCs, which are thought to provide broad lateral inhibition in this circuit (Kato et al., 2013; Miyamichi et al., 2013). Under resting conditions, and similar to the MOB FS (MOB; FS: 34.6 ± 8.7 Hz, n = 14; GC: 4.9 ± 0.9 Hz, n = 25, p = 0.00000000007), AOB extGCs exhibited a

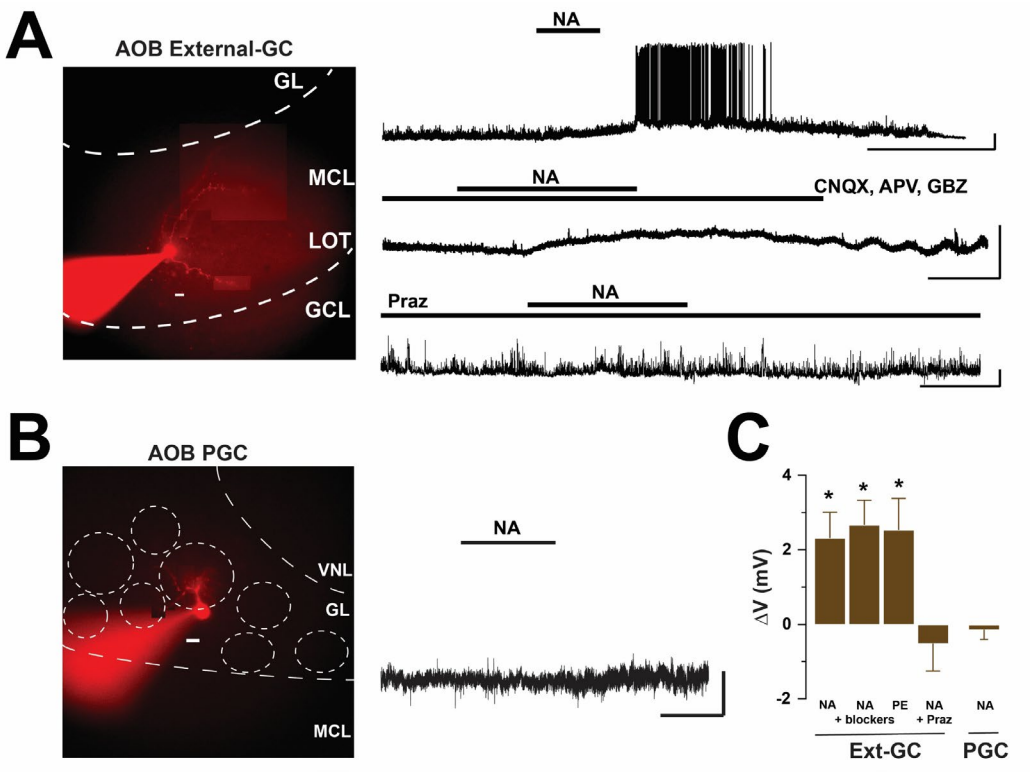


**Figure 5. NA excites extGCs but not PGCs of the AOB**
A. Left, image of a loaded extGC of the AOB filled with the Alexa594 dye (red). Calibration: 10 µm. Right, NA (10 µM) produces a depolarization in extGCs (top, $V_{rest}$ = –65 mV), which persists in the presence of blockers of fast synaptic transmission (middle; CNQX 10 µM, APV 50 µM, GBZ 10 µM; $V_{rest}$ = –62 mV). Bottom, in the presence of the α1-AR antagonist Praz (1 µM) the depolarization by NA was completely abolished ($V_{rest}$ = –71 mV). Calibration: 10 mV, 2 min. B. Left, image of a periglomerular cell (PGC) of the AOB filled with the Alexa594 dye (red). Calibration: 10 µm. Right, NA failed to produce a response in this PGC. The resting membrane potential is –62 mV. Calibration 10 mV, 2 min. C. Summary bar graphs for voltage responses for selective pharmacology in extGCs of in the AOB (NA, n = 5, p = 0.02; NA + blockers, n = 5, p = 0.006; PE, n = 6, p = 0.03; NA + Praz, n = 4, p = 0.9), and PGCs (n = 6, p = 0.6).

much higher sEPSC frequency compared to AOB internal GCs (AOB; extGC = 15.1 ± 2.1 Hz, n = 9; internal GC = 5.3 ± 1.5 Hz, n = 8, p = .001), suggesting they may also have a dense connectivity with MCs. In the presence of NA, extGCs exhibited a significant depolarization, that persisted in the presence of

synaptic blockers (Fig 5A. NA, ΔV: 5.7 ± 3.4 mV, n = 5, p = .02; NA + blockers, ΔV: 2.8 ± .5 mV, n = 5, p = .005). Furthermore, the depolarizing effect of NA in extGCs is mimicked by the $\alpha_1$ agonist PE and was abolished by the $\alpha_1$ antagonist Prazosin (Fig 5A. PE, ΔV: 2.5 ± .8 mV, n = 6, p = .03; NA + Praz, ΔV: -0.5 ± .7 mV, n = 4, p = .92). In contrast, extGCs were not activated by the β-AR agonist ISO (ΔV: 0.9 ± .5 mV, n = 3, p = 0.22; not shown). These results suggest the additional sIPSC population recruited in the presence of NA results from a direct excitation of extGCs via $\alpha_1$-AR activation. Although, we cannot rule out the possibility that NA is acting in additional inhibitory types, it is noteworthy that AOB periglomerular neurons failed to show a response to the application of NA (Fig 5B; ΔV: –0.1 ± .3 mV, n = 6, p = 0.65).

We next examined whether NA could affect other primary interneurons in the MOB besides the GCs. Interestingly, while NA depolarized FS interneurons (Fig 6A. ΔV: 6.2 ± 1.3 mV, n = 7, p = 0.001), this depolarization was abolished with pre-application of blockers of fast-synaptic transmission (Fig 6A. ΔV: 0.5 ± 0.5 mV, n = 7, p = 0.23), suggesting a di-synaptic origin. In contrast, NA depolarized GAD2+ GFP-labeled interneurons of the glomerular layer in the MOB, and this effect persisted in the presence of blockers of synaptic transmission and TTX (Fig 6B. NA, ΔV: 6.8 ± 2.3 mV, n = 9, p = .02; NA + blockers, ΔV: 3.1 ± 1.2 mV, n = 7, p = .04). Application of specific

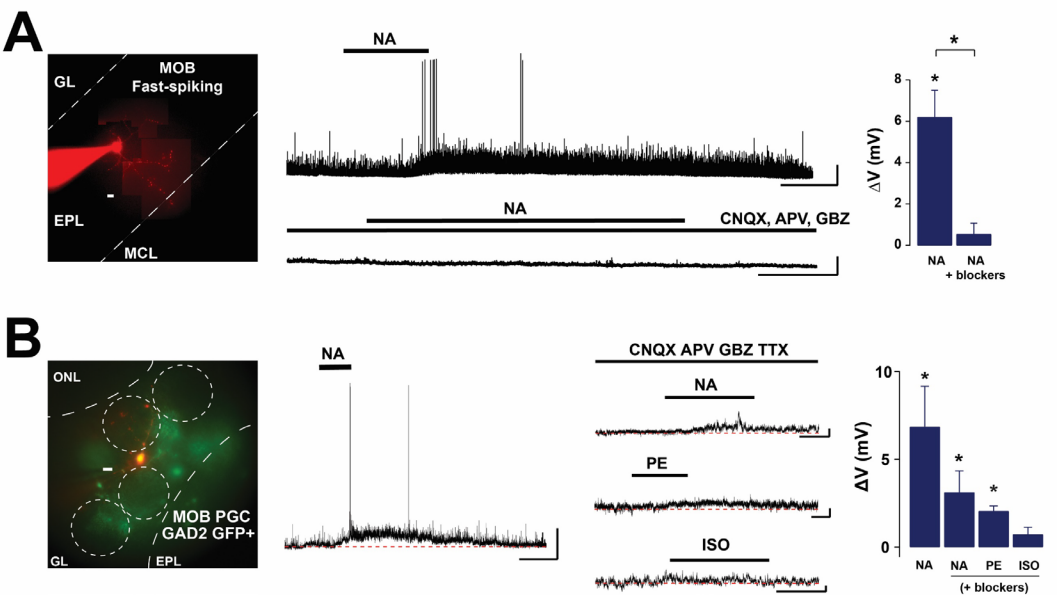


**Figure 6. NA induces extrinsic excitation in the FS interneurons and intrinsic excitation of PGCs of the MOB**

A. Left, image of a loaded FS of the MOB filled with the Alexa594 dye (red). Calibration: 10 μm. Middle, NA (10 μM) produces a depolarization of the FS (top, $V_{rest}$ = –70 mV), which was abolished by the presence of blockers of fast synaptic transmission (bottom; CNQX 10 μM, APV 50 μM, GBZ 10 μM; $V_{rest}$ = –71 mV). Right, summary bar graphs for the response of FS interneurons to NA (NA, n = 7, p = 0.005; NA + blockers, n = 4, p = 0.2). Calibration: 20 mV, 2 min. B. Left, image of a GFP+ tagged (green) uni-glomerular PGC of the MOB filled with the Alexa594 dye (red). Calibration: 10 μm. Middle, NA excited the PGC (Vrest = –65 mV; Calibration: 20 mV, 2 min), and this effect persisted in the presence of blockers of synaptic transmission and TTX. Additional selective agonists for NA showed an $\alpha_1$ excitation in PGCs (PE), while a β-AR agonist (ISO) to produced no effect. The resting membrane potential was –65 mV for both PE and ISO. Calibration: 5 mV, 1 min. Right, summary bar graphs for voltage responses for GAD2+ PGCs (NA, n = 9, p = 0.02; NA + blockers, n = 7, p = 0.04; PE + blockers, n = 6, p = 0.0008; ISO + blockers, n = 5, p = 0.14).

agonists of ARs indicated that excitation could be mimicked by the $\alpha_1$ agonist PE (Fig 6B. ΔV: 2.1 ± 0.3 mV, n = 6, p = 0.001), but not the β-AR agonist ISO (ΔV: 0.7 ± 0.4 mV, n = 5, p = 0.14). Taken together, these results suggest that NA recruits different subpopulations of primary inhibitory interneurons across layers between the MOB and AOB.

**NA produces differential changes in spike precision between MOB and AOB MCs**

GABAergic inhibition has key role in regulating spike timing of principal neurons as well as network synchrony in cortex and hippocampus (Bartos et al., 2007; Cardin, 2018). Given the differential modulation of inhibition by NA in these two regions, we next examined how spike precision of MCs is regulated by NA. To this extent, we simulated physiological 8 synaptic inputs of increasing suprathreshold intensities overlaid on a 4 Hz respiration-like Gaussian process (see methods) in MCs of the MOB and AOB (Fig 7A; AOB: n = 8; MOB n = 8). These suprathreshold stimuli were adjusted to elicit a similar firing rate (FR) across these trials (Fig 7B; MOB FR = 7.1 ± 0.2 Hz, AOB FR = 8.0 ± 1.3 Hz, p = 0.12). Across a given trial, the increase in the amplitude of events (1-8) is accompanied by an increase in the synchrony of spikes that occur at the peak of the stimulus, which is accompanied by a general decrease in the spike jitter (SJ) in both MOB and AOB (Fig 7A; MOB, SJ1 = 20.6 ± 3.4 ms , SJ8 = 15.6 ± 4.1 ms, p = 0.006; AOB, SJ1 = 29.1 ± 6.6 ms , SJ8 = 25.2 ± 7.2 ms, p = 0.07). When we averaged the first 4 stimuli (representing lower synchrony) and the last 4 stimuli (representing higher synchrony) we found that the spike jitters are significantly lower in the MOB (Fig 7B: SJ at low intensity: MOB = 21.6 ± 1.5 ms, AOB = 29.9 ± 2.9 ms, p = 0.013: SJ at high intensity: MOB = 17.9 ± 1.8 ms, AOB = 27.0 ± 3.2 ms, p =

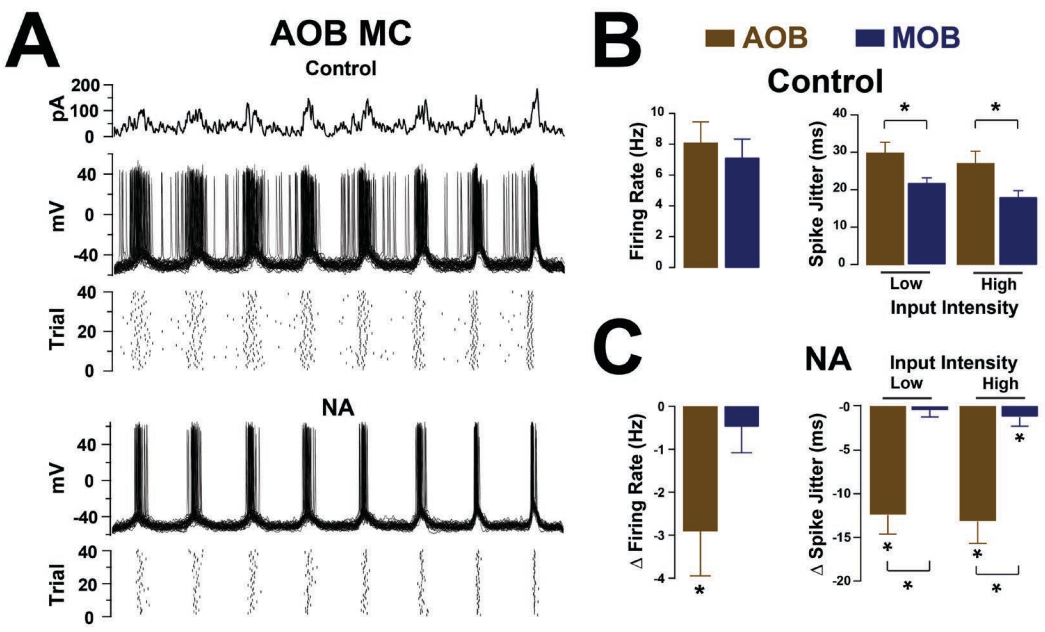


**Figure 7. NA produces a greater enhancement of spike precision in AOB MCs.**

A. MCs were stimulated with fluctuating currents that simulate sensory input of increasing synchrony at 4 Hz (upper trace). The simulated current injection had low (first 4 current bursts) and high synchrony (last 4 current bursts). Overlaid voltage traces from a MC in response to the current stimuli, during control (upper traces) and NA (10 μM; bottom). Raster plots underneath show single cell responses in 40 trials. In the presence of NA, the membrane potential was maintained close to the baseline value, –58 mV, by current injection. B. Left, in control, the overall firing rate of MCs was not different between MOB and AOB, however the spike jitters were lower (i.e. more precise) in MOB than in AOB (right, AOB, n = 8, MOB, n = 8, $p < 0.02$). C. Left, in the presence of NA the firing rate of MCs was significantly decreased compared to control in the AOB but not in the MOB (AOB, $p = 0.02$, MOB, $p = 0.46$). Right, NA increases spike precision for events of low and high synchrony in the AOB ($p < 0.0001$), but only the spike precision to high input synchrony stimuli is increased in the MOB (low, $p = 0.41$; high, $p = 0.01$).

0.017). Thus, under control conditions, spike timing in MOB MCs occurs with more precision, perhaps facilitating synchronized firing.

In the presence of NA, while preventing changes in the membrane potential by current injection, spike precision increased in AOB MCs, that is there was a decrease in SJ in both synchrony conditions (Fig. 7C; low ΔSJ= –

12.5 ± 2.2 ms, p = 0.00002; ΔSJ = –13.2 ± 2.5 ms, p = 0.0001). Despite preventing changes in membrane potential, there was also an overall decrease in FR in the presence of NA (Fig 7C; ΔFR = –2.9 ± 1.0 Hz, p = 0.02). In contrast, in the MOB MCs, NA produced a small but significant decrease in SJ only in high intensity stimuli (Fig 7C; low: ΔSJ= –1.1 ± 1.3 ms, p = 0.41; high: Δ SJ= –2.3 ± 1.0 ms, p = 0.01), with no significant change in FR (ΔFR = –0.47 ± 0.6 Hz, p = 0.46). These results are in agreement with a model in which the overall suppression of excitability in AOB MCs enhances the selectivity of MC spiking across different stimuli intensity. In MOB MCs, the increase in excitability of MCs together with enhancement of inhibitory inputs produced by NA, increases spike precision during more salient stimuli.

## Discussion

The circuits in the MOB and AOB function under similar principles, with odor signals relayed to the principal neurons, which undergo regulation by a large and diverse group of local inhibitory neurons, while conveying odor information to upstream processing areas. Yet, how NA regulates the excitation-inhibition balance of these circuits and whether similar mechanisms exist in these two regions remains unknown. Here we show that NA produces dramatically different effects on the output neurons of the AOB and MOB: NA reduced the overall excitability of MCs in the AOB, while producing the opposite effect in the MOB. This differential regulation could be explained by two opposite mechanisms: a direct excitatory adrenergic effect on MOB MCs, but not AOB, and activation of local inhibitory inputs onto MCs that in the AOB is more prominent and exhibits different kinetics. At the circuit level, NA increased the spike precision of output neurons in the AOB, in a stimulus-intensity independent manner, while in the MOB, this increase in spike precision occurred only at higher intensity stimuli, suggesting that adrenergic regulation of spike timing in MCs of the MOB is activity-dependent.

Previous work has shown a robust $\alpha_{1A}$-adrenergic excitation of the GCs, suggesting an overall enhancement of inhibition onto MCs throughout the bulb (Araneda & Firestein, 2006; Smith et al., 2009; Zimnik et al., 2013). However, we found a striking difference in the overall effect of NA on the output neurons. In the MOB, NA produces a dual effect: excitation of GCs

increases inhibition onto MCs, but NA also produces a direct excitation of MCs, which is mediated by activation of both $\alpha_{1A}$- and $\beta_1$- adrenergic receptors. Moreover, despite the increase in inhibition resulting from GC activation, the overall effect of NA was an increase in excitability of MCs. In contrast, in the AOB, the overall effect of NA in output neurons is inhibition, mediated by excitation of GCs. These results are consistent with findings in other sensory systems, in which noradrenaline can modulate the intrinsic cell excitability of principal neurons, as well as circuit excitation and inhibition through concurrent activation of multiple adrenergic receptor classes (Hurley et al., 2004; Kossl & Vater, 1989; McCormick et al., 1991; Rogawski & Aghajanian, 1980; Waterhouse et al., 1990).

The combination of both intrinsic excitation and extrinsic inhibition elicited by NA also increased subthreshold oscillations in the gamma frequency range in the MOB. Interestingly, this effect was sensitive to GABAergic blockade, suggesting that enhanced inhibition from GCs is a major contribution, yet, these subthreshold oscillations were not observed in the AOB, where the GABAergic inhibition is more prominent. Odor processing in the MOB relies on a temporal code built on network oscillatory activity (Bathellier et al., 2008; Gschwend et al., 2015; Rebello et al., 2014; Smear et al., 2011). Gamma-frequency oscillations are thought to arise from dendrodendritic interactions between MCs and GCs and this network oscillation is a prominent feature of circuit activity during odor discrimination

tasks (Beshel et al., 2007; Kay, 2014; Lepousez & Lledo, 2013;  a. Li et al., 2015). Therefore, we propose that by increasing membrane potential fluctuations in the gamma frequency range, NA can potentiate dendrodendritic interactions, thereby facilitating network oscillations. Interestingly, a previous report also showed a robust increase in the power of gamma frequency, in MOB slices, that outlasted the NA application (Gire & Schoppa, 2008).

A potential mechanism by which NA differentially shapes the output of MCs in the OB lies in different inhibitory mechanisms regulating these output neurons. Inhibitory synaptic currents in MOB MCs exhibit fast kinetics, in agreement with previous studies (Castillo & Carleton, 1999; Schoppa et al., 1998); however, the decay of the IPSCs in AOB MCs is significantly slower than in the MOB. Furthermore, the single channel conductances determined by non-stationary fluctuation analysis, suggested that this difference could be due to the activity of $GABA_A$ receptors of different characteristics. This possibility is in agreement with previous *in situ* hybridization studies for $GABA_A$ receptor subunits, which shows the expression of  α1, β2, and γ2 subunits in MOB MCs, and α1, α2, β1, and γ2 subunits AOB MCs (Angelotti & Macdonald, 1993; Brickley et al., 1999; De Koninck & Mody, 1994; Laurie et al., 1992; Lein et al., 2007; Panzanelli et al., 2005). $GABA_A$ receptors containing the β1 subunit have been previously shown to produce greater currents than β2-containing receptors (Mortensen et al., 2012), which is in

agreement with the larger conductance we observed in AOB MCs. Likewise, the slower decay kinetics of the IPSC in the AOB could be due to presence of the α2 subunit, which renders $GABA_A$ receptors with decay kinetics 5 times slower compared α1-containing receptors (Dixon et al., 2014; Lavole et al., 1997; McClellan & Twyman, 1999). Further experiments should address the expression of these receptors in MCs of the AOB and MOB.

In AOB MCs, the recruitment of a high amplitude, fast rise time population of sIPSCs and its potential correspondence with extGCs is in agreement with anatomical findings showing that extGCs provide perisomatic inhibition whereas internal GCs contact the lateral dendrites of AOB MCs (Larriva-Sahd, 2008; Takami et al., 1992). Taken together, the combination of the relatively slower decay of the IPSCs and the larger amplitude of the current, summed to the recruitment of two interneuron populations (the GCs and the extGCs), may lead to a shunting effect when inhibition is enhanced by NA, and could explain the robust hyperpolarization and suppression of action potential firing, with minimal change in high frequency synaptic noise. In contrast, in MOB MCs the faster decay of the IPSC is posed to contribute to faster field potentials oscillations, as previously described in hippocampus (Bartos et al., 2007; Chow et al., 1998; Traub et al., 1996), and the recruitment of these inhibitory currents by NA could strengthen these network dynamics. In sum, differences in the kinetics of the inhibitory synaptic inputs

combined with the changes in excitability results in distinct changes in network-level activity by NA in the MOB and AOB.

Across sensory networks, the regulation of the balance of excitation and inhibition play a major role in the coding of sensory information, for example by the adjustment of signal-to-noise ratios, gain control (Harris & Mrsic-Flogel, 2013; H. Y. He & Cline, 2019; S. Zhou & Yu, 2018). In the visual thalamus, neuromodulation by noradrenaline alters the balance of network excitation and inhibition, resulting in alterations in spike-timing, and in turn the fidelity of information transfer to higher cortical regions (Le Masson et al., 2002; Shu et al., 2003). Despite the slower sensory drive from the vomeronasal organ (Meredith, 1994), previous experiments have shown that pheromonal investigation elicits network oscillations in AOB *in vivo* with increased power in lower frequency ranges (< 10 Hz) (Binns & Brennan, 2005), allowing for the possibility of a temporal element in pheromonal coding. In the AOB MCs, the strong shift towards inhibition produced by NA resulted in a dramatic increase in spike precision regardless of the stimulus intensity. In contrast, in the MOB, an increase in spike precision in MCs was only observed for more salient stimuli, due to the dual effect on intrinsic excitation and extrinsic inhibition. Because the odor code in the MOB relies on precisely timed spikes as well as the spatial organization of active MCs (Gschwend et al., 2015; Haddad et al., 2013; Shusterman et al., 2011; Smear et al., 2011; Uchida et al., 2013). It is possible that the enhancement of spike

precision by NA with more salient stimuli could ensure more efficient coding of olfactory cues at the population level across MCs.

In conclusion, despite the similarities in both olfactory circuits, noradrenergic modulation differentially affects individual circuit components between the two regions. The differences in cell-specific adrenergic modulation with regards to the MCs and local interneuron populations of both regions highlight the specialized function of these two olfactory pathways with regards to stimulus specificity, input modes, and their respective roles in animal behavior.

# Chapter 5: Long-term plasticity elicited by NA in MCs of the MOB and AOB

## Introduction

Social learning and recognition in most mammals rely on olfactory signaling. Several studies have indicated that learning of conspecific chemosensory cues involves neural plasticity at synapses in the the olfactory bulb (OB), the first region of olfactory processing in the brain. In the main and accessory olfactory bulb (MOB and AOB, respectively), this neuronal plasticity, in the context of social odor learning, is expressed as changes in intrinsic cell excitability as well as changes in synaptic connectivity and strength in the OB (Brennan & Keverne, 1997; Cansler et al., 2017; Gao et al., 2017; Vinograd et al., 2017).

In both the MOB and AOB, odor learning and neuronal plasticity rely on state-dependent neuromodulation, with noradrenaline (NA) released by neurons in the locus coeruleus (LC)(McLean & Shipley, 1991; Mclean, Shipley, Nickell, Aston-Jones, & Reyher, 1989; Shipley, Halloran, & de la Torre, 1985). Accordingly, antagonism of adrenergic receptors occluded odor (Doucette et al., 2007; Mandairon et al., 2008; Vinera et al., 2015), as well as, pheromonal learning in female mice (Dluzen et al., 2000; Kaba & Keverne, 1988). Several studies have shed light on the cellular mechanisms of noradrenergic modulation on AOB and MOB circuit function (Smith et al., 2009; Zimnik et al., 2013), including the results presented in the preceding

chapters; however, it remains unknown how these short-terms effects of NA result in long-term changes in circuit function and plasticity. To fill this gap we have begun to examine the long-term effects of an acute exposure to NA. Using, whole-cell recordings we find that NA produced a long-term change in the excitability of output neurons in both AOB and MOB. After NA, MOB MCs of males and females showed increased excitability that lasted throughout the recording (more than one hour). Surprisingly, we found a significant sexually dimorphic effect in the AOB. The excitability of MCs in females was decreased after the NA application, while in males, it increased. These differences in long-term excitability with NA, compounded by region-specific sexual dimorphism, illustrate a potential mechanism by which early stages of olfactory processing can exhibit flexibility in adjusting towards different social and behavioral contexts.

**Materials and methods**

*Animals:* All experiments were conducted following the IACUC guidelines at the University of Maryland in College Park. Experiments were performed on group-housed male and female wild-type (C57/BL6) mice at 3 months of age (and older).

*Slice preparation:* Experiments were performed in OB slices using methods previously described (Zimnik et al., 2013). Briefly, slices were prepared in an oxygenated ice-cold artificial cerebrospinal fluid (ACSF) containing low $Ca^{2+}$ (0.5 mM) and high $Mg^{2+}$ (6 mM). Sagittal and horizontal sections of the OB (250 μm) were then transferred to an incubation chamber containing normal ACSF (see below) and left to recuperate for at least 30 minutes at 37°C, before the recordings. In all experiments, unless otherwise stated, the extracellular solution is ACSF of the following composition (in mM): 125 NaCl, 26 NaHCO3, 1.25 NaH2PO4, 2.5 KCl, 2 CaCl2, 1 MgCl2, 1 myo-inositol, 0.4 ascorbic acid, 2 Na-pyruvate, and 15 glucose, continuously oxygenated (95% O2-5% CO2) to give a pH 7.4 and an osmolarity of ~305 mOsm.

*Electrophysiological recordings:* Neurons were visualized using an Olympus BX51W1 microscope and recorded in voltage and current clamp modes using a dual EPC10 amplifier controlled by the PatchMaster software (HEKA, Holliston, MA). Experiments were performed at room temperature (~22° C) and cells were recorded using standard patch pipettes (2-6 MΩ resistance). The internal solution had the following composition (in mM): 130 K-gluconate,

4 KCl, 10 HEPES-K, 10 Na phosphocreatine, 2 Na-ATP, 4 Mg-ATP, and 0.3 GTP adjusted to pH 7.3 with KOH. The osmolarity of the internal solutions was adjusted to 290–305 mOsm.

*Data analysis:* Data was analyzed using custom programs written in MATLAB (Mathworks). We used a minimum of 5 adult group-housed animals for each experimental category (AOB, MOB, males, females). To examine changes in excitability in MCs we adapted an experimental paradigm used by Gao et al 2017. We recorded from MCs and injected 500 ms, –20 pA to –50 pA test pulses to measure input resistance and capacitance, followed by depolarizing 20 s square current pulses at 1 minute intervals to examine spiking responses across successive stimulations. To standardize across cells, the resting membrane potential was set to –62 ± 0.5 mV, and the initial depolarizing current injection intensity was set to produce average spike rates between 2 and 10 Hz in both MOB and AOB MCs (overall: 5 ± 1 Hz). We conducted at least 10 control trials before applying NA (10 μM) for 10 minutes, which was then washed out for over 30 minutes. The current injection protocols were also executed throughout the NA application and washout. After the washout, the membrane potential was reset to the initial value recorded at the start of the pre-NA trials, and 10 trials were run again. Rate change ratios were calculated as the rate of the $10^{th}$ trial over the $1^{st}$ trial (RCR). There were no significant correlations between the starting spike rate versus the control or washout RCR in any of the groups (general linear model), suggesting the

long-term plasticity effects were independent of the starting value of spike rates.

Baseline measurements indicated that MCs in the AOB of females and males had higher input resistance and lower cell capacitance than those in MOB males and females (AOB input resistance: females = 375 ± 23 MΩ, n = 26, males = 482 ± 55 MΩ, n = 29; AOB capacitance: females = 143 ± 12 pF, males = 135 ± 15 pF; MOB input resistance: females = 160 ± 24 MΩ, males = 116 ± 12 MΩ, p = 0.12; MOB capacitance: females 322 ± .38 pF, males 290 ± 33 pF, p = 0.54; not shown; input resistance AOB vs MOB, $p = 9*10^{-11}$; capacitance AOB vs MOB, $p = 1*10^{-5}$). Statistical significance was calculated using a student's t-test, ANOVA with Tukey's posthoc correction method, and general or generalized linear models.

## Results

### NA induces sexually dimorphic long-term changes in MC excitability in the AOB

Previous studies have proposed a central role for NA in social recognition and learning during mating in female mice and mother-offspring bonding in ewes, which are thought to rely on neural plasticity at the level of the OB (Brennan & Kendrick, 2006; Brennan & Keverne, 1997; Griffiths & Brennan, 2015). More recently, both aggression in males and mating in female mice were shown to induce changes in the excitability of AOB neurons (Cansler et al., 2017; Gao et al., 2017). Therefore, we hypothesized that exposure to NA alone, could drive these long-term changes in excitability. To measure changes in excitability elicited by NA in the AOB, we stimulated MCs with a long current pulse (20 s) at 1 min intervals across 10 trials (Gao et al., 2017) (Fig 1). This protocol was used to reveal changes in AOB MCs excitability after mating behavior. Before the application of NA, MCs from males and females exhibited sustained firing across the 10 trials. However, there was a significant reduction in the firing across the trials in the female but not in the males. This is highlighted when we quantified changes in excitability as a rate-change ratio (RCR = trial 10 rate / trial 1 rate; see methods), where a value less than 1 correspond to a reduction in firing elicited by the current stimuli across the trials. Thus, the initial RCR in females was 0.74 ± 0.07 ($p = 0.000006$) versus of 1.1 ± 0.13 in males ($p = 0.99$).

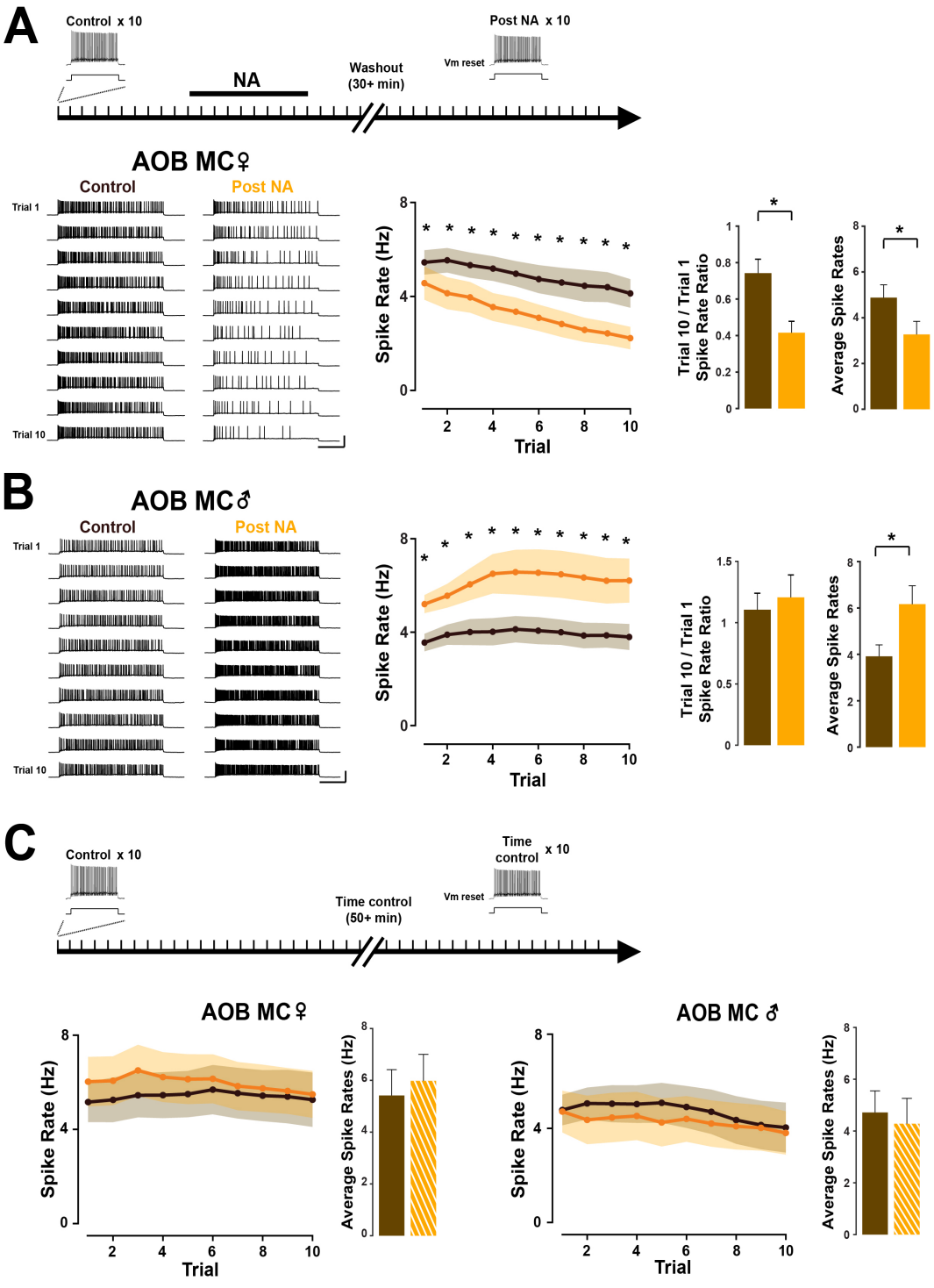


To determine the long-term effect of NA exposure in the AOB, we

**Figure 1. NA elicits different long-term changes in excitability in AOB MCs of female and males.**
A. Top, diagram of the time course of the stimulation protocol. MCs from male and females were stimulated by 10 consecutive trials of square current pulses (20 s; 1 min intervals), before the application of NA (10 μM, 10 min, control), and throughout the enter application and washout of NA. 30 min after the NA application, the resting membrane potential was reset and 10 consecutive trials were collected (post-NA). Bottom, left, responses to current stimulation in a MC from a female, before (left) and after NA. Middle graph, across trials the frequency of firing decreases both in control (brown) and after NA (yellow, n= 18, $p < 0.03$). However, the decrease is more pronounced post-NA. The ratio of spike rates in the tenth trial vs. the first trial, and the average firing rate across trials were significantly reduced post-NA ($p = 0.006$, left; $p= 0.003$, right). B. Left, responses in a MC from a male, before and after NA. The responses were constant across trials, however, the firing frequency was higher post-NA across trials (middle graph; n=19, $p < 0.02$). The spike ratio was not different post-NA (left bar graph, $p = 0.7$), however the average firing rate across trials was significantly higher (right bar graph, $p = 0.02$). The resting potential in A is –60 mV and –62 mV in B. the calibration is 80 mV and 5 s in A and B. C. Top, diagram of the control stimulation protocol with no NA. MCs from females and males were stimulated with square current pulses (20 s; 1 min intervals). After a minimum of 50 minutes of stimulation, the Vm was reset and 10 stimulation trials were initiated. In both females (n = 9) and males (n = 12), time control firing rates (hashed yellow) across trials were not significantly different than those in the initial control trials (brown). Similarly, the average firing rates was not significantly different.

examined the excitability of MCs 30 min after NA exposure (10 μM; 10 min). Surprisingly, MCs of females, but not males, showed a significant decrease in the input resistance post-NA application (female control = 356 ± 30 MΩ, post-NA = 313 ± 29 MΩ, n = 18, $p = 0.000006$; male control= 516 ± 71 MΩ, post-NA = 517 ± 79 MΩ, n = 19, $p = 0.99$). We note capacitance was not significantly different between the sexes (AOB females vs. males: resistance, $p = 0.09$, capacitance, $p = 0.67$, see methods). Furthermore, post- NA application, there was a stronger suppression of firing across the 10 trials in females (Fig 1A; RCR control = 0.74 ± 0.07; post-NA = 0.41 ± 0.06, $p = 0.006$), as well as an overall reduction in the average spike rates (Fig 1A;

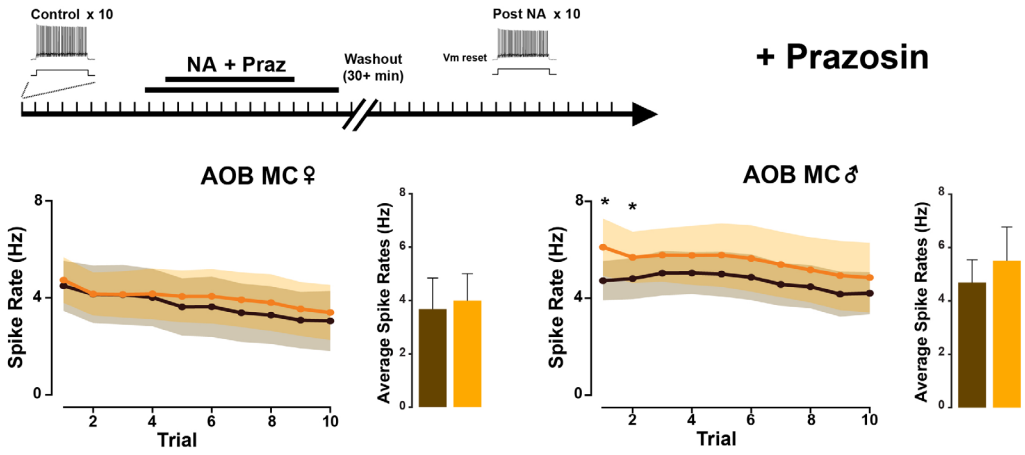


**Figure 2. Long-term excitability in AOB MCs is mediated by $\alpha_1$-ARs**
Top, diagram of stimulation protocol for the application of NA in the presence of the $\alpha_1$-AR antagonist Prazosin (Praz, 1 µM). MCs were stimulated by 10 consecutive trials of square current pulses, and Praz was applied for 10 minutes prior to perfusion of NA (10 min). Post-NA trials were collected 30 minutes after NA and Praz washout. Left, in the AOB MCs of females (n = 9), pre-application of Praz occluded the long-term changes elicited by NA spike rates across trials and averaged firing rates (control, brown; post-NA, yellow). Right, in the AOB MCs of males (n = 9), spike rates were significantly higher only in the first two trials post-NA ($p < 0.04$), but the overall spike rate averages were not significantly different.

control = 4.9 ± 0.6 Hz, post-NA = 3.3 ± 0.6 Hz, p = 0.003). It should be noted that in control experiments, in which we conducted the same stimulation protocol but without applying NA, there were no differences in the average spike rates (Fig 1C;, initial trials = 5.4 ± 1.0 Hz; end trials = 6.0 ± 1.0 Hz, n = 9, p = 0.36), suggesting that the observed changes in excitability were induced by NA. In contrast, post NA, there was no change in the RCR in MCs from males (RCR control = 1.00 ± 0.23, post-NA = 1.20 ± 0.18, p = 0.71). However, post NA, the overall spike rates were significantly higher in MCs from males (Fig 1B; averaged spike rates, control = 3.9 ± 0.5 Hz, post-NA = 6.2 ± 0.8 Hz, p = 0.02). Similar to the MCs from females, control experiments

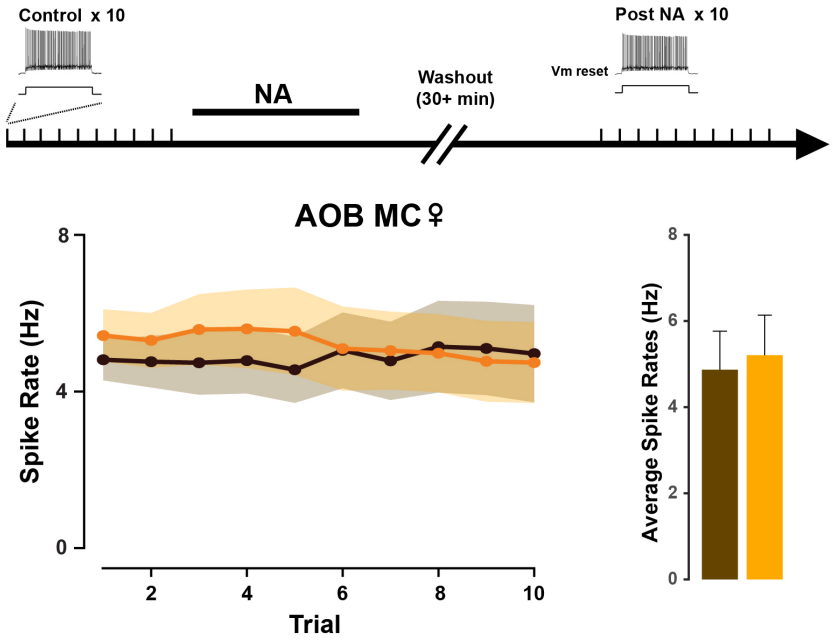


**Figure 3. Long-term excitability changes in AOB MCs from females require concurrent MC stimulation during NA application**
Top, diagram of the stimulation protocol for the NA application in the absence of continuous stimulation. MCs from females (n = 9) were stimulated with square current pulses (20 s; 1 min intervals) for 10 trials. Afterwards, NA was bath applied for 10 minutes. Post-NA trials were collected 30 minutes after NA washout. In the absence of MC stimulation during the NA application, spike rates across trials (left) and averaged spike rates (right) were not significantly different between control (brown) and post-NA conditions (yellow).

show no changes in the averaged spike rates, in the absence of NA (Fig 1C; initial trials = 4.7 ± 0.8 Hz, end trials = 4.3 ± 1.0 Hz, n = 12, p = 0.51).

Our data indicates that the predominant modulation in the AOB circuit by NA results from activation of $\alpha_1$-ARs. Therefore, we examined the possibility that the changes in plasticity by NA are mediated by activation of these receptors. In agreement with our previous findings, the $\alpha_1$ antagonist Praz (1 μM) occluded the long-term changes produced by NA in the RCR,

input resistance, and average spike rates of MCs from females (Fig 2; Praz, n = 9; control vs. post-NA: RCR = 0.53 ± 0.17 vs. 0.64 ± 0.17, p = 0.63; input resistance = 425 ± 29 MΩ vs. 464 ± 55 MΩ, p = 0.98; average spike rates = 3.7 ± 1.2  Hz vs. 4.0 ± 1.0 Hz, p = 0.83). In addition, in MC of males, the averaged firing rates were also not significantly different with pre-application of Praz (Fig 2; Praz, n = 9; average spike rates = 4.7 ± 0.9 Hz vs. 5.5 ± 1.3 Hz, p = 0.55).

To determine the activity-dependence of this long-term plasticity induction, we tested whether we could induce this plasticity in the absence of concurrent stimulation of the MC. After collecting the control stimulation trials, the NA application and the wash out period were conducted in the absence of MC stimulation. Surprisingly, the averaged firing rates were not significantly different post-NA (Fig 3; control = 4.9 ± 0.9 Hz, post-NA = 5.2 ± 0.9 Hz, p = 0.64). These results suggest that the induction of this long-term suppression of excitability in AOB MCs of females requires activation of MCs when NA is present.

**NA induces a long-term increase in MC excitability in the MOB**

As with the MCs of the AOB, the stimulation protocols elicited sustained firing across trials in MCs of the MOB. However, unlike the MCs of the AOB, the firing across the trials were relatively consistent (RCR: female = 0.82 ± 0.09, p = 0.68, n = 15; male = 1.00 ± 0.23, p = 0.99, n = 14). Intriguingly, we did not observe sexually dimorphic changes in the excitability

in MOB MCs post-NA. The input resistance in MCs of females and males was not significantly different post-NA (MOB females: 160 ± 24 MΩ vs. 169 ± 23 MΩ, , p = 0.99; MOB males: 116 ± 12 MΩ vs. 128 ± 16 MΩ, , p = 0.36). However, MCs from both female and males exhibited notably higher firing rate post-NA (Fig 3; females: averaged spike rates, control = 6 .2 ± 0.9 Hz, post-NA = 10.3 ± 1.6 Hz, p = 0.008; males: averaged spike rates, control = 5.1 ± 0.8 Hz, post-NA = 12.6 ± 2.6 Hz, p = 0.007).

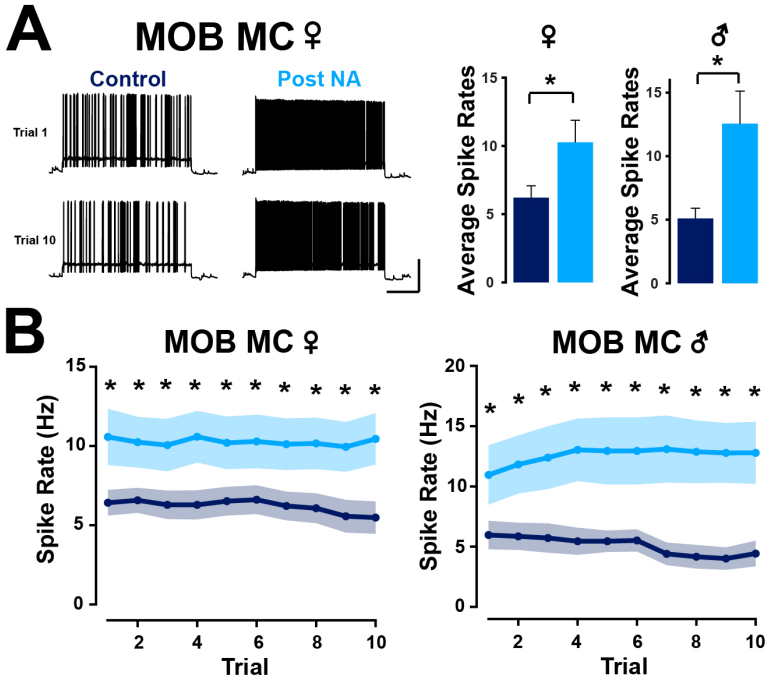


**Figure 4. Long-term changes in intrinsic excitability produced by NA in MCs of the MOB**
A. Sample responses to current stimulation in a MC from a female, before (left) and after NA. Only the first and tenth trials are shown. The resting membrane potential is–64 mV. Calibration: 40 mV and 5 s. Right, on average, firing rates were significantly higher both in females (left, n =15, p = 0.008) and males (bottom,n = 14, p = 0.007). B. The responses were generally consistent across trials, however, the firing frequency was higher post-NA (cyan) than in control (blue) in both females and males (female, p < 0.00001; male, p < 0.002).

## Discussion

Regulation of OB circuits by NA plays an important role in odor-driven social recognition and learning, across a myriad of behavioral contexts (i.e. aggression, mating). These behaviors rely on the activation of two parallel streams of information through the MOB and AOB, regions that receive dense noradrenergic input from the locus coeruleus (LC). The circuits in the MOB and AOB function under similar principles, with odor signals relayed to the principal neurons, which undergo regulation by local inhibitory neurons, and convey odor information to downstream processing areas. Yet how NA mediates plasticity in both circuits remains unknown. Here we show that NA produced long-term changes in excitability in MCs of both the MOB and AOB. Surprisingly, these changes in plasticity were sexually dimorphic in MCs of the AOB but not in the MOB. Together, these results indicate that parallel streams of olfactory signals by OB can be regulated using distinct mechanisms and that these changes can occur in a sex-dependent manner.

Several studies have indicated the crucial role of NA in several important odor-mediated behavioral responses (Brennan et al., 1995; Brennan & Keverne, 1997; Fletcher & Chen, 2010; Gervais et al., 1988; Rosser & Keverne, 1985). Microdialysis experiments in the OB as well as LC lesion experiments suggest that NA is required to form long-term social memories in the AOB (Brennan et al., 1995; Kaba & Keverne, 1988; Rosser & Keverne, 1985), however the mechanisms underlying this memory formation

are unknown. We found NA produced a sexually dimorphic and distinct long-term effects in the AOB and MOB. In the AOB, MCs in females undergo a general decrease in excitability, while MCs in males exhibit an increased excitability. Furthermore, in the AOB MCs of females, we show that the induction of this plasticity requires the excitation of MCs in the presence of NA. This result is in agreement with proposed models of plasticity associated with the learning of male odors in females, including the Bruce effect (Brennan & Keverne, 2014), in which MCs activated by the stud's pheromones selectively undergo plasticity and are less responsive to future exposure to the stud's odors. While prior models posit that the suppression of MC activity encoding the stud pheromones is mediated by an increase in GABAergic inhibition (Brennan & Keverne, 2014), our results suggest that additional mechanisms, such as a decrease in intrinsic excitability in MCs from the female maybe also involved. In the MOB, MCs in both females and males exhibit an increase in excitability after exposure to NA. Interestingly, recent studies revealed changes in intrinsic excitability as well as circuit physiology after mating in both the AOB and MOB (Cansler et al., 2017; Gao et al., 2017; Vinograd et al., 2017). In females, AOB MCs exhibit decreases in intrinsic excitability after mating (Gao et al., 2017). Likewise, MOB MCs exhibit stronger calcium responses to natural odors post-parturition, suggesting an increase in excitability (Vinograd et al., 2017). Together, our results suggest that a surge in NA concentration in the OB could be sufficient

to drive mating-induced plasticity in AOB MCs from females, as well as excitability changes in MOB MCs post-parturition. It would be important in future experiments to examine the specific adrenergic receptors and subcellular mechanisms responsible for these effects.

Sex-differences in responses to neuromodulators, or neuromodulator receptor expression have been described in various subcortical areas, including limbic and hypothalamic centers (Rhodes & Rubin, 1999; Riters & Ball, 2002), and further sexual divergence has been described when these monoaminergic systems interact with hormonal or peptidergic systems in the brain (Bangasser et al., 2019; Stone et al., 1989). While sex differences regarding noradrenergic neuromodulation in sensory circuits have been characterized in avian birdsong models (Ball, 1994; Castelino & Schmidt, 2010; Riters & Ball, 2002), to the best of our knowledge, our findings are the first to report sexual dimorphism in noradrenergic in an early sensory circuit in mammals. In the OB, we posit that the sexual divergence in network physiology and plasticity mediated by NA depends on behavioral context. An increase in NA concentrations is thought to occur during aggressive fight-or-flight encounters, but also in mating and during parturition (Brennan et al., 1995; Brennan & Keverne, 1997; Haller et al., 1997; Marino et al., 2005; R. J. Nelson & Trainor, 2007; Rosser & Keverne, 1985). The changes in MC excitability promoted by NA in females could be involved in the learning of pheromones associated with the male stud. In this model, the learning

mechanism leads to a suppression of MC activity and potential downstream processes such as pregnancy block (Brennan & Keverne, 1997; Kaba et al., 1989; Lloyd-Thomas & Keverne, 1982). On the contrary, an increase in AOB MC excitability in the context of male aggression could help trigger faster fight or flight responses to conspecific males (R. J. Nelson & Trainor, 2007). Further experiments antagonizing adrenergic receptors *in vivo* in combination with electrophysiology are necessary to confirm these mechanisms. In the MOB, it is possible that the long-term increase in excitability sensitizes the MCs to future presentations of those same odors. In a social context, sensitization of a volatile social odor can allow a mouse to alter how its behavior before getting closer to another mouse. In summary, our results indicate that even at an early stage of olfactory processing, a single neuromodulator can produce a complex set of short- and long-term phenotypes, which is dependent on the OB circuit, and the animal's sex.

# Chapter 6: Concluding remarks and future directions

In the present studies, we described the presence of $I_h$ in GCs, which acts as a novel mechanism of intrinsic excitability that can contribute to the participation of GCs in circuit oscillations, Furthermore, we demonstrated that NA acting on $\alpha_2$-ARs modulates $I_h$, and that this regulation can affect the inhibitory output from GCs, indicating a novel mechanism by which NA can modulate dendrodendritic inhibition (Chapters 2, 3). Surprisingly, despite a similar regulation of GC function by NA in both AOB and MOB, we describe overall divergent effects of NA on the function of MCs in these regions, which can be partially explained by the region-specific effects of NA on the MCs as well as the recruitment of distinct inhibitory types, in addition to GCs (Chapter 4). Finally, in Chapter 5, we began to explore how NA produces long-term changes in the MOB and AOB circuits. Preliminary data indicates that NA produces differential changes in long-term excitability in these regions, with sex-specific changes in excitability in the AOB and a sex-independent increase in excitability in the MOB. Together these studies raise exciting new questions regarding how NA may affect cell- and circuit-level function in these parallel pathways of chemosensory processing, and work that remains to be accomplished will be described here.

Despite the fundamental role of inhibition by GCs as a neurophysiological mechanism underlying olfactory processing in the OB,

very little is known on the intrinsic regulation of GCs that contributes to this function. Here, we described for the first time the presence of the HCN current (Ih) in GCs, and its contribution towards subthreshold resonance. Throughout the brain, HCN channels contribute to network oscillatory dynamics and neuronal excitability, exemplified by the bursting behavior in thalamocortical neurons (McCormick & Pape, 1990), as well as the filtering of synaptic inputs in the context of dendritic integration and computation, in pyramidal neurons of the hippocampus and cortex (Beaulieu-Laroche et al., 2018; Harnett et al., 2015; Magee, 1999). In the MOB, odor discrimination relies on coordinated neuronal activity of output neurons, and network oscillations (Kay, 2014). In this context, GCs have been shown to contribute to gamma frequency (30 – 100 Hz) field oscillations (Lagier et al., 2004), while PGCs contribute to theta range (2 – 12 Hz) oscillations (Fukunaga et al., 2014). As $I_h$ and electrical resonance contributes to spike generation and spike timing (Das & Narayanan, 2017; Gastrein et al., 2011), the contribution of intrinsic theta resonance towards PGC output and its effects on theta frequency network oscillations is relatively clear. However, because MOB GCs are deemed necessary for gamma frequency network oscillations, whether a relationship exists between GCs' intrinsic theta resonance due to $I_h$ and their contribution to gamma oscillations is not known. In the hippocampus, which also utilizes theta and gamma network oscillations in information processing, pyramidal neurons exhibit a theta resonance (Hua Hu

et al., 2009; Narayanan & Johnston, 2007). Electrophysiology and biophysical modeling have suggested that $I_h$-mediated theta resonance shifts the phase coupling between dendritic compartments and the soma with respect to synaptic inputs (Narayanan & Johnston, 2008; Sinha & Narayanan, 2015; Vaidya & Johnston, 2013). Furthermore, $I_h$ may work in tandem with the geometry and capacitance of the hippocampal pyramidal neuron to produce a preference for both theta and gamma-frequency input stimuli for spike generation (Vaidya & Johnston, 2013). Future electrophysiological and dendritic calcium imaging experiments in MC or stimulation of PCx excitatory feedback are necessary to examine how subthreshold resonance in GCs contributes to dendritic integration and whether there is any frequency preference in input stimuli for spike generation or eliciting dendritic spikes.

GCs are axon-less and their output is at the level of their distal dendrites (Jahr & Nicoll, 1980; Price & Powell, 1970). Therefore, the control of dendritic excitability is crucial for GCs in circuit function. Because dendritic patch-clamping is feasible in pyramidal neurons, a number of studies have characterized the distribution of ionic conductances along their dendrites. These studies have shown that the density of $I_h$ increases with distance from the soma (Harnett et al., 2015; Kole, 2006; Magee, 1998; Narayanan & Johnston, 2007). Although, due to their small size, we were unable to directly record the $I_h$ current from GC dendrites, our studies suggested that $I_h$ can contribute to the dendritic output of GCs. However, the relative density of $I_h$

along the somatodendritic axis of GCs is still unresolved. Finer patch clamp methods for dual-patching the soma and distal dendrite of a single GC with 2-photon guidance may allow for electrophysiological measurements of $I_h$ densities with greater spatial resolution (Jayant et al., 2017).

The neuromodulation of $I_h$ has been implicated as a mechanism that can support working memory in cortex (Paspalas et al., 2013; M. Wang et al., 2007). Specifically, the activation of dendritic $\alpha_2$-ARs can increase dendritic excitability in pyramidal neurons by reducing $I_h$, within the time frame required for working memory (Barth et al., 2008; Labarrera et al., 2018; M. Wang et al., 2007). Our results are consistent with the possibility that $\alpha_2$-ARs suppress $I_h$ in GCs via reduction of cAMP, and that this affects dendritic excitability and the degree of inhibition at dendrodendritic synapses. Specifically, $\alpha_2$-ARs suppression $I_h$ produces a negligible change in reciprocal inhibition but enhances lateral inhibition. A main difference between these types of inhibition is the reliance on different mechanisms for calcium signaling; reciprocal inhibition is dependent on the activation of NMDA receptors, and therefore sensitive to voltage-dependent block by Mg++, while lateral

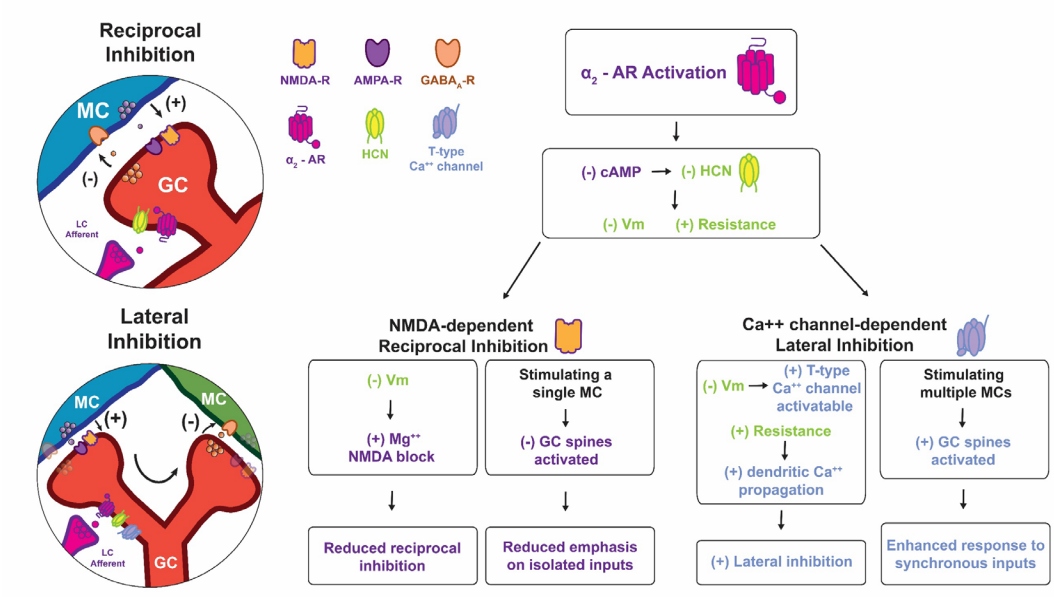


**Figure 1. $\alpha_2$-AR modulation of $I_h$ on two distinct modes of dendrodendritic inhibition**
Theoretical diagrams of experimental findings. Reciprocal inhibition relies on NMDA activation, and a suppression of $I_h$ by $\alpha_2$-ARs would hyperpolarize local compartments, but also increase the compartment resistance, leading to changes in ability to meet requirements for $Mg^{++}$ block removal on NMDA-Rs. This mechanism may de-emphasize lone inputs onto GC distal dendrites. In a model of lateral inhibition, the hyperpolarization from the suppression of $I_h$ would allow low-threshold T-type $Ca^{++}$ channels to enter a more readily-activatable state, and an increase in dendritic resistance would enhance dendritic propagation of $Ca^{++}$ signaling for enhanced lateral inhibition. This mechanism may enhance the GC response to synchronous inputs when optogenetically exciting multiple MCs.

inhibition is dependent on the activation of low-threshold T-type calcium channels. How the activation of $\alpha_2$-ARs, and suppression of $I_h$, affects odor coding *in vivo* has not been explored, but we propose that activation of $\alpha_2$-ARs by NA can serve as a mechanism to sharpen of MC odor tuning by shifting the relative weights of reciprocal versus lateral inhibition. In this model, enhancing lateral inhibition but not reciprocal inhibition would allow strongly activated MCs to more effectively inhibit the activity of MCs

innervated by weakly activated glomeruli, enhancing the signal to noise ratio of the system.

We hypothesize that in the presence of $\alpha_2$-mediated $I_h$ suppression, the dendritic compartments would hyperpolarize, allowing for low threshold calcium channels to enter a more readily activatable state, as well as increase the local membrane resistance. In addition, this hyperpolarization would oppose the effect of depolarization by single inputs onto GC dendritic arbors or spines, which would prevent the unblocking of Mg++ in NMDA receptors. It is also possible that the increase in membrane resistance together with the recruitment of low-threshold calcium channels, can enhance spike probability or the probability of NMDA receptor activation by the coincident activation of multiple inputs. These in turn can affect long-term synaptic plasticity. A previous study has shown that MC-GC synapses can engage in NMDA-dependent spike-time dependent plasticity (Gao & Strowbridge, 2009). Thus, $\alpha_2$-adrenergic modulation of Ih may affect the timing windows for spike-time dependent plasticity (Froemke et al., 2010). In this model, $\alpha_2$-AR modulation of Ih in GCs may serve to widen the spike-time plasticity timing window and increase the likelihood for synapse potentiation. Furthermore, our studies showed that the $\alpha_2$-adrenergic modulation of Ih is present in adult-born neurons during their critical period, thus, it is possible that this mechanism could participate in activity-dependent integration and survival of adult born GCs. Prior work indicated that infusions of $\alpha_2$-AR antagonists in the OB

affected abGC survival (Moreno et al., 2012), however, these studies failed to dissociate the contribution of other adrenergic receptors on abGC functional integration and survival. Therefore, a more direct way to test whether $\alpha_2$-ARs affect abGC integration and survival, would be to selectively delete the $\alpha_2$-AR gene in abGCs migrating along the rostral migratory stream, and subsequently assess cell physiology and survival.

Generally, the LC exhibits three modes of firing. During sleep, the activity of the LC is reduced, but after the transition to wakefulness and low arousal states, LC neurons engage in tonic firing (1 - 6 Hz) (Atzori et al., 2016; Foote et al., 1980); in response to salient stimuli, or novel objects and contexts, LC neurons can engage in phasic burst firing (10 - 15 Hz) (Aston-Jones & Bloom, 1981; Clayton et al., 2004); and during states of heightened arousal, stress, or anxiety, LC neurons can consistently fire over 10 Hz (McCall et al., 2015; Weiss et al., 1994). Furthermore, microdialysis experiments have shown that stimulation of the LC by 10 Hz stimulus train can increase local NA concentrations by over 170% in prefrontal cortex (Florin-Lechner et al., 1996). Amongst adrenergic receptor subtypes, $\alpha_2$-ARs exhibit the highest binding affinity to NA, followed by $\alpha_1$-ARs, with β-ARs exhibiting the lowest sensitivity (Molinoff, 1984; Rang, 2012), suggesting that different modes of LC activity may selectively activate different receptor subtypes. Thus, given that local concentrations of NA correlate with LC

spiking activity (Florin-Lechner et al., 1996), recruitment of $\alpha_2$- and $\alpha_1$- ARs and the state of OB circuit activity could depend on LC activity.

It is possible that in a state of low arousal, in which the animal is awake but not actively engaged in a task, the predominant action of NA on the OB circuit is mediated by $\alpha_2$-ARs. As mentioned above, activation of this receptor could favor the enhancement of lateral inhibition over reciprocal inhibition. We propose that this inhibition may allow for higher fidelity in the relaying of salient signals by the MCs to the cortex, enabling the animal to better notice the presence of potentially relevant stimuli. This mode would place a higher emphasis on simple detection over discrimination of odors. Upon odor detection, the activity of the LC and attention-related circuits increases, driving active odor investigation and discrimination. When the animal is attentively engaged in active odor sampling, the phasic LC bursting leads to an increase in the NA concentration in the OB, which now can activate both $\alpha_2$- and $\alpha_1$-ARs, thereby dramatically enhancing overall inhibitory tone onto MCs via the $\alpha_1$-ARs. In this context, active odor investigation should also dramatically increase the excitation onto MCs, with sniff rates increasing from baseline levels of 2 to 4 Hz up to 12 Hz (Díaz-Quesada et al., 2018; Manabe & Mori, 2013). Therefore, we surmise that during active odor investigation or when the animal engages in an olfactory-related task (e.g. odor discrimination in an go-no/go paradigm), the enhancement of inhibitory tone via $\alpha_1$-ARs counteracts the increase in excitatory drive from the OSNs onto the MCs,

balancing overall excitation and inhibition in the circuit. In support of this possibility *in vivo* studies have shown that GCs exhibit higher baseline firing rates during awake states compared to anesthetized states (Cazakoff et al., 2014), and the stimulation of the LC suppresses the response of MCs to odors (Shea et al., 2008). These experiments were accomplished in head-fixed animals, therefore, future studies should be conducted in the freely-behaving animals, to examine MC and GC activity in the context of locomotion, which is directly associated with LC activity and general increased adrenergic tone (Joshi et al., 2016; Polack et al., 2013). In fact, several recent studies highlight the role of motor function in sensory processing (Iwata et al., 2017; Polack et al., 2013; Ranade et al., 2013; Schneider et al., 2014). In the olfactory system, the activity of the OB can be modulated by whisker and nose movements in the absence of odor stimuli (Musall et al., 2019).

Given the varying nature of LC activity and the fast time scales in which state-dependent changes in global brain activity occur, it is crucial to determine with fine temporal resolution the fluctuations in NA concentrations in the OB during tasks. As head-mounted fluorescence imaging techniques in freely behaving animals and new fluorescent noradrenaline sensors are developed and refined (Feng et al., 2019), we will be able to examine this during various behavioral states and specific behaviors such as odor investigation and learning, general locomotion, stress, or various social

| | AOB | | | | MOB | | | |
|---|---|---|---|---|---|---|---|---|
| | MC | GC | extGC | PGC | MC | GC | FS | PGC |
| $\alpha_2$ | ? | ? | ? | ? | ? | + | ? | ? |
| $\alpha_1$ | - | + | + | - | + | + | - | + |
| β | - | - | - | - | + | - | - | - |

**Table 1. Summary of known adrenergic receptor expression across cell types between AOB and MOB**
Selective pharmacology with agonists and antagonists of adrenergic receptors on the presence (+) or absence (-) of adrenergic receptor subtypes across interneuron populations and principal neurons between the MOB and AOB in which an electrophysiological effect has been observed in our present studies.

behaviors (e.g. mating and aggression). These experiments can lead to a better understanding of the neural activity in the OB in relation to general noradrenergic modulation and behavioral context.

While we have shown that GCs express both $\alpha_2$- and $\alpha_1$- ARs, it is still unclear whether other inhibitory interneurons express $\alpha_2$- ARs (Table 1). $\alpha_2$-AR activation has been shown to suppress Ih in a subtype of PGC that also are dopaminergic (Pignatelli et al., 2013), but whether it acts similarly in other interneurons expressing Ih, such as the FS and glomerular GAD2+ PGCs of the MOB or interneurons of the AOB is unknown (Table 1). Interestingly, in all the inhibitory interneurons of the MOB we have examined, the excitation elicited by NA occurs by activation of $\alpha_1$-ARs, while an excitatory effect by activation of β-ARs occurs only in MOB MCs. This is similar to cortex where multiple classes of inhibitory interneurons have been shown to exhibit an

intrinsic $\alpha_1$- but not β-AR excitation (Kawaguchi & Shindou, 1998). The $\alpha_1$-adrenergic modulation of inhibitory interneurons in cortical and subcortical areas has been proposed to act as a gain control mechanism in sensory brain areas (Polack et al., 2013; Rodenkirch et al., 2019), therefore, it is possible that the general role of LC activity and $\alpha_1$-adrenergic modulation of broad inhibitory interneuron populations in the OB, serves a similar purpose.

In addition to general physiological arousal, noradrenergic modulation is involved in social behaviors and is recruited in the OB in kin recognition and long-term plasticity in social odor learning (Brennan & Keverne, 1997). In our studies examining long-term changes in excitability produced by NA, MOB MCs exhibited an increase in excitability with higher stimulus-elicited spiking. This could serve as a potential mechanism underlying the observed increase in odor responses in MCs in females post-parturition, using calcium imaging *in vivo* (Vinograd et al., 2017). Furthermore, in new born rats, β-ARs are necessary for odor preference learning and long-term plasticity (Sullivan et al., 1989, 1992; Sullivan & Wilson, 1991). Therefore, it is possible that in adult mice, β-ARs also mediate the long-term increase in excitability in MOB MCs. Future experiments will test this possibility by using selective blockade of β-ARs *in vivo*, and also assess the intracellular signaling pathways that mediate this effect. In hippocampal CA1, β-ARs can facilitate LTP through a cAMP-dependent mechanism that involves the downstream activation of protein kinase A or C (PKA, PKC) depending on the plasticity induction protocol

(Marzo et al., 2009; Winder et al., 1999). Furthermore, increasing cAMP by activation of adenylyl cyclase or activation of β-ARs can enhance voltage-gated sodium currents, effectively lowering spike thresholds (Matsuda et al., 1992; Ono et al., 1993). Activation of β-AR has been shown to enhance the persistent sodium currents in external tufted cells (F.-W. Zhou et al., 2016), we will also test whether this conductance is also involved in the observed increase in long-term intrinsic excitability in MCs.

Interestingly, in the AOB, the long-term changes in excitability produced by NA were sexually dimorphic; MCs of females showed a reduction in excitability while males showed an increase in excitability. Because we did not observe a direct effect of NA on the AOB MCs, we hypothesize the source of this difference may reside in the $\alpha_1$-AR excitation of inhibitory interneurons, including GCs and extGCs. Adrenergic excitation of GCs in the AOB dramatically increases inhibition onto MCs (Araneda & Firestein, 2006), and microdialysis studies have shown that during mating, both NA and GABA is highly increased in the AOB (Brennan et al., 1995). Expression of metabotropic $GABA_B$ receptors was observed in the MC layer of AOB (Panzanelli et al., 2004), it is possible that a surge of GABAergic input onto AOB MCs activates $GABA_B$ receptors. Activation of these receptors has been shown to affect synaptic plasticity in cortical circuits (Ainsworth et al., 2016), which could be mediated by any of the changes in conductances and cAMP signaling associated with their activity (Chalifoux & Carter, 2011).

However, the function of $GABA_B$ receptors on AOB MCs has not been characterized. In the AOB MCs of females, the observed decrease in the input resistance, which could be attributed to the enhancement of a leak potassium conductance, and calcium suppression could decrease spike probability across a long stimulus train. Whether $GABA_B$ receptor activation is necessary is still puzzling because the plasticity was not observed in males, as MCs of both females and males receive an increase in inhibition with NA in our slice experiments. It should be noted that it is not known if a sex difference in the expression $GABA_B$ in the AOB exists.

Regarding the AOB MCs from males, experiments involving GPCRs in other regions of the central nervous system may provide an insight. When cerebellar Golgi cells or neurons in the vestibular nuclei are hyperpolarized by activation of group 2 metabotropic glutamate receptors (mGluR2) or direct current injections, this hyperpolarization is followed by a prolonged enhancement of spike rates above control levels, and a decrease in the action potential after-hyperpolarization (Hull et al., 2013; A. B. Nelson et al., 2003). In these examples, during the prolonged hyperpolarization, calmodulin-dependent protein kinase II (CaMKII) activity is dramatically reduced, and in turn provides a long-term reduction of BK-type calcium-activated potassium currents (A. B. Nelson et al., 2005; van Welie & du Lac, 2011). This hypothesis could be tested by examining action potential waveforms and using CaMKII inhibitors, which are expected to mimic the NA-

induced increase in excitability in the MCs of males. Nevertheless, this still would not explain the effect in females, in which the majority of MCs from females show a hyperpolarization and a decrease in stimulus-elicited spiking after NA, instead of increase in excitability. This suggests that sexual differences in other cellular properties of MCs in the AOB are still unknown. One method to find potential differences would be to use RNA sequencing of AOB MC populations between males and female to find what genes are actively expressed by the cells in adult animals. Furthermore, single-cell RNA sequencing of AOB cell populations after mating in females or agonistic encounters in males may also provide insights into the mechanisms underlying our plasticity experiments.

Another avenue for future research is to examine how noradrenergic modulation is affected by the neuroendocrine system. The cyclical fluctuations of sex hormones in females can interact with circuit and synaptic plasticity mechanisms in the brain. For example, estrogens produce changes in spine density of hippocampal pyramidal neurons through a NMDA receptor-dependent mechanism (Woolley et al., 1990), as well as nitric oxide signaling in the barrel cortex for experience-dependent potentiation with whisker stimulation (Dachtler et al., 2012). In the olfactory bulb, estrogen receptors are expressed in cells of both MOB and AOB across all layers with differential expression of estrogen receptor (ER) α and β isoforms. The ER-α and -β are expressed in the MOB but only ER-β expressed in the AOB (Guo et al., 2001;

Hoyk et al., 2014). Activation of ER-β in the MOB prolonged odor memory in an olfactory habituation paradigm, however no sex differences were observed (Samuel Dillon et al., 2013). In contrast, immediate early gene staining in AOB with estrogen or testosterone treatments showed sex differences in the number of cells activated in the MC layer when the animal was presented with male or female bedding (Halem et al., 2001). Whether there is an interaction between noradrenergic modulation in the MOB and AOB and sex hormone modulation is unknown. In other systems, altering levels of sex hormones in the brain can alter the expression levels of neuromodulatory receptors in a region-specific manner (Biegon et al., 1983). Castration of adult male rats leads to an increase in $\alpha_2$-AR mRNA expression in brain stem regions but a decrease in frontal cortex and these effects are reversed by testosterone injection (Dygalo et al., 2002). In ovariectomized female rats, estrogen treatment increases $\alpha_1$-AR mRNA expression in the hypothalamus pre-optic area, but decreases expression in cortex (Karkanias et al., 1996). Therefore, more studies are necessary to determine sex-specific expression levels of adrenergic receptors between in the AOB and MOB. In addition, one method to examine whether there is an interaction between noradrenergic modulation and sex hormones with regards to the long-term plasticity in the AOB between males and females is to repeat the slice electrophysiology experiments in ovariectomized females and castrated males. Finally, *in situ*

*hybridization* for adrenergic receptor mRNAs could test whether removal of sex hormones affects adrenergic receptor expression.

In conclusion, across the AOB and MOB, the combination of cell-intrinsic properties with extrinsic noradrenergic modulation produce cell- and region-specific differences in function and plasticity. Remaining questions include: 1) How does Ih-mediated electrical resonance in GCs of the OB affect odor processing and network oscillations in both regions? 2) How does the $\alpha_2$-AR modulation of Ih in GCs affect synaptic plasticity and functional integration? 3) Under what behavioral contexts does the activation of $\alpha_2$- and $\alpha_1$-ARs occur? 4) What are the cellular mechanisms that mediate the long-term plasticity in AOB and MOB MCs and what is the role of the sexual dimorphism observed in the AOB but not in the MOB?

# Bibliography


Accili, E. a, Proenza, C., Baruscotti, M., & DiFrancesco, D. (2002). From funny current to HCN channels: 20 years of excitation. *News in Physiological Sciences : An International Journal of Physiology Produced Jointly by the International Union of Physiological Sciences and the American Physiological Society*, *17*(6), 32–37. http://www.ncbi.nlm.nih.gov/pubmed/11821534

Ainsworth, M., Lee, S., Kaiser, M., Simonotto, J., Kopell, N. J., & Whittington, M. A. (2016). GABAB receptor-mediated, layer-specific synaptic plasticity reorganizes gamma-frequency neocortical response to stimulation. *Proceedings of the National Academy of Sciences of the United States of America*, *113*(19), E2721–E2729. https://doi.org/10.1073/pnas.1605243113

Aizenman, C. D., & Linden, D. J. (1999). Regulation of the rebound depolarization and spontaneous firing patterns of deep nuclear neurons in slices of rat cerebellum. *Journal of Neurophysiology*, *82*(4), 1697–1709. http://www.ncbi.nlm.nih.gov/pubmed/10515960

Altman, J. (1962). Are new neurons formed in the brains of adult mammals? *Science (New York, N.Y.)*, *135*(3509), 1127–1128. https://doi.org/10.1126/science.135.3509.1127

Altman, J., & Das, G. D. (1965). Post-natal origin of microneurones in the rat brain. *Nature*, *207*(5000), 953–956. https://doi.org/10.1038/207953a0

Angelo, K., & Margrie, T. W. (2011). Population diversity and function of hyperpolarization-activated current in olfactory bulb mitral cells. *Scientific Reports*, *1*, 50. https://doi.org/10.1038/srep00050

Angelotti, T. P., & Macdonald, R. L. (1993). Assembly of GABAA receptor subunits: alpha 1 beta 1 and alpha 1 beta 1 gamma 2S subunits produce unique ion channels with dissimilar single-channel properties. *The Journal of Neuroscience : The Official Journal of the Society for Neuroscience*, *13*(4), 1429–1440. https://doi.org/10.1007/1-4020-4733-9_2

Araneda, R. C., & Firestein, S. (2006). Adrenergic enhancement of inhibitory transmission in the accessory olfactory bulb. *The Journal of Neuroscience : The Official Journal of the Society for Neuroscience*, *26*(12), 3292–3298. https://doi.org/10.1523/JNEUROSCI.4768-05.2006

Araneda, R. C., Kini, a D., & Firestein, S. (2000). The molecular receptive range of an odorant receptor. *Nature Neuroscience*, *3*(12), 1248–1255. https://doi.org/10.1038/81774

Araneda, R. C., Peterlin, Z., Zhang, X., Chesler, A., & Firestein, S. (2004). A pharmacological profile of the aldehyde receptor repertoire in rat olfactory epithelium. *The Journal of Physiology*, *555*(Pt 3), 743–756. https://doi.org/10.1113/jphysiol.2003.058040

Aston-Jones, G., & Bloom, F. E. (1981). Norepinephrine-containing locus coeruleus neurons in behaving rats exhibit pronounced responses to non-noxious environmental stimuli. *The Journal of Neuroscience : The Official Journal of the Society for Neuroscience*, *1*(8), 887–900. http://www.ncbi.nlm.nih.gov/pubmed/7346593

Aston-Jones, G., & Cohen, J. D. (2005). AN INTEGRATIVE THEORY OF LOCUS COERULEUS-NOREPINEPHRINE FUNCTION: Adaptive Gain and Optimal Performance. *Annual Review of Neuroscience*, *28*(1), 403–450. https://doi.org/10.1146/annurev.neuro.28.061604.135709

Atzori, M., Cuevas-Olguin, R., Esquivel-Rendon, E., Garcia-Oscos, F., Salgado-Delgado, R. C., Saderi, N., Miranda-Morales, M., Treviño, M., Pineda, J. C., & Salgado, H. (2016). Locus Ceruleus Norepinephrine Release: A Central Regulator of CNS Spatio-Temporal Activation? In *Frontiers in Synaptic Neuroscience* (Vol. 8, Issue August). https://doi.org/10.3389/fnsyn.2016.00025

Ball, G. F. (1994). Neurochemical Specializations Associated with Vocal Learning and Production in Songbirds and Budgerigars. *Brain, Behavior and Evolution*, *44*(4–5), 234–246. https://doi.org/10.1159/000113579

Banerjee, A., Marbach, F., Anselmi, F., Koh, M. S., Davis, M. B., Garcia da Silva, P., Delevich, K., Oyibo, H. K., Gupta, P., Li, B., & Albeanu, D. F. (2015). An Interglomerular Circuit Gates Glomerular Output and Implements Gain Control in the Mouse Olfactory Bulb. *Neuron*, *87*(1), 193–207. https://doi.org/10.1016/j.neuron.2015.06.019

Bangasser, D. A., Eck, S. R., & Ordoñes Sanchez, E. (2019). Sex differences in stress reactivity in arousal and attention systems. *Neuropsychopharmacology*, *44*(1), 129–139. https://doi.org/10.1038/s41386-018-0137-2

Barth, A. M. I., Vizi, E. S., & Lendvai, B. (2007). Noradrenergic enhancement of Ca2+ responses of basal dendrites in layer 5 pyramidal neurons of the prefrontal cortex. *Neurochemistry International*, *51*(5), 323–327. https://doi.org/10.1016/j.neuint.2007.05.008

Barth, A. M. I., Vizi, E. S., Zelles, T., & Lendvai, B. (2008). α 2 -Adrenergic Receptors Modify Dendritic Spike Generation Via HCN Channels in the Prefrontal Cortex. *Journal of Neurophysiology*, *99*(1), 394–401. https://doi.org/10.1152/jn.00943.2007

Bartos, M., Vida, I., & Jonas, P. (2007). Synaptic mechanisms of synchronized gamma oscillations in inhibitory interneuron networks. *Nature Reviews Neuroscience*, *8*(1), 45–56. https://doi.org/10.1038/nrn2044

Bathellier, B., Buhl, D. L., Accolla, R., & Carleton, A. (2008). Dynamic Ensemble Odor Coding in the Mammalian Olfactory Bulb: Sensory Information at Different Timescales. *Neuron*, *57*(4), 586–598. https://doi.org/10.1016/j.neuron.2008.02.011

Batista-Brito, R., Close, J., Machold, R., & Fishell, G. (2008). The Distinct Temporal Origins of Olfactory Bulb Interneuron Subtypes. *Journal of Neuroscience*, *28*(15), 3966–3975. https://doi.org/10.1523/JNEUROSCI.5625-07.2008

Bauer, S., Moyse, E., Jourdan, F., Colpaert, F., Martel, J. C., & Marien, M. (2003). Effects of

the α2-adrenoreceptor antagonist dexefaroxan on neurogenesis in the olfactory bulb of the adult rat in vivo: Selective protection against neuronal death. *Neuroscience*, *117*(2), 281–291. https://doi.org/10.1016/S0306-4522(02)00757-1

Beaulieu-Laroche, L., Toloza, E. H. S., van der Goes, M. S., Lafourcade, M., Barnagian, D., Williams, Z. M., Eskandar, E. N., Frosch, M. P., Cash, S. S., & Harnett, M. T. (2018). Enhanced Dendritic Compartmentalization in Human Cortical Neurons. *Cell*, *175*(3), 643-651.e14. https://doi.org/10.1016/j.cell.2018.08.045

Bekkers, J. M., & Suzuki, N. (2013). Neurons and circuits for odor processing in the piriform cortex. *Trends in Neurosciences*, *36*(7), 429–438. https://doi.org/10.1016/j.tins.2013.04.005

Belluzzi, O., Benedusi, M., Ackman, J., & LoTurco, J. J. (2003). Electrophysiological differentiation of new neurons in the olfactory bulb. *The Journal of Neuroscience : The Official Journal of the Society for Neuroscience*, *23*(32), 10411–10418. https://doi.org/10.1371/journal.pone.0037742

Ben-Shaul, Y., Katz, L. C., Mooney, R., & Dulac, C. (2010). In vivo vomeronasal stimulation reveals sensory encoding of conspecific and allospecific cues by the mouse accessory olfactory bulb. *Proceedings of the National Academy of Sciences*, *107*(11), 5172–5177. https://doi.org/10.1073/pnas.0915147107

Benarroch, E. E. (2013). HCN channels: function and clinical implications. *Neurology*, *80*(3), 304–310. https://doi.org/10.1212/WNL.0b013e31827dec42

Berridge, C. W., & Waterhouse, B. D. (2003). The locus coeruleus-noradrenergic system: Modulation of behavioral state and state-dependent cognitive processes. *Brain Research Reviews*, *42*(1), 33–84. https://doi.org/10.1016/S0165-0173(03)00143-7

Beshel, J., Kopell, N., & Kay, L. M. (2007). Olfactory bulb gamma oscillations are enhanced with task demands. *Journal of Neuroscience*, *27*(31), 8358–8365. https://doi.org/10.1523/JNEUROSCI.1199-07.2007

Biegon, A., Reches, A., Snyder, L., & McEwen, B. S. (1983). Serotonergic and noradrenergic receptors in the rat brain: Modulation by chronic exposure to ovarian hormones. *Life Sciences*, *32*(17), 2015–2021. https://doi.org/10.1016/0024-3205(83)90053-X

Binns, K. E., & Brennan, P. A. (2005). Changes in electrophysiological activity in the accessory olfactory bulb and medial amygdala associated with mate recognition in mice. *European Journal of Neuroscience*, *21*(9), 2529–2537. https://doi.org/10.1111/j.1460-9568.2005.04090.x

Bokil, H., Andrews, P., Kulkarni, J. E., Mehta, S., & Mitra, P. P. (2010). Chronux: A platform for analyzing neural signals. *Journal of Neuroscience Methods*, *192*(1), 146–151. https://doi.org/10.1016/j.jneumeth.2010.06.020

Bouret, S., & Sara, S. J. (2004). Reward expectation, orientation of attention and locus coeruleus-medial frontal cortex interplay during learning. *European Journal of Neuroscience*, *20*(3), 791–802. https://doi.org/10.1111/j.1460-9568.2004.03526.x

Boyd, A. M., Sturgill, J. F., Poo, C., & Isaacson, J. S. (2012). Cortical feedback control of olfactory bulb circuits. *Neuron*, *76*(6), 1161–1174. https://doi.org/10.1016/j.neuron.2012.10.020

Brennan, P. A., & Kendrick, K. M. (2006). Mammalian social odours: Attraction and individual recognition. *Philosophical Transactions of the Royal Society B: Biological Sciences*, *361*(1476), 2061–2078. https://doi.org/10.1098/rstb.2006.1931

Brennan, P. A., Kendrick, K. M., & Keverne, E. B. (1995). Neurotransmitter release in the accessory olfactory bulb during and after the formation of an olfactory memory in mice. *Neuroscience*, *69*(4), 1075–1086. https://doi.org/10.1016/0306-4522(95)00309-7

Brennan, P. A., & Keverne, E. B. (1997). Neural mechanisms of mammalian olfactory learning. *Progress in Neurobiology*, *51*(4), 457–481. https://doi.org/10.1016/S0301-0082(96)00069-X

Brennan, P. A., & Keverne, E. B. (2014). Biological complexity and adaptability of simple mammalian olfactory memory systems. *Neuroscience & Biobehavioral Reviews*. https://doi.org/10.1016/j.neubiorev.2014.10.020

Brennan, P. A., Schellinck, H. M., De La Riva, C., Kendrick, K. M., & Keverne, E. B. (1998). Changes in neurotransmitter release in the main olfactory bulb following an olfactory conditioning procedure in mice. *Neuroscience*, *87*(3), 583–590. https://doi.org/10.1016/S0306-4522(98)00182-1

Breton-Provencher, V., Bakhshetyan, K., Hardy, D., Bammann, R. R., Cavarretta, F., Snapyan, M., Côté, D., Migliore, M., & Saghatelyan, A. (2016). Principal cell activity induces spine relocation of adult-born interneurons in the olfactory bulb. *Nature Communications*, *7*, 12659. https://doi.org/10.1038/ncomms12659

Brickley, S. G., Cull-Candy, S. G., & Farrant, M. (1999). Single-channel properties of synaptic and extrasynaptic GABA(A) receptors suggest differential targeting of receptor subtypes. *Journal of Neuroscience*, *19*(8), 2960–2973. https://doi.org/10.1523/jneurosci.19-08-02960.1999

Brignall, A. C., & Cloutier, J.-F. (2015). Neural map formation and sensory coding in the vomeronasal system. *Cellular and Molecular Life Sciences*. https://doi.org/10.1007/s00018-015-2029-5

Brody, C. D. and J. J. H. (2003). *Simple Networks for Spike-Timing-Based\nComputation: with applications to olfactory processing. 37*, 843–852.

Buck, L., & Axel, R. (1991). A novel multigene family may encode odorant receptors: a molecular basis for odor recognition. *Cell*, *65*(1), 175–187. https://doi.org/10.1016/0092-8674(91)90418-X

Burton, S. D., & Urban, N. N. (2015). Rapid Feedforward Inhibition and Asynchronous Excitation Regulate Granule Cell Activity in the Mammalian Main Olfactory Bulb. *Journal of Neuroscience*, *35*(42), 14103–14122. https://doi.org/10.1523/JNEUROSCI.0746-15.2015

Bywalez, W. G., Patirniche, D., Rupprecht, V., Stemmler, M., Herz, A. V. M., P??lfi, D., R??zsa, B., & Egger, V. (2015). Local postsynaptic voltage-gated sodium channel activation in dendritic spines of olfactory bulb granule cells. *Neuron*, *85*(3), 590–601. https://doi.org/10.1016/j.neuron.2014.12.051

Cang, J., & Isaacson, J. S. (2003). In vivo whole-cell recording of odor-evoked synaptic transmission in the rat olfactory bulb. *The Journal of Neuroscience : The Official Journal of the Society for Neuroscience*, *23*(10), 4108–4116. https://doi.org/23/10/4108 [pii]

Cansler, H. L., Maksimova, M. A., & Meeks, J. P. (2017). Experience-dependent plasticity in accessory olfactory bulb interneurons following male–male social interaction. *Journal of Neuroscience*, *37*(30), 7240–7252. https://doi.org/10.1523/JNEUROSCI.1031-17.2017

Cardin, J. A. (2018). Inhibitory Interneurons Regulate Temporal Precision and Correlations in Cortical Circuits. *Trends in Neurosciences*, *41*(10), 689–700. https://doi.org/10.1016/j.tins.2018.07.015

Carleton, A., Petreanu, L. T., Lansford, R., Alvarez-Buylla, A., & Lledo, P.-M. (2003). Becoming a new neuron in the adult olfactory bulb. *Nature Neuroscience*, *6*(5), 507–518. https://doi.org/10.1038/nn1048

Carr, D. B., Andrews, G. D., Glen, W. B., & Lavin, A. (2007). α 2 -Noradrenergic receptors activation enhances excitability and synaptic integration in rat prefrontal cortex pyramidal neurons via inhibition of HCN currents. *The Journal of Physiology*, *584*(2), 437–450. https://doi.org/10.1113/jphysiol.2007.141671

Castelino, C. B., & Schmidt, M. F. (2010). What birdsong can teach us about the central noradrenergic system. *Journal of Chemical Neuroanatomy*, *39*(2), 96–111. https://doi.org/10.1016/j.jchemneu.2009.08.003

Castillo, P., & Carleton, A. (1999). Multiple and opposing roles of cholinergic transmission in the main olfactory bulb. *The Journal of …*, *19*(21), 9180–9191. http://www.ncbi.nlm.nih.gov/pubmed/10531421

Castro, J. B., Hovis, K. R., & Urban, N. N. (2007). Recurrent dendrodendritic inhibition of accessory olfactory bulb mitral cells requires activation of group I metabotropic glutamate receptors. *The Journal of Neuroscience : The Official Journal of the Society for Neuroscience*, *27*(21), 5664–5671. https://doi.org/10.1523/JNEUROSCI.0613-07.2007

Cazakoff, B. N., Lau, B. Y. B., Crump, K. L., Demmer, H. S., & Shea, S. D. (2014). Broadly tuned and respiration-independent inhibition in the olfactory bulb of awake mice. *Nature Neuroscience*, *October 2013*. https://doi.org/10.1038/nn.3669

Chalifoux, J. R., & Carter, A. G. (2011). GABAB receptor modulation of synaptic function. *Current Opinion in Neurobiology*, *21*(2), 339–344. https://doi.org/10.1016/j.conb.2011.02.004

Chamero, P., Leinders-Zufall, T., & Zufall, F. (2012). From genes to social communication: Molecular sensing by the vomeronasal organ. *Trends in Neurosciences*, *35*(10), 597–606. https://doi.org/10.1016/j.tins.2012.04.011

Chow, C. C., White, J. A., Ritt, J., & Kopell, N. (1998). Frequency control in synchronized networks of inhibitory neurons. *Journal of Computational Neuroscience*, *5*(4), 407–420. https://doi.org/10.1023/A:1008889328787

Cichy, a., Ackels, T., Tsitoura, C., Kahan, a., Gronloh, N., Sochtig, M., Engelhardt, C. H., Ben-Shaul, Y., Muller, F., Spehr, J., & Spehr, M. (2015). Extracellular pH Regulates Excitability of Vomeronasal Sensory Neurons. *Journal of Neuroscience*, *35*(9), 4025–4039. https://doi.org/10.1523/JNEUROSCI.2593-14.2015

Ciombor, K. J., Ennis, M., & Shipley, M. T. (1999). Norepinephrine increases rat mitral cell excitatory responses to weak olfactory nerve input via alpha-1 receptors in vitro. *Neuroscience*, *90*(2), 595–606. https://doi.org/10.1016/S0306-4522(98)00437-0

Clayton, E. C., Rajkowski, J., Cohen, J. D., & Aston-Jones, G. (2004). Phasic activation of monkey locus ceruleus neurons by simple decisions in a forced-choice task. *Journal of Neuroscience*, *24*(44), 9914–9920. https://doi.org/10.1523/JNEUROSCI.2446-04.2004

Craven, K. B., & Zagotta, W. N. (2006). CNG and HCN channels: two peas, one pod. *Annual Review of Physiology*, *68*, 375–401. https://doi.org/10.1146/annurev.physiol.68.040104.134728

Dachtler, J., Hardingham, N. R., & Fox, K. (2012). The role of nitric oxide synthase in cortical plasticity is sex specific. *Journal of Neuroscience*, *32*(43), 14994–14999. https://doi.org/10.1523/JNEUROSCI.3189-12.2012

Das, A., & Narayanan, R. (2017). Theta-frequency selectivity in the somatic spike triggered average of rat hippocampal pyramidal neurons is dependent on HCN channels. *Journal of Neurophysiology*, *250*, jn.00356.2017. https://doi.org/10.1152/jn.00356.2017

De Koninck, Y., & Mody, I. (1994). Noise analysis of miniature IPSCs in adult rat brain slices: properties and modulation of synaptic GABAA receptor channels. *Journal of Neurophysiology*, *71*(4), 1318–1335. http://jn.physiology.org/cgi/reprint/71/4/1318%5Cnpapers3://publication/uuid/A5C39871-0560-448C-B518-69CB49A24136

Díaz-Quesada, M., Youngstrom, I. A., Tsuno, Y., Hansen, K. R., Economo, M. N., & Wachowiak, M. (2018). Inhalation frequency controls reformatting of mitral/tufted cell odor representations in the olfactory bulb. *Journal of Neuroscience*, *38*(9), 2189–2206. https://doi.org/10.1523/JNEUROSCI.0714-17.2018

Dibattista, M., Mazzatenta, A., Grassi, F., Tirindelli, R., & Menini, A. (2008). Hyperpolarization-activated cyclic nucleotide-gated channels in mouse vomeronasal sensory neurons. *Journal of Neurophysiology*, *100*(2), 576–586. https://doi.org/10.1152/jn.90263.2008

Dixon, C., Sah, P., Lynch, J. W., & Keramidas, A. (2014). GABAa receptor α and γ subunits shape synaptic currents via different mechanisms. *Journal of Biological Chemistry*, *289*(9), 5399–5411. https://doi.org/10.1074/jbc.M113.514695

Dluzen, D. E., Muraoka, S., Engelmann, M., Ebner, K., & Landgraf, R. (2000). Oxytocin induces preservation of social recognition in male rats by activating α-adrenoceptors of

the olfactory bulb. *European Journal of Neuroscience*, *12*(2), 760–766. https://doi.org/10.1046/j.1460-9568.2000.00952.x

Doucette, W., Milder, J., & Restrepo, D. (2007). Adrenergic modulation of olfactory bulb circuitry affects odor discrimination. *Learn Mem*, *14*(8), 539–547. https://doi.org/10.1101/lm.606407

Doving, Kjell B;Trotier, D. (1998). Strucure and functions of the vomeronasal organ. *The Journal of Experimental Biology*, *201*, 2913–2925.

Doyle, W. I., & Meeks, J. P. (2017). Heterogeneous effects of noradrenaline on spontaneous and stimulus-driven activity in the male accessory olfactory bulb. *Journal of Neurophysiology*, jn.00871.2016. https://doi.org/10.1152/jn.00871.2016

Dulac, C., & Wagner, S. (2006). Genetic Analysis of Brain Circuits Underlying Pheromone Signaling. *Annual Review of Genetics*, *40*(1), 449–467. https://doi.org/10.1146/annurev.genet.39.073003.093937

Dygalo, N. N., Kalinina, T. S., Sournina, N. Y., & Shishkina, G. T. (2002). Effects of testosterone on alpha2A-adrenergic receptor expression in the rat brain. *Psychoneuroendocrinology*, *27*(5), 585–592. https://doi.org/10.1016/S0306-4530(01)00094-4

Economo, M. N., Hansen, K. R., Economo, M. N., Hansen, K. R., & Wachowiak, M. (2016). Control of Mitral / Tufted Cell Output by Selective Inhibition among Olfactory Bulb Glomeruli Article Control of Mitral / Tufted Cell Output by Selective Inhibition among Olfactory Bulb Glomeruli. *Neuron*, 1–15. https://doi.org/10.1016/j.neuron.2016.06.001

Egger, V., Svoboda, K., & Mainen, Z. F. (2003). Mechanisms of lateral inhibition in the olfactory bulb: efficiency and modulation of spike-evoked calcium influx into granule cells. *The Journal of Neuroscience : The Official Journal of the Society for Neuroscience*, *23*(20), 7551–7558. https://doi.org/23/20/7551 [pii]

Egger, V., Svoboda, K., & Mainen, Z. F. (2005). Dendrodendritic synaptic signals in olfactory bulb granule cells: local spine boost and global low-threshold spike. *The Journal of Neuroscience : The Official Journal of the Society for Neuroscience*, *25*(14), 3521–3530. https://doi.org/10.1523/JNEUROSCI.4746-04.2005

Engbers, J. D. T., Anderson, D., Tadayonnejad, R., Mehaffey, W. H., Molineux, M. L., & Turner, R. W. (2011). Distinct roles for $I_T$ and $I_H$ in controlling the frequency and timing of rebound spike responses. *The Journal of Physiology*, *589*(22), 5391–5413. https://doi.org/10.1113/jphysiol.2011.215632

Fallon, J. H., & Moore, R. Y. (1978). Catecholamine innervation of the basal forebrain III. Olfactory bulb, anterior olfactory nuclei, olfactory tubercle and piriform cortex. *Journal of Comparative Neurology*, *180*(3), 533–544. https://doi.org/10.1002/cne.901800309

Fan, Y., Fricker, D., Brager, D. H., Chen, X., Lu, H.-C., Chitwood, R. a, & Johnston, D. (2005). Activity-dependent decrease of excitability in rat hippocampal neurons through increases in I(h). *Nature Neuroscience*, *8*(11), 1542–1551. https://doi.org/10.1038/nn1568

Feng, J., Zhang, C., Lischinsky, J. E., Jing, M., Zhou, J., Wang, H., Zhang, Y., Dong, A., Wu, Z., Wu, H., Chen, W., Zhang, P., Zou, J., Hires, S. A., Zhu, J. J., Cui, G., Lin, D., Du, J., & Li, Y. (2019). A Genetically Encoded Fluorescent Sensor for Rapid and Specific In Vivo Detection of Norepinephrine. *Neuron*, *102*(4), 745-761.e8. https://doi.org/10.1016/j.neuron.2019.02.037

Firestein, S. (2001). How the olfactory system makes sense of scents. *Nature*, *413*(6852), 211–218. https://doi.org/10.1038/35093026

Fletcher, M. L., & Chen, W. R. (2010). Neural correlates of olfactory learning: Critical role of centrifugal neuromodulation. *Learning & Memory (Cold Spring Harbor, N.Y.)*, *17*(11), 561–570. https://doi.org/10.1101/lm.941510

Florin-Lechner, S. M., Druhan, J. P., Aston-Jones, G., & Valentino, R. J. (1996). Enhanced norepinephrine release in prefrontal cortex with burst stimulation of the locus coeruleus. *Brain Research*, *742*(1–2), 89–97. https://doi.org/10.1016/S0006-8993(96)00967-5

Foote, S. L., Aston-Jones, G., & Bloom, F. E. (1980). Impulse activity of locus coeruleus neurons in awake rats and monkeys is a function of sensory stimulation and arousal. *Proceedings of the National Academy of Sciences of the United States of America*, *77*(5), 3033–3037. https://doi.org/10.1073/pnas.77.5.3033

Forest, J., Chalençon, L., Midroit, M., Terrier, C., Caillé, I., Sacquet, J., Benetollo, C., Martin, K., Richard, M., Didier, A., & Mandairon, N. (2020). Role of Adult-Born Versus Preexisting Neurons Born at P0 in Olfactory Perception in a Complex Olfactory Environment in Mice. *Cerebral Cortex (New York, N.Y. : 1991)*, *30*(2), 534–549. https://doi.org/10.1093/cercor/bhz105

Fried, H. U., Kaupp, U. B., & Müller, F. (2010). Hyperpolarization-activated and cyclic nucleotide-gated channels are differentially expressed in juxtaglomerular cells in the olfactory bulb of mice. *Cell and Tissue Research*, *339*, 463–479. https://doi.org/10.1007/s00441-009-0904-9

Froemke, R. C., Letzkus, J. J., Kampa, B. M., Hang, G. B., & Stuart, G. J. (2010). Dendritic synapse location and neocortical spike-timingdependent plasticity. *Frontiers in Synaptic Neuroscience*, *2*(JUL), 1–14. https://doi.org/10.3389/fnsyn.2010.00029

Fukunaga, I., Herb, J. T., Kollo, M., Boyden, E. S., & Schaefer, A. T. (2014). Independent control of gamma and theta activity by distinct interneuron networks in the olfactory bulb. *Nature Neuroscience*, *July*. https://doi.org/10.1038/nn.3760

Gao, Y., Budlong, C., Durlacher, E., & Davison, I. G. (2017). Neural mechanisms of social learning in the female mouse. *ELife*, *6*, e25421. https://doi.org/10.7554/eLife.25421

Gao, Y., & Strowbridge, B. W. (2009). Long-term plasticity of excitatory inputs to granule cells in the rat olfactory bulb. *Nature Neuroscience*, *12*(6), 731–733. https://doi.org/10.1038/nn.2319

Gastrein, P., Campanac, É., Gasselin, C., Cudmore, R. H., Bialowas, A., Carlier, E., Fronzaroli-Molinieres, L., Ankri, N., & Debanne, D. (2011). The role of hyperpolarization-activated cationic current in spike-time precision and intrinsic resonance in cortical

neurons in vitro. *Journal of Physiology*, *589*(15), 3753–3773. https://doi.org/10.1113/jphysiol.2011.209148

Gee, J. M. M., Smith, N. A., Fernandez, F. R., Economo, M. N., Brunert, D., Rothermel, M., Morris, S. C. C., Talbot, A., Palumbos, S., Ichida, J. M., Shepherd, J. D., West, P. J., Wachowiak, M., Capecchi, M. R., Wilcox, K. S., White, J. A., & Tvrdik, P. (2014). Imaging Activity in Neurons and Glia with a Polr2a-Based and Cre-Dependent GCaMP5G-IRES-tdTomato Reporter Mouse. *Neuron*, *83*(5), 1–15. https://doi.org/10.1016/j.neuron.2014.07.024

George, M. S., Abbott, L. F., & Siegelbaum, S. a. (2009). HCN hyperpolarization-activated cation channels inhibit EPSPs by interactions with M-type K(+) channels. *Nature Neuroscience*, *12*(5), 577–584. https://doi.org/10.1038/nn.2307

Gervais, R., Holley, A., & Keverne, B. (1988). The importance of central noradrenergic influences on the olfactory bulb in the processing of learned olfactory cues. *Chemical Senses*, *13*(1), 3–12.

Gheusi, G., & Lledo, P.-M. (2014). Adult neurogenesis in the olfactory system shapes odor memory and perception. In *Progress in brain research* (1st ed., Vol. 208). Elsevier B.V. https://doi.org/10.1016/B978-0-444-63350-7.00006-1

Ghosh, S., Larson, S. D., Hefzi, H., Marnoy, Z., Cutforth, T., Dokka, K., & Baldwin, K. K. (2011). Sensory maps in the olfactory cortex defined by long-range viral tracing of single neurons. *Nature*, *472*(7342), 217–220. https://doi.org/10.1038/nature09945

Gire, D. H., & Schoppa, N. E. (2008). Long-term enhancement of synchronized oscillations by adrenergic receptor activation in the olfactory bulb. *Journal of Neurophysiology*, *99*(4), 2021–2025. https://doi.org/10.1152/jn.01324.2007

Glezer, I., & Malnic, B. (2019). Olfactory receptor function. In *Handbook of Clinical Neurology* (1st ed., Vol. 164). Elsevier B.V. https://doi.org/10.1016/B978-0-444-63855-7.00005-8

Gorin, M., Tsitoura, C., Kahan, A., Watznauer, K., Drose, D. R., Arts, M., Mathar, R., O'Connor, S., Hanganu-Opatz, I. L., Ben-Shaul, Y., & Spehr, M. (2016). Interdependent Conductances Drive Infraslow Intrinsic Rhythmogenesis in a Subset of Accessory Olfactory Bulb Projection Neurons. *Journal of Neuroscience*, *36*(11), 3127–3144. https://doi.org/10.1523/JNEUROSCI.2520-15.2016

Gottfried, J. a. (2010). Central mechanisms of odour object perception. *Nature Reviews. Neuroscience*, *11*(9), 628–641. https://doi.org/10.1038/nrn2883

Griffen, T. C., & Maffei, A. (2014). GABAergic synapses: Their plasticity and role in sensory cortex. *Frontiers in Cellular Neuroscience*, *8*(MAR), 1–22. https://doi.org/10.3389/fncel.2014.00091

Griffiths, P. R., & Brennan, P. A. (2015). Roles for learning in mammalian chemosensory responses. *Hormones and Behavior*, *68*, 91–102. https://doi.org/10.1016/j.yhbeh.2014.08.010

Gschwend, O., Abraham, N. M., Lagier, S., Begnaud, F., Rodriguez, I., & Carleton, A. (2015).

Neuronal pattern separation in the olfactory bulb improves odor discrimination learning. *Nature Neuroscience*, *August*. https://doi.org/10.1038/nn.4089

Gu, Q. (2002). Neuromodulatory transmitter systems in the cortex and their role in cortical plasticity. *Neuroscience*, *111*(4), 815–835. https://doi.org/10.1016/S0306-4522(02)00026-X

Guo, X. Z., Su, J. Da, Sun, Q. W., & Jiao, B. H. (2001). Expression of estrogen receptor (ER) -α and -β transcripts in the neonatal and adult rat cerebral cortex, cerebellum, and olfactory bulb. *Cell Research*, *11*(4), 321–324. https://doi.org/10.1038/sj.cr.7290103

Gutfreund, Y., Yarom, Y., & Segev, I. (1995). Subthreshold oscillations and resonant frequency in guinea-pig cortical neurons: physiology and modelling. *The Journal of Physiology*, *483 ( Pt 3*(1995), 621–640. http://www.pubmedcentral.nih.gov/articlerender.fcgi?artid=1157807&tool=pmcentrez&rendertype=abstract

Gutkin, B., & Ermentrout, G. B. (2003). *Spike Generating Dynamics and the Conditions for Spike-Time*. 91–103.

Haas, H. L., & Rose, G. M. (1987). Noradrenaline blocks potassium conductance in rat dentate granule cells in vitro. *Neuroscience Letters*, *78*(2), 171–174. https://doi.org/10.1016/0304-3940(87)90628-8

Haddad, R., Lanjuin, A., Madisen, L., Zeng, H., Murthy, V. N., & Uchida, N. (2013). Olfactory cortical neurons read out a relative time code in the olfactory bulb. *Nature Neuroscience*, *16*(7), 949–957. https://doi.org/10.1038/nn.3407

Haga, S., Hattori, T., Sato, T., & Sato, K. (2010). The male mouse pheromone ESP1 enhances female sexual receptive behaviour through a specific vomeronasal receptor. *Nature*, *466*(7302), 118–122. https://doi.org/10.1038/nature09142

Halabisky, B., & Strowbridge, B. W. (2003). Gamma-frequency excitatory input to granule cells facilitates dendrodendritic inhibition in the rat olfactory Bulb. *Journal of Neurophysiology*, *90*(2), 644–654. https://doi.org/10.1152/jn.00212.2003

Halem, H. A., Baum, M. J., & Cherry, J. A. (2001). Sex difference and steroid modulation of pheromone-induced immediate early genes in the two zones of the mouse accessory olfactory system. *Journal of Neuroscience*, *21*(7), 2474–2480. https://doi.org/10.1523/JNEUROSCI.21-07-02474.2001

Haller, J., Makara, G. B., & Kruk, M. R. (1997). Catecholaminergic involvement in the control of aggression: Hormones, the peripheral sympathetic, and central noradrenergic systems. *Neuroscience and Biobehavioral Reviews*, *22*(1), 85–97. https://doi.org/10.1016/S0149-7634(97)00023-7

Harnett, M. T., Magee, J. C., Williams, S. R., MT, H., JC, M., & SR, W. (2015). Distribution and Function of HCN Channels in the Apical Dendritic Tuft of Neocortical Pyramidal Neurons. *The Journal of Neuroscience : The Official Journal of the Society for Neuroscience*, *35*(3), 1024–1037. https://doi.org/10.1523/JNEUROSCI.2813-14.2015.

Harris, K. D., & Mrsic-Flogel, T. D. (2013). Cortical connectivity and sensory coding. *Nature*, *503*(7474), 51–58. https://doi.org/10.1038/nature12654

He, C., Chen, F., Li, B., & Hu, Z. (2014). Neurophysiology of HCN channels: From cellular functions to multiple regulations. *Progress in Neurobiology*, *112*, 1–23. https://doi.org/10.1016/j.pneurobio.2013.10.001

He, H. Y., & Cline, H. T. (2019). What Is Excitation/Inhibition and How Is It Regulated? A Case of the Elephant and the Wisemen. *Journal of Experimental Neuroscience*, *13*, 10–12. https://doi.org/10.1177/1179069519859371

Hein, L. (2006). Adrenoceptors and signal transduction in neurons. *Cell and Tissue Research*, *326*(2), 541–551. https://doi.org/10.1007/s00441-006-0285-2

Holderith, N. B., Shigemoto, R., & Nusser, Z. (2003). Cell type-dependent expression of HCN1 in the main olfactory bulb. *European Journal of Neuroscience*, *18*(April), 344–354. https://doi.org/10.1046/j.1460-9568.2003.02756.x

Hong, W., Kim, D. W., & Anderson, D. J. (2014). Antagonistic control of social versus repetitive self-grooming behaviors by separable amygdala neuronal subsets. *Cell*, *158*(6), 1348–1361. https://doi.org/10.1016/j.cell.2014.07.049

Hoyk, Z., Csákvári, E., Gyenes, A., Siklós, L., Harada, N., & Párducz, Á. (2014). Aromatase and estrogen receptor beta expression in the rat olfactory bulb: Neuroestrogen action in the first relay station of the olfactory pathway? *Acta Neurobiologiae Experimentalis*, *74*(1), 1–14.

Hsieh, Y. W., Alqadah, A., & Chuang, C. F. (2017). Mechanisms controlling diversification of olfactory sensory neuron classes. *Cellular and Molecular Life Sciences*, *74*(18), 3263–3274. https://doi.org/10.1007/s00018-017-2512-2

Hu, H., Vervaeke, K., & Storm, J. F. (2002). Two forms of electrical resonance at theta frequencies, generated by M-current, h-current and persistent Na+ current in rat hippocampal pyramidal cells. *The Journal of Physiology*, *545*(3), 783–805. https://doi.org/10.1113/jphysiol.2002.029249

Hu, Hua, Vervaeke, K., Graham, L. J., & Storm, J. F. (2009). Complementary theta resonance filtering by two spatially segregated mechanisms in CA1 hippocampal pyramidal neurons. *The Journal of Neuroscience : The Official Journal of the Society for Neuroscience*, *29*(46), 14472–14483. https://doi.org/10.1523/JNEUROSCI.0187-09.2009

Hu, R., Ferguson, K. A., Whiteus, C. B., Meijer, D. H., & Araneda, R. C. (2016). Hyperpolarization-Activated Currents and Subthreshold Resonance in Granule Cells of the Olfactory Bulb. *ENeuro*, *3*(5), 9817. https://doi.org/10.1523/ENEURO.0197-16.2016

Huang, H., & Trussell, L. O. (2014). Presynaptic HCN Channels Regulate Vesicular Glutamate Transport. *Neuron*, *84*(2), 340–346. https://doi.org/10.1016/j.neuron.2014.08.046

Hull, C. A., Chu, Y. X., Thanawala, M., & Regehr, W. G. (2013). Hyperpolarization induces a

long-term increase in the spontaneous firing rate of cerebellar Golgi cells. *Journal of Neuroscience*, *33*(14), 5895–5902. https://doi.org/10.1523/JNEUROSCI.4052-12.2013

Hurley, L. M., Devilbiss, D. M., & Waterhouse, B. D. (2004). A matter of focus: Monoaminergic modulation of stimulus coding in mammalian sensory networks. *Current Opinion in Neurobiology*, *14*(4), 488–495. https://doi.org/10.1016/j.conb.2004.06.007

Hutcheon, B., & Yarom, Y. (2000). Resonance, oscillation and the intrinsic frequency preferences of neurons. *Trends in Neurosciences*, *2236*(1980). http://www.sciencedirect.com/science/article/pii/S0166223600015472

Imamura, F., & Greer, C. a. (2015). Segregated labeling of olfactory bulb projection neurons based on their birthdates. *European Journal of Neuroscience*, *41*(2), 147–156. https://doi.org/10.1111/ejn.12784

Isaacson, J. S. (2001). Mechanisms governing dendritic γ-aminobutyric acid (GABA) release in the rat olfactory bulb. *Proceedings of the National Academy of Sciences of the United States of America*, *98*(1), 337–342. https://doi.org/10.1073/pnas.021445798

Isaacson, J. S., & Scanziani, M. (2011). How inhibition shapes cortical activity. *Neuron*, *72*(2), 231–243. https://doi.org/10.1016/j.neuron.2011.09.027

Isaacson, J. S., & Strowbridge, B. W. (1998). Olfactory reciprocal synapses: Dendritic signaling in the CNS. *Neuron*, *20*(4), 749–761. https://doi.org/10.1016/S0896-6273(00)81013-2

Iwata, R., Kiyonari, H., & Imai, T. (2017). Mechanosensory-Based Phase Coding of Odor Identity in the Olfactory Bulb. *Neuron*, *96*(5), 1139-1152.e7. https://doi.org/10.1016/j.neuron.2017.11.008

Jahr, C. E., & Nicoll, R. a. (1980). Dendrodendritic inhibition: demonstration with intracellular recording. *Science (New York, N.Y.)*, *207*(4438), 1473–1475. https://doi.org/10.1126/science.7361098

Jahr, C. E., & Nicoll, R. a. (1982). Noradrenergic modulation of dendrodendritic inhibition in the olfactory bulb. In *Nature* (Vol. 297, Issue 5863, pp. 227–229). https://doi.org/10.1038/297227a0

Jayant, K., Hirtz, J. J., Plante, I. J., Tsai, D. M., De Boer, W. D. A. M., Semonche, A., Peterka, D. S., Owen, J. S., Sahin, O., Shepard, K. L., & Yuste, R. (2017). Targeted intracellular voltage recordings from dendritic spines using quantum-dot-coated nanopipettes. *Nature Nanotechnology*, *12*(4), 335–342. https://doi.org/10.1038/nnano.2016.268

Jia, C., Chen, W. R., & Shepherd, G. M. (1999). Synaptic organization and neurotransmitters in the rat accessory olfactory bulb. *Journal of Neurophysiology*, *81*(1), 345–355.

Jones, S. W. (1998). Overview of voltage-dependent calcium channels. *Journal of Bioenergetics and Biomembranes*, *30*(4), 299–312. https://doi.org/10.1023/A:1021977304001

Joshi, S., Li, Y., Kalwani, R. M., & Gold, J. I. (2016). Relationships between Pupil Diameter and Neuronal Activity in the Locus Coeruleus, Colliculi, and Cingulate Cortex. *Neuron*, *89*(1), 221–234. https://doi.org/10.1016/j.neuron.2015.11.028

Kaba, H., & Keverne, E. B. (1988). The effect of microinfusions of drugs into the accessory olfactory bulb on the olfactory block to pregnancy. *Neuroscience*, *25*(3), 1007–1011. https://doi.org/10.1016/0306-4522(88)90053-X

Kaba, H., Rosser, A., & Keverne, B. (1989). Neural basis of olfactory memory in the context of pregnancy block. *Neuroscience*, *32*(3), 657–662. https://doi.org/10.1016/0306-4522(89)90287-X

Karkanias, G. B., Ansonoff, M. A., & Etgen, A. M. (1996). Estradiol regulation of α(1b)-adrenoceptor mRNA in female rat hypothalamus-preoptic area. *Journal of Neuroendocrinology*, *8*(6), 449–455. https://doi.org/10.1046/j.1365-2826.1996.04716.x

Kato, H. H. K., Gillet, S. S. N., Peters, A. J. A., Isaacson, J. S., & Komiyama, T. (2013). Parvalbumin-expressing interneurons linearly control olfactory bulb output. *Neuron*, *80*(5), 1218–1231. https://doi.org/10.1016/j.neuron.2013.08.036

Kaupp, U. B., & Seifert, R. (2001). Molecular diversity of pacemaker ion channels. *Annual Review of Physiology*, *63*(52), 235–257. https://doi.org/10.1146/annurev.physiol.63.1.235

Kawaguchi, Y., & Shindou, T. (1998). Noradrenergic excitation and inhibition of GABAergic cell types in rat frontal cortex. *The Journal of Neuroscience : The Official Journal of the Society for Neuroscience*, *18*(17), 6963–6976.

Kay, L. M. (2014). Circuit oscillations in odor perception and memory. In *Progress in brain research* (1st ed., Vol. 208). Elsevier B.V. https://doi.org/10.1016/B978-0-444-63350-7.00009-7

Kay, L. M., & Sherman, S. M. (2007). An argument for an olfactory thalamus. *Trends in Neurosciences*, *30*(2), 47–53. https://doi.org/10.1016/j.tins.2006.11.007

Kelsch, W., Lin, C. W., & Lois, C. (2008). Sequential development of synapses in dendritic domains during adult neurogenesis. *Proceedings of the National Academy of Sciences of the United States of America*, *105*(43), 16803–16808. https://doi.org/10.1073/pnas.0807970105

Kelsch, W., Lin, C. W., Mosley, C. P., & Lois, C. (2009). A critical period for activity-dependent synaptic development during olfactory bulb adult neurogenesis. *Journal of Neuroscience*, *29*(38), 11852–11858. https://doi.org/10.1523/JNEUROSCI.2406-09.2009

Keverne, E. B. (1999). The Vomeronasal Organ. *Science*, *286*(5440), 716–720. https://doi.org/10.1126/science.286.5440.716

Khvotchev, M., & Kavalali, E. T. (2008). Pharmacology of neurotransmitter release: Measuring exocytosis. In *Handbook of Experimental Pharmacology* (Vol. 184). https://doi.org/10.1007/978-3-540-74805-2-2

Kimchi, T., Xu, J., & Dulac, C. (2007). A functional circuit underlying male sexual behaviour in the female mouse brain. *Nature*, *448*(7157), 1009–1014. https://doi.org/10.1038/nature06089

Kole, M. H. P. (2006). Single Ih Channels in Pyramidal Neuron Dendrites: Properties, Distribution, and Impact on Action Potential Output. *Journal of Neuroscience*, *26*(6), 1677–1687. https://doi.org/10.1523/JNEUROSCI.3664-05.2006

Kondo, Y., & Arai, Y. (1995). Functional association between the medial amygdala and the medial preoptic area in regulation of mating behavior in the male rat. *Physiology and Behavior*, *57*(1), 69–73. https://doi.org/10.1016/0031-9384(94)00205-J

Kossl, M., & Vater, M. (1989). Noradrenaline enhances temporal auditory contrast and neuronal timing precision in the cochlear nucleus of the mustached bat. *Journal of Neuroscience*, *9*(12), 4169–4178. https://doi.org/10.1523/jneurosci.09-12-04169.1989

Kuhn, H. G. (2016). *Control of Cell Survival in Adult Mammalian Neurogenesis*.

Kunisawa, Y., Kawabe, K., Niijima, T., Honda, K., & Takenaka, T. (1985). A pharmacological study of alpha-adrenergic receptor subtypes in smooth muscle of human urinary bladder base and prostatic urethra. *Journal of Urology*, *134*(2), 396–398. https://doi.org/10.1016/S0022-5347(17)47185-0

Labarrera, C., Deitcher, Y., Dudai, A., Weiner, B., Kaduri Amichai, A., Zylbermann, N., & London, M. (2018). Adrenergic Modulation Regulates the Dendritic Excitability of Layer 5 Pyramidal Neurons In Vivo. *Cell Reports*, *23*(4), 1034–1044. https://doi.org/10.1016/j.celrep.2018.03.103

Lagier, S., Carleton, A., & Lledo, P.-M. (2004). Interplay between local GABAergic interneurons and relay neurons generates gamma oscillations in the rat olfactory bulb. *The Journal of Neuroscience : The Official Journal of the Society for Neuroscience*, *24*(18), 4382–4392. https://doi.org/10.1523/JNEUROSCI.5570-03.2004

Larriva-Sahd, J. (2008). The accessory olfactory bulb in the adult rat: A cytological study of its cell types, neuropil, neuronal modules, and interactions with the main olfactory system. *Journal of Comparative Neurology*, *510*(3), 309–350. https://doi.org/10.1002/cne.21790

Laurie, D. J., Seeburg, P. H., & Wisden, W. (1992). The distribution of 13 GABA(A) receptor subunit mRNAs in the rat brain. II. Olfactory bulb and cerebellum. *Journal of Neuroscience*, *12*(3), 1063–1076. https://doi.org/10.1523/jneurosci.12-03-01063.1992

Lavole, A. M., Tingey, J. J., Harrison, N. L., Pritchett, D. B., & Twyman, R. E. (1997). Activation and deactivation rates of recombinant GABA(A) receptor channels are dependent on α-subunit isoform. *Biophysical Journal*, *73*(5), 2518–2526. https://doi.org/10.1016/s0006-3495(97)78280-8

Le Masson, G., Renaud-Le Masson, S., Debay, D., & Bal, T. (2002). Feedback inhibition controls spike transfer in hybrid thalamic circuits. *Nature*, *417*(6891), 854–858. https://doi.org/10.1038/nature00825

Lein, E. S., Hawrylycz, M. J., Ao, N., Ayres, M., Bensinger, A., Bernard, A., Boe, A. F.,

Boguski, M. S., Brockway, K. S., Byrnes, E. J., Chen, L., Chen, L., Chen, T. M., Chin, M. C., Chong, J., Crook, B. E., Czaplinska, A., Dang, C. N., Datta, S., … Jones, A. R. (2007). Genome-wide atlas of gene expression in the adult mouse brain. *Nature*, *445*(7124), 168–176. https://doi.org/10.1038/nature05453

Lepousez, G., & Lledo, P.-M. (2013). Odor discrimination requires proper olfactory fast oscillations in awake mice. *Neuron*, *80*(4), 1010–1024. https://doi.org/10.1016/j.neuron.2013.07.025

Lepousez, G., Valley, M. T., & Lledo, P.-M. (2013). The impact of adult neurogenesis on olfactory bulb circuits and computations. *Annual Review of Physiology*, *75*, 339–363. https://doi.org/10.1146/annurev-physiol-030212-183731

Leszkowicz, E., Khan, S., Ng, S., Ved, N., Swallow, D. L., & Brennan, P. A. (2012). Noradrenaline-induced enhancement of oscillatory local field potentials in the mouse accessory olfactory bulb does not depend on disinhibition of mitral cells. *European Journal of Neuroscience*, *35*(9), 1433–1445. https://doi.org/10.1111/j.1460-9568.2012.08070.x

Li, a., Gire, D. H., & Restrepo, D. (2015). Spike-Field Coherence in a Population of Olfactory Bulb Neurons Differentiates between Odors Irrespective of Associated Outcome. *Journal of Neuroscience*, *35*(14), 5808–5822. https://doi.org/10.1523/JNEUROSCI.4003-14.2015

Li, Y., Mathis, A., Grewe, B. F., Osterhout, J. A., Ahanonu, B., Schnitzer, M. J., Murthy, V. N., & Dulac, C. (2017). Neuronal Representation of Social Information in the Medial Amygdala of Awake Behaving Mice. *Cell*, *171*(5), 1176-1190.e17. https://doi.org/10.1016/j.cell.2017.10.015

Li, Y. W., Bayliss, D. A., & Guyenet, P. G. (1995). C1 neurons of neonatal rats: intrinsic beating properties and alpha 2-adrenergic receptors. *American Journal of Physiology-Regulatory, Integrative and Comparative Physiology*, *269*(6), R1356–R1369. https://doi.org/10.1152/ajpregu.1995.269.6.R1356

Liberles, S. D. (2014). Mammalian pheromones. *Annual Review of Physiology*, *76*(August), 151–175. https://doi.org/10.1146/annurev-physiol-021113-170334

Livneh, Y., & Mizrahi, A. (2011). Long-term changes in the morphology and synaptic distributions of adult-born neurons. *Journal of Comparative Neurology*, *519*(11), 2212–2224. https://doi.org/10.1002/cne.22625

Lledo, P.-M., Alonso, M., & Grubb, M. S. (2006). Adult neurogenesis and functional plasticity in neuronal circuits. *Nature Reviews. Neuroscience*, *7*(3), 179–193. https://doi.org/10.1038/nrn1867

Lledo, P.-M., Merkle, F. T., & Alvarez-Buylla, A. (2008). Origin and function of olfactory bulb interneuron diversity. *Trends in Neurosciences*, *31*(8), 392–400. https://doi.org/10.1016/j.tins.2008.05.006

Lledo, P.-M., & Saghatelyan, A. (2005). Integrating new neurons into the adult olfactory bulb: joining the network, life-death decisions, and the effects of sensory experience. *Trends*

*in Neurosciences*, *28*(5), 248–254. https://doi.org/10.1016/j.tins.2005.03.005

Lledo, P., Gheusi, G., & Vincent, J. (2005). Information processing in the mammalian olfactory system. *Physiological Reviews*, *85*(227), 281–317. https://doi.org/10.1152/physrev.00008.2004.

Lloyd-Thomas, A., & Keverne, E. B. (1982). Role of the brain and accessory olfactory system in the block to pregnancy in mice. *Neuroscience*, *7*(4). https://doi.org/10.1016/0306-4522(82)90051-3

Lodovichi, C., & Belluscio, L. (2012). Odorant receptors in the formation of the olfactory bulb circuitry. *Physiology (Bethesda, Md.)*, *27*(4), 200–212. https://doi.org/10.1152/physiol.00015.2012

Lois, C., & Alvarez-Buylla, a. (1994). Long-distance neuronal migration in the adult mammalian brain. *Science (New York, N.Y.)*, *264*(5162), 1145–1148. https://doi.org/10.1126/science.8178174

Ludwig, A., Zong, X., Jeglitsch, M., Hofmann, F., & Biel, M. (1998). A family of hyperpolarization-activated mammalian cation channels. *Nature*, *393*(6685), 587–591. https://doi.org/10.1038/31255

Luethi, A., & McCormick, D. A. (1998). H-Current: Minireview Properties of a Neuronal and Network Pacemaker. *Neuron*, *21*, 9–12. http://www.med.yale.edu/neurobio/mccormick/pubs/minireview.pdf

Luo, M., Fee, M. S., & Katz, L. C. (2003). Encoding Pheromonal Signals in the Accessory Olfactory Bulb of Behaving Mice. *Science*, *299*(February), 1196–1201. https://doi.org/10.1126/science.1082133

Ma, L., Qiu, Q., Gradwohl, S., Scott, A., Yu, E. Q., Alexander, R., Wiegraebe, W., & Yu, C. R. (2012). Distributed representation of chemical features and tunotopic organization of glomeruli in the mouse olfactory bulb. *Proceedings of the National Academy of Sciences of the United States of America*, *109*(14), 5481–5486. https://doi.org/10.1073/pnas.1117491109

Magavi, S. S. P., Mitchell, B. D., Szentirmai, O., Carter, B. S., & Macklis, J. D. (2005). Adult-born and preexisting olfactory granule neurons undergo distinct experience-dependent modifications of their olfactory responses in vivo. *The Journal of Neuroscience : The Official Journal of the Society for Neuroscience*, *25*(46), 10729–10739. https://doi.org/10.1523/JNEUROSCI.2250-05.2005

Magee, J. C. (1998). Dendritic hyperpolarization-activated currents modify the integrative properties of hippocampal CA1 pyramidal neurons. *The Journal of Neuroscience : The Official Journal of the Society for Neuroscience*, *18*(19), 7613–7624.

Magee, J. C. (1999). Dendritic Ih normalizes temporal summation in hippocampal CA1 neurons. *Nature Neuroscience*, *2*(6), 508–514. https://doi.org/10.1038/9158

Mainen, Z. F., & Sejnowski, T. J. (1995). Reliability of Spike Timing in Neocortical Neurons. *Science*, *268*(5216), 1503–1506. https://doi.org/10.1126/science.7770778

Maksimova, M. A., Cansler, H. L., Zuk, K. E., Torres, J. M., Roberts, D. J., & Meeks, J. P. (2019). Interneuron functional diversity in the mouse accessory olfactory bulb. *ENeuro*, *6*(4). https://doi.org/10.1523/ENEURO.0058-19.2019

Manabe, H., & Mori, K. (2013). Sniff rhythm-paced fast and slow gamma-oscillations in the olfactory bulb: relation to tufted and mitral cells and behavioral states. *J Neurophysiol*, *110*(7), 1593–1599. https://doi.org/10.1152/jn.00379.2013

Mandairon, N., Peace, S., Karnow, A., Kim, J., Ennis, M., & Linster, C. (2008). Noradrenergic modulation in the olfactory bulb influences spontaneous and reward-motivated discrimination, but not the formation of habituation memory. *European Journal of Neuroscience*, *27*(5), 1210–1219. https://doi.org/10.1111/j.1460-9568.2008.06101.x

Manella, L. C., Petersen, N., & Linster, C. (2017). Stimulation of the locus ceruleus modulates signal-to-noise ratio in the olfactory bulb. *Journal of Neuroscience*, *37*(48), 11605–11615. https://doi.org/10.1523/JNEUROSCI.2026-17.2017

Marder, E., & Goaillard, J.-M. (2006). Variability, compensation and homeostasis in neuron and network function. *Nature Reviews. Neuroscience*, *7*(7), 563–574. https://doi.org/10.1038/nrn1949

Marino, M. D., Bourdélat-Parks, B. N., Cameron Liles, L., & Weinshenker, D. (2005). Genetic reduction of noradrenergic function alters social memory and reduces aggression in mice. *Behavioural Brain Research*, *161*(2), 197–203. https://doi.org/10.1016/j.bbr.2005.02.005

Markopoulos, F., Rokni, D., Gire, D. D. H., & Murthy, V. N. V. (2012). Functional properties of cortical feedback projections to the olfactory bulb. *Neuron*, *76*(6), 1–6. https://doi.org/10.1016/j.neuron.2012.10.028

Marzo, A., Bai, J., & Otani, S. (2009). Neuroplasticity Regulation by Noradrenaline in Mammalian Brain. *Current Neuropharmacology*, *7*(4), 286–295. https://doi.org/10.2174/157015909790031193

Matsuda, J. J., Lee, H., & Shibata, E. F. (1992). Enhancement of rabbit cardiac sodium channels by β-adrenergic stimulation. *Circulation Research*, *70*(1), 199–207. https://doi.org/10.1161/01.res.70.1.199

McCall, J. G., Al-Hasani, R., Siuda, E. R., Hong, D. Y., Norris, A. J., Ford, C. P., & Bruchas, M. R. (2015). CRH Engagement of the Locus Coeruleus Noradrenergic System Mediates Stress-Induced Anxiety. *Neuron*, *87*(3), 605–620. https://doi.org/10.1016/j.neuron.2015.07.002

McClellan, A. M. L., & Twyman, R. E. (1999). Receptor system response kinetics reveal functional subtypes of native murine and recombinant human GABA(A) receptors. *Journal of Physiology*, *515*(3), 711–727. https://doi.org/10.1111/j.1469-7793.1999.711ab.x

McCormick, D. A., & Pape, H. C. (1990). Properties of a hyperpolarization-activated cation current and its role in rhythmic oscillation in thalamic relaty neurones. *J.Phys.*, *431*, 319–342.

McCormick, D. A., Pape, H. C., & Williamson, A. (1991). Actions of norepinephrine in the cerebral cortex and thalamus: Implications for function of the central noradrenergic system. *Progress in Brain Research*, *88*(C), 293–305. https://doi.org/10.1016/S0079-6123(08)63817-0

McCormick, D. A., & Wang, Z. (1991). Serotonin and noradrenaline excite GABAergic neurones of the guinea-pig and cat nucleus reticularis thalami. *The Journal of Physiology*, *442*(1), 235–255. https://doi.org/10.1113/jphysiol.1991.sp018791

McLean, J. H., & Shipley, M. T. (1991). Postnatal development of the noradrenergic projection from locus coeruleus to the olfactory bulb in the rat. *Journal of Comparative Neurology*, *304*(3), 467–477. https://doi.org/10.1002/cne.903040310

Mclean, J. H., Shipley, M. T., Nickell, W. T., Aston-Jones, G., & Reyher, C. K. H. (1989). *Chemoanatomical Organization of the Noradrenergic Input From Locus Coeruleus to the Olfactory Bulb of the Adult Rat*. *349*.

McTavis, T. S., Migliore, M., Shepherd, G. M., & Hines, M. L. (2012). Mitral cell spike synchrony modulated by dendrodendritic synapse location. *Frontiers in Computational Neuroscience*, *6*(JANUARY 2012), 1–12. https://doi.org/10.3389/fncom.2012.00003

Meredith, M. (1994). Chronic recording of vomeronasal pump activation in awake behaving hamsters. *Physiology and Behavior*, *56*(2), 345–354. https://doi.org/10.1016/0031-9384(94)90205-4

Mistrik, P., Mader, R., Michalakis, S., Weidinger, M., Pfeifer, A., & Biel, M. (2005). The Murine HCN3 Gene Encodes a Hyperpolarization-activated Cation Channel with Slow Kinetics and Unique Response to Cyclic Nucleotides. *Journal of Biological Chemistry*, *280*(29), 27056–27061. https://doi.org/10.1074/jbc.M502696200

Miura, K., Mainen, Z. F., & Uchida, N. (2012). Odor representations in olfactory cortex: distributed rate coding and decorrelated population activity. *Neuron*, *74*(6), 1087–1098. https://doi.org/10.1016/j.biotechadv.2011.08.021.Secreted

Miyamichi, K., Shlomai-Fuchs, Y., Shu, M., Weissbourd, B. C., Luo, L., & Mizrahi, A. (2013). Dissecting Local Circuits: Parvalbumin Interneurons Underlie Broad Feedback Control of Olfactory Bulb Output. *Neuron*, *80*(5), 1232–1245. https://doi.org/10.1016/j.neuron.2013.08.027

Molinoff, P. B. (1984). α- and β-Adrenergic Receptor Subtypes: Properties, Distribution and Regulation. *Drugs*, *28*(2), 1–15. https://doi.org/10.2165/00003495-198400282-00002

Mombaerts, P., Wang, F., Dulac, C., Chao, S. K., Nemes, A., Mendelsohn, M., Edmondson, J., & Axel, R. (1996). Visualizing an olfactory sensory map. *Cell*, *87*(4), 675–686. https://doi.org/10.1016/S0092-8674(00)81387-2

Moreno, M. M., Bath, K., Kuczewski, N., Sacquet, J., Didier, a., & Mandairon, N. (2012). Action of the Noradrenergic System on Adult-Born Cells Is Required for Olfactory Learning in Mice. *Journal of Neuroscience*, *32*(11), 3748–3758. https://doi.org/10.1523/JNEUROSCI.6335-11.2012

Mori, K., & Sakano, H. (2011). How is the olfactory map formed and interpreted in the mammalian brain? *Annual Review of Neuroscience*, *34*, 467–499. https://doi.org/10.1146/annurev-neuro-112210-112917

Mortensen, M., Patel, B., & Smart, T. G. (2012). GABA potency at GABA A receptors found in synaptic and extrasynaptic zones. *Frontiers in Cellular Neuroscience*, *6*(JANUARY), 1–10. https://doi.org/10.3389/fncel.2012.00001

Musall, S., Kaufman, M. T., Juavinett, A. L., Gluf, S., & Churchland, A. K. (2019). Single-trial neural dynamics are dominated by richly varied movements. *Nature Neuroscience*, *22*(10), 1677–1686. https://doi.org/10.1038/s41593-019-0502-4

Nagayama, S., Homma, R., & Imamura, F. (2014). Neuronal organization of olfactory bulb circuits. *Frontiers in Neural Circuits*, *8*(September), 98. https://doi.org/10.3389/fncir.2014.00098

Nai, Q., Dong, H.-W., Hayar, A., Linster, C., & Ennis, M. (2009). Noradrenergic Regulation of GABAergic Inhibition of Main Olfactory Bulb Mitral Cells Varies as a Function of Concentration and Receptor Subtype. *J Neurophysiol*, *101*, 2472–2484. https://doi.org/10.1152/jn.91187.2008

Narayanan, R., & Johnston, D. (2007). Long-term potentiation in rat hippocampal neurons is accompanied by spatially widespread changes in intrinsic oscillatory dynamics and excitability. *Neuron*, *56*(6), 1061–1075. https://doi.org/10.1016/j.neuron.2007.10.033

Narayanan, R., & Johnston, D. (2008). The h channel mediates location dependence and plasticity of intrinsic phase response in rat hippocampal neurons. *The Journal of Neuroscience : The Official Journal of the Society for Neuroscience*, *28*(22), 5846–5860. https://doi.org/10.1523/JNEUROSCI.0835-08.2008

Nelson, A. B., Gittis, A. H., & Du Lac, S. (2005). Decreases in CaMKII activity trigger persistent potentiation of intrinsic excitability in spontaneously firing vestibular nucleus neurons. *Neuron*, *46*(4), 623–631. https://doi.org/10.1016/j.neuron.2005.04.009

Nelson, A. B., Krispel, C. M., Sekirnjak, C., & Lac, S. Du. (2003). Long-lasting increases in intrinsic excitability triggered by inhibition. *Neuron*, *40*(3), 609–620. https://doi.org/10.1016/S0896-6273(03)00641-X

Nelson, R. J., & Trainor, B. C. (2007). Neural mechanisms of aggression. *Nature Reviews Neuroscience*, *8*(7), 536–546. https://doi.org/10.1038/nrn2174

Notomi, T., & Shigemoto, R. (2004). Immunohistochemical localization of Ih channel subunits, HCN1-4, in the rat brain. *The Journal of Comparative Neurology*, *471*(3), 241–276. https://doi.org/10.1002/cne.11039

Ono, K., Fozzard, H. A., & Hanck, D. A. (1993). Mechanism of cAMP-dependent modulation of cardiac sodium channel current kinetics. *Circulation Research*, *72*(4), 807–815. https://doi.org/10.1161/01.RES.72.4.807

Osinski, B. L., & Kay, L. M. (2016). Granule cell excitability regulates gamma and beta oscillations in a model of the olfactory bulb dendrodendritic microcircuit. *Journal of*

*Neurophysiology*, ajpheart 00684 2015. https://doi.org/doi:10.1152/jn.00988.2015 1

Panzanelli, P., López-Bendito, G., Luján, R., & Sassoé-Pognetto, M. (2004). Localization and developmental expression of GABA B receptors in the rat olfactory bulb. *Journal of Neurocytology*, *33*(1 SPEC. ISS.), 87–99. https://doi.org/10.1023/B:NEUR.0000029650.28943.b2

Panzanelli, P., Perazzini, A. Z., Fritschy, J. M., & Sassoè-Pognetto, M. (2005). Heterogeneity of γ-aminobutyric acid type A receptors in mitral and tufted cells of the rat main olfactory bulb. *Journal of Comparative Neurology*, *484*(1), 121–131. https://doi.org/10.1002/cne.20440

Pape, H. C., & McCormick, D. a. (1989). Noradrenaline and serotonin selectively modulate thalamic burst firing by enhancing a hyperpolarization-activated cation current. *Nature*, *340*(6236), 715–718. https://doi.org/10.1038/340715a0

Pardo-Bellver, C., Martínez-Bellver, S., Martínez-García, F., Lanuza, E., & Teruel-Martí, V. (2017). Synchronized Activity in the Main and Accessory Olfactory Bulbs and Vomeronasal Amygdala Elicited by Chemical Signals in Freely Behaving Mice. *Scientific Reports*, *7*(1), 1–16. https://doi.org/10.1038/s41598-017-10089-4

Paspalas, C. D., Wang, M., & Arnsten, A. F. T. (2013). Constellation of HCN channels and cAMP regulating proteins in dendritic spines of the primate prefrontal cortex: Potential substrate for working memory deficits in schizophrenia. *Cerebral Cortex*, *23*(7), 1643–1654. https://doi.org/10.1093/cercor/bhs152

Pawlak, V., Wickens, J. R., Kirkwood, A., & Kerr, J. N. D. (2010). Timing is not Everything: Neuromodulation Opens the STDP Gate. *Frontiers in Synaptic Neuroscience*, *2*(October), 146. https://doi.org/10.3389/fnsyn.2010.00146

Petreanu, L., & Alvarez-Buylla, A. (2002). Maturation and death of adult-born olfactory bulb granule neurons: role of olfaction. *The Journal of Neuroscience : The Official Journal of the Society for Neuroscience*, *22*(14), 6106–6113. https://doi.org/20026588

Phillips, M. E., Sachdev, R. N. S., Willhite, D. C., & Shepherd, G. M. (2012). Respiration drives network activity and modulates synaptic and circuit processing of lateral inhibition in the olfactory bulb. *Journal of Neuroscience*, *32*(1), 85–98. https://doi.org/10.1523/JNEUROSCI.4278-11.2012

Pignatelli, A., Borin, M., Fogli Iseppe, A., Gambardella, C., & Belluzzi, O. (2013). The h-Current in Periglomerular Dopaminergic Neurons of the Mouse Olfactory Bulb. *PLoS ONE*, *8*(2). https://doi.org/10.1371/journal.pone.0056571

Platel, J. C., Angelova, A., Bugeon, S., Wallace, J., Ganay, T., Chudotvorova, I., Deloulme, J. C., Béclin, C., Tiveron, M. C., Coré, N., Murthy, V. N., & Cremer, H. (2019). Neuronal integration in the adult mouse olfactory bulb is a non-selective addition process. *ELife*, *8*, 1–21. https://doi.org/10.7554/eLife.44830

Polack, P. O., Friedman, J., & Golshani, P. (2013). Cellular mechanisms of brain state-dependent gain modulation in visual cortex. *Nature Neuroscience*, *16*(9), 1331–1339. https://doi.org/10.1038/nn.3464

Pressler, R. T., Inoue, T., & Strowbridge, B. W. (2007). Muscarinic receptor activation modulates granule cell excitability and potentiates inhibition onto mitral cells in the rat olfactory bulb. *Journal Of Neuroscience*, *27*(41), 10969–10981. https://doi.org/10.1523/JNEUROSCI.2961-07.2007

Price, J. L., & Powell, T. P. (1970). The morphology of the granule cells of the olfactory bulb. *Journal of Cell Science*, *7*(1), 91–123.

Ramirez-Gordillo, D., Ma, M., & Restrepo, D. (2018). Precision of classification of odorant value by the power of olfactory bulb oscillations is altered by optogenetic silencing of local adrenergic innervation. *Frontiers in Cellular Neuroscience*, *12*(March). https://doi.org/10.3389/fncel.2018.00048

Ranade, S., Hangy, B., & Kepecs, A. (2013). Multiple modes of phase locking between sniffing and whisking during active exploration. *Journal of Neuroscience*, *33*(19), 8250–8256. https://doi.org/10.1523/JNEUROSCI.3874-12.2013

Rang, J. R. R. F. G. H. H. (2012). *Rang & Dale's Pharmacology*. https://www.elsevier.com/books/rang-and-dales-pharmacology/rang/978-1-4377-1933-8

Rebello, M. R., McTavish, T. S., Willhite, D. C., Short, S. M., Shepherd, G. M., & Verhagen, J. V. (2014). Perception of Odors Linked to Precise Timing in the Olfactory System. *PLoS Biology*, *12*(12). https://doi.org/10.1371/journal.pbio.1002021

Rhodes, M. E., & Rubin, R. T. (1999). Functional sex differences ('sexual diergism') of central nervous system cholinergic systems, vasopressin, and hypothalamic-pituitary-adrenal. *Brain Research Reviews*, *30*(2), 135–152. https://doi.org/10.1016/S0165-0173(99)00011-9

Riters, L. V., & Ball, G. F. (2002). Sex differences in the densities of α2-adrenergic receptors in the song control system, but not the medial preoptic nucleus in zebra finches. *Journal of Chemical Neuroanatomy*, *23*(4), 269–277. https://doi.org/10.1016/S0891-0618(02)00005-4

Rodenkirch, C., Liu, Y., Schriver, B. J., & Wang, Q. (2019). Locus coeruleus activation enhances thalamic feature selectivity via norepinephrine regulation of intrathalamic circuit dynamics. *Nature Neuroscience*, *22*(1), 120–133. https://doi.org/10.1038/s41593-018-0283-1

Rodriguez, I., Feinstein, P., & Mombaerts, P. (1999). Variable patterns of axonal projections of sensory neurons in the mouse vomeronasal system. *Cell*, *97*(2), 199–208. https://doi.org/10.1016/S0092-8674(00)80730-8

Rogawski, M. A., & Aghajanian, G. K. (1980). Activation of lateral geniculate neurons by norepinephrine: Mediation by an α-adrenergic receptor. *Brain Research*, *182*(2), 345–359. https://doi.org/10.1016/0006-8993(80)91193-2

Rosser, A. E., & Keverne, E. B. (1985). The importance of central noradrenergic neurones in the formation of an olfactory memory in the prevention of pregnancy block. *Neuroscience*, *15*(4), 1141–1147. https://doi.org/10.1016/0306-4522(85)90258-1

Sahay, A., Wilson, D. a, & Hen, R. (2011). Pattern separation: a common function for new neurons in hippocampus and olfactory bulb. *Neuron*, *70*(4), 582–588. https://doi.org/10.1016/j.neuron.2011.05.012

Sailor, K. A., Valley, M. T., Wiechert, M. T., Riecke, H., Sun, G. J., Adams, W., Dennis, J. C., Sharafi, S., Ming, G., Song, H., & Lledo, P.-M. (2016). Persistent Structural Plasticity Optimizes Sensory Information Processing in the Olfactory Bulb. *Neuron*, *91*(2), 384–396. https://doi.org/10.1016/j.neuron.2016.06.004

Salgado, H., Treviño, M., & Atzori, M. (2016). Layer- and area-specific actions of norepinephrine on cortical synaptic transmission. *Brain Research*, *1641*, 163–176. https://doi.org/10.1016/j.brainres.2016.01.033

Samuel Dillon, T., Fox, L. C., Han, C., & Linster, C. (2013). 17β-Estradiol enhances memory duration in the main olfactory bulb in CD-1 mice. *Behavioral Neuroscience*, *127*(6), 923–931. https://doi.org/10.1037/a0034839

Sara, S. J. (2009). The locus coeruleus and noradrenergic modulation of cognition. *Nature Reviews Neuroscience*, *10*(3), 211–223. https://doi.org/10.1038/nrn2573

Scalia, F., & Winans, S. S. (1975). The differential projections of the olfactory bulb and accessory olfactory bulb in mammals. *Journal of Comparative Neurology*, *161*(1), 31–55. https://doi.org/10.1002/cne.901610105

Schneider, D. M., Nelson, A., & Mooney, R. (2014). A synaptic and circuit basis for corollary discharge in the auditory cortex. *Nature*, *513*(7517), 189–194. https://doi.org/10.1038/nature13724

Schoppa, N. E. (2006). Synchronization of olfactory bulb mitral cells by precisely timed inhibitory inputs. *Neuron*, *49*(2), 271–283. https://doi.org/10.1016/j.neuron.2005.11.038

Schoppa, N. E., Kinzie, J. M., Sahara, Y., Segerson, T. P., & Westbrook, G. L. (1998). Dendrodendritic inhibition in the olfactory bulb is driven by NMDA receptors. *The Journal of Neuroscience : The Official Journal of the Society for Neuroscience*, *18*(17), 6790–6802. http://www.ncbi.nlm.nih.gov/pubmed/9712650

Schoppa, N. E., & Urban, N. N. (2003). Dendritic processing within olfactory bulb circuits. *Trends in Neurosciences*, *26*(9), 501–506. https://doi.org/10.1016/S0166-2236(03)00228-5

Schoppa, N. E., & Westbrook, G. L. (1999). Regulation of synaptic timing in the olfactory bulb by an A-type potassium current. *Nature Neuroscience*, *2*(12), 1106–1113. https://doi.org/10.1038/16033

Shah, M. M. (2014). Cortical HCN channels: Function, trafficking and plasticity. *Journal of Physiology*, *592*(13), 2711–2719. https://doi.org/10.1113/jphysiol.2013.270058

Shea, S. D., Katz, L. C., & Mooney, R. (2008). Noradrenergic Induction of Odor-Specific Neural Habituation and Olfactory Memories. *Journal of Neuroscience*, *28*(42), 10711–10719. https://doi.org/10.1523/JNEUROSCI.3853-08.2008

Shepherd, G M. (1972). Synaptic organization of the mammalian olfactory bulb. *Physiological Reviews*, *52*(4), 864–917.

Shepherd, Gordon M. (2004). The Synaptic Organization of the Brain. In *Oxford University Press*. https://doi.org/DOI:10.1093/acprof:oso/9780195159561.001.1

Shipley, M. T., Halloran, F. J., & de la Torre, J. (1985). Surprisingly rich projection from locus coeruleus to the olfactory bulb in the rat. *Brain Research*, *329*(1–2), 294–299. https://doi.org/10.1016/0006-8993(85)90537-2

Shu, Y., Hasenstaub, A., Badoual, M., Bal, T., & McCormick, D. A. (2003). Barrages of synaptic activity control the gain and sensitivity of cortical neurons. *The Journal of Neuroscience : The Official Journal of the Society for Neuroscience*, *23*(32), 10388–10401. http://www.ncbi.nlm.nih.gov/pubmed/14614098

Shusterman, R., Smear, M. C., Koulakov, A. a, & Rinberg, D. (2011). Precise olfactory responses tile the sniff cycle. *Nature Neuroscience*, *14*(8), 1039–1044. https://doi.org/10.1038/nn.2877

Sinha, M., & Narayanan, R. (2015). HCN channels enhance spike phase coherence and regulate the phase of spikes and LFPs in the theta-frequency range. *Proceedings of the National Academy of Sciences*, 201419017. https://doi.org/10.1073/pnas.1419017112

Small, K. M., McGraw, D. W., & Liggett, S. B. (2003). Pharmacology and Physiology of Human Adrenergic Receptor polymorphisms. *Annual Review of Pharmacology and Toxicology*, *43*(1), 381–411. https://doi.org/10.1146/annurev.pharmtox.43.100901.135823

Smear, M., Shusterman, R., O'Connor, R., Bozza, T., & Rinberg, D. (2011). Perception of sniff phase in mouse olfaction. *Nature*, *479*(7373), 397–400. https://doi.org/10.1038/nature10521

Smith, R. S., Hu, R., DeSouza, A., Eberly, C. L., Krahe, K., Chan, W., & Araneda, R. C. (2015). Differential Muscarinic Modulation in the Olfactory Bulb. *Journal of Neuroscience*, *35*(30), 10773–10785. https://doi.org/10.1523/JNEUROSCI.0099-15.2015

Smith, R. S., Weitz, C. J., & Araneda, R. C. (2009). Excitatory actions of noradrenaline and metabotropic glutamate receptor activation in granule cells of the accessory olfactory bulb. *Journal of Neurophysiology*, *102*(2), 1103–1114. https://doi.org/10.1152/jn.91093.2008

Sosulski, D. L., Bloom, M. L., Cutforth, T., Axel, R., & Datta, S. R. (2011). Distinct representations of olfactory information in different cortical centres. *Nature*, *472*(7342), 213–216. https://doi.org/10.1038/nature09868

Spehr, M. (2006). Essential Role of the Main Olfactory System in Social Recognition of Major Histocompatibility Complex Peptide Ligands. *Journal of Neuroscience*, *26*(7), 1961–1970. https://doi.org/10.1523/JNEUROSCI.4939-05.2006

Stettler, D., & Axel, R. (2009). Representations of odor in the piriform cortex. *Neuron*, *63*(6),

854–864. https://doi.org/10.1016/j.neuron.2009.09.005

Stone, J. D., Crofton, J. T., & Share, L. (1989). Sex differences in central adrenergic control of vasopressin release. *American Journal of Physiology - Regulatory Integrative and Comparative Physiology*, *257*(5). https://doi.org/10.1152/ajpregu.1989.257.5.r1040

Stowers, L., Holy, T. E., Meister, M., Dulac, C., & Koentges, G. (2002). Loss of sex discrimination and male-male aggression in mice deficient for TRP2. *Science (New York, N.Y.)*, *295*(5559), 1493–1500. https://doi.org/10.1126/science.1069259

Stroh, O., Freichel, M., Kretz, O., Birnbaumer, L., Hartmann, J., & Egger, V. (2012). NMDA Receptor-Dependent Synaptic Activation of TRPC Channels in Olfactory Bulb Granule Cells. *Journal of Neuroscience*, *32*(17), 5737–5746. https://doi.org/10.1523/JNEUROSCI.3753-11.2012

Sullivan, R. M., & Wilson, D. a. (1991). The role of norepinephrine in the expression of learned olfactory neurobehavioral responses in infant rats. *Psychobiology*, *19*(4), 308–312. https://doi.org/10.3758/BF03332084

Sullivan, R. M., Wilson, D. a, & Leon, M. (1989). Norepinephrine and learning-induced plasticity in infant rat olfactory system. *The Journal of Neuroscience : The Official Journal of the Society for Neuroscience*, *9*(11), 3998–4006. https://doi.org/10.1016/j.biotechadv.2011.08.021.Secreted

Sullivan, R. M., Zyzak, D. R., Skierkowski, P., & Wilson, D. A. (1992). The Role of Olfactory-Bulb Norepinephrine in Early Olfactory Learning. *Developmental Brain Research*, *70*(2), 279–282.

Surges, R., Brewster, A. L., Bender, R. A., Beck, H., Feuerstein, T. J., & Baram, T. Z. (2006). Regulated expression of HCN channels and cAMP levels shape the properties of the h current in developing rat hippocampus. *European Journal of Neuroscience*, *24*(1), 94–104. https://doi.org/10.1111/j.1460-9568.2006.04880.x

Takami, S., Fernandez, G. D., & Graziadei, P. P. C. (1992). The morphology of GABA-immunoreactive neurons in the accessory olfactory bulb of rats. *Brain Research*, *588*(2), 317–323. https://doi.org/10.1016/0006-8993(92)91593-4

Takami, S., & Graziadei, P. P. (1991). Light microscopic Golgi study of mitral/tufted cells in the accessory olfactory bulb of the adult rat. *The Journal of Comparative Neurology*, *311*(1), 65–83. https://doi.org/10.1002/cne.903110106

Timmons, S. D., Geisert, E., Stewart, A. E., Lorenzon, N. M., & Foehring, R. C. (2004). α2-Adrenergic receptor-mediated modulation of calcium current in neocortical pyramidal neurons. *Brain Research*, *1014*(1–2), 184–196. https://doi.org/10.1016/j.brainres.2004.04.025

Tirindelli, R., Dibattista, M., Pifferi, S., & Menini, A. (2009). From pheromones to behavior. *Physiological Reviews*, *89*(3), 921–956. https://doi.org/10.1152/physrev.00037.2008

Tolokh, I. I., Fu, X., & Holy, T. E. (2013). Reliable Sex and Strain Discrimination in the Mouse Vomeronasal Organ and Accessory Olfactory Bulb. *Journal of Neuroscience*, *33*(34),

13903–13913. https://doi.org/10.1523/JNEUROSCI.0037-13.2013

Traub, R. D., Whittington, M. A., Colling, S. B., Buzsáki, G., & Jefferys, J. G. R. (1996). Analysis of gamma rhythms in the rat hippocampus in vitro and in vivo. *Journal of Physiology*, *493*(2), 471–484. https://doi.org/10.1113/jphysiol.1996.sp021397

Trombley, P. Q., & Shepherd, G. M. (1992). Noradrenergic inhibition of synaptic transmission between mitral and granule cells in mammalian olfactory bulb cultures. *The Journal of Neuroscience : The Official Journal of the Society for Neuroscience*, *12*(10), 3985–3991.

Uchida, N., Poo, C., & Haddad, R. (2013). Coding and Transformations in the Olfactory System. *Annual Review of Neuroscience*, *May*, 363–385. https://doi.org/10.1146/annurev-neuro-071013-013941

Ulrich, D. (2002). Dendritic resonance in rat neocortical pyramidal cells. *Journal of Neurophysiology*, *87*(6), 2753–2759. https://doi.org/10.1152/jn.01000.2001

Ulrich, D. (2014). Subthreshold delta-frequency resonance in thalamic reticular neurons. *The European Journal of Neuroscience*, *April*, 1–8. https://doi.org/10.1111/ejn.12630

Umemura, S., Smyth, D. D., & Pettinger, W. A. (1986). Alpha 2-adrenoceptor stimulation and cellular cAMP levels in microdissected rat glomeruli. *American Journal of Physiology-Renal Physiology*, *250*(1), F103–F108. https://doi.org/10.1152/ajprenal.1986.250.1.F103

Vaidya, S. P., & Johnston, D. (2013). Temporal synchrony and gamma-to-theta power conversion in the dendrites of CA1 pyramidal neurons. *Nature Neuroscience*, *16*(12), 1812–1820. https://doi.org/10.1038/nn.3562

Valsecchi, F., Ramos-Espiritu, L. S., Buck, J., Levin, L. R., & Manfredi, G. (2013). cAMP and mitochondria. *Physiology (Bethesda, Md.)*, *28*(3), 199–209. https://doi.org/10.1152/physiol.00004.2013

van Brederode, J. F. M., & Berger, a J. (2011). GAD67-GFP+ neurons in the Nucleus of Roller. II. Subthreshold and firing resonance properties. *Journal of Neurophysiology*, *105*(1), 249–278. https://doi.org/10.1152/jn.00492.2010

van Welie, I., & du Lac, S. (2011). Bidirectional control of BK channel open probability by CAMKII and PKC in medial vestibular nucleus neurons. *Journal of Neurophysiology*, *105*(4), 1651–1659. https://doi.org/10.1152/jn.00058.2011

Vera, J., Pezzoli, M., Pereira, U., Bacigalupo, J., & Sanhueza, M. (2014). Electrical resonance in the θ frequency range in olfactory amygdala neurons. *PloS One*, *9*(1), e85826. https://doi.org/10.1371/journal.pone.0085826

Veyrac, A., Sacquet, J., Nguyen, V., Marien, M., Jourdan, F., & Didier, A. (2009). Novelty determines the effects of olfactory enrichment on memory and neurogenesis through noradrenergic mechanisms. *Neuropsychopharmacology*, *34*(3), 786–795. https://doi.org/10.1038/npp.2008.191

Vinera, J., Kermen, F., Sacquet, J., Didier, A., Mandairon, N., & Richard, M. (2015). Olfactory

perceptual learning requires action of noradrenaline in the olfactory bulb: comparison with olfactory associative learning. *Learning & Memory (Cold Spring Harbor, N.Y.)*, *22*(3), 192–196. https://doi.org/10.1101/lm.036608.114

Vinograd, A., Fuchs-shlomai, Y., Stern, M., Mukherjee, D., Gao, Y., Citri, A., Davison, I., Mizrahi, A., Vinograd, A., Fuchs-shlomai, Y., Stern, M., Mukherjee, D., Gao, Y., Citri, A., & Davison, I. (2017). Functional Plasticity of Odor Representations during Article Functional Plasticity of Odor Representations during Motherhood. *CellReports*, *21*(2), 351–365. https://doi.org/10.1016/j.celrep.2017.09.038

Von Campenhausen, H., & Mori, K. (2000). Convergence of segregated pheromonal pathways from the accessory olfactory bulb to the cortex in the mouse. *European Journal of Neuroscience*, *12*(1), 33–46. https://doi.org/10.1046/j.1460-9568.2000.00879.x

Wagner, S., Gresser, A. L., Torello, A. T., & Dulac, C. (2006). A Multireceptor Genetic Approach Uncovers an Ordered Integration of VNO Sensory Inputs in the Accessory Olfactory Bulb. *Neuron*, *50*(5), 697–709. https://doi.org/10.1016/j.neuron.2006.04.033

Wainger, B. J., DeGennaro, M., Santoro, B., Siegelbaum, S. a, & Tibbs, G. R. (2001). Molecular mechanism of cAMP modulation of HCN pacemaker channels. *Nature*, *411*(6839), 805–810. https://doi.org/10.1038/35081088

Wallace, J. L., Wienisch, M., & Murthy, V. N. (2017). Development and Refinement of Functional Properties of Adult-Born Neurons. *Neuron*, *96*(4), 883-896.e7. https://doi.org/10.1016/j.neuron.2017.09.039

Wang, M., Ramos, B. P., Paspalas, C. D., Shu, Y., Simen, A., Duque, A., Vijayraghavan, S., Brennan, A., Dudley, A., Nou, E., Mazer, J. A., McCormick, D. A., & Arnsten, A. F. T. (2007). α2A-Adrenoceptors Strengthen Working Memory Networks by Inhibiting cAMP-HCN Channel Signaling in Prefrontal Cortex. *Cell*, *129*(2), 397–410. https://doi.org/10.1016/j.cell.2007.03.015

Wang, Y., He, Z., Zhao, C., & Li, L. (2013). Medial amygdala lesions modify aggressive behavior and immediate early gene expression in oxytocin and vasopressin neurons during intermale exposure. *Behavioural Brain Research*, *245*, 42–49. https://doi.org/10.1016/j.bbr.2013.02.002

Wanner, A. A., & Friedrich, R. W. (2020). Whitening of odor representations by the wiring diagram of the olfactory bulb. *Nature Neuroscience*, *23*(3), 433–442. https://doi.org/10.1038/s41593-019-0576-z

Waterhouse, B. D., Ausim Azizi, S., Burne, R. A., & Woodward, D. J. (1990). Modulation of rat cortical area 17 neuronal responses to moving visual stimuli during norepinephrine and serotonin microiontophoresis. *Brain Research*, *514*(2), 276–292. https://doi.org/10.1016/0006-8993(90)91422-D

Weiss, J. M., Stout, J. C., Aaron, M. F., Quan, N., Owens, M. J., Butler, P. D., & Nemeroff, C. B. (1994). Depression and anxiety: Role of the locus coeruleus and corticotropin-releasing factor. *Brain Research Bulletin*, *35*(5–6), 561–572. https://doi.org/10.1016/0361-9230(94)90170-8

Wiechert, M. T., Judkewitz, B., Riecke, H., & Friedrich, R. W. (2010). Mechanisms of pattern decorrelation by recurrent neuronal circuits. *Nature Neuroscience*, *13*(8), 1003–1010. https://doi.org/10.1038/nn.2591

Wilson, R. I., & Mainen, Z. F. (2006). Early Events in Olfactory Processing. *Annual Review of Neuroscience*, *29*(1), 163–201. https://doi.org/10.1146/annurev.neuro.29.051605.112950

Winder, D. G., Martin, K. C., Muzzio, I. A., Rohrer, D., Chruscinski, A., Kobilka, B., & Kandel, E. R. (1999). ERK plays a regulatory role in induction of LTP by theta frequency stimulation and its modulation by β-adrenergic receptors. *Neuron*, *24*(3), 715–726. https://doi.org/10.1016/S0896-6273(00)81124-1

Winner, B., Cooper-Kuhn, C. M., Aigner, R., Winkler, J., & Kuhn, H. G. (2002a). Long-term survival and cell death of newly generated neurons in the adult rat olfactory bulb. *European Journal of Neuroscience*, *16*(9), 1681–1689. https://doi.org/10.1046/j.1460-9568.2002.02238.x

Winner, B., Cooper-Kuhn, C. M., Aigner, R., Winkler, J., & Kuhn, H. G. (2002b). Long-term survival and cell death of newly generated neurons in the adult rat olfactory bulb. *European Journal of Neuroscience*, *16*(9), 1681–1689. https://doi.org/10.1046/j.1460-9568.2002.02238.x

Woolley, C. S., Gould, E., Frankfurt, M., & McEwen, B. S. (1990). Naturally occurring fluctuation in dendritic spine density on adult hippocampal pyramidal neurons. *Journal of Neuroscience*, *10*(12), 4035–4039. https://doi.org/10.1523/jneurosci.10-12-04035.1990

Yamaguchi, M., & Mori, K. (2005). Critical period for sensory experience-dependent survival of newly generated granule cells in the adult mouse olfactory bulb. *… of the National Academy of Sciences …*, *102*(27), 9697–9702. https://doi.org/10.1073/pnas.0406082102

Yokoi, M., Mori, K., & Nakanishi, S. (1995). Refinement of odor molecule tuning by dendrodendritic synaptic inhibition in the olfactory bulb. *Proceedings of the National Academy of Sciences of the United States of America*, *92*(8), 3371–3375. https://doi.org/10.1073/pnas.92.8.3371

Yoles-Frenkel, M., Kahan, A., & Ben-Shaul, Y. (2018). Temporal response properties of accessory olfactory bulb neurons: Limitations and opportunities for decoding. *Journal of Neuroscience*, *38*(21), 4957–4976. https://doi.org/10.1523/JNEUROSCI.2091-17.2018

Yoon, H., Enquist, L. W., & Dulac, C. (2005). Olfactory inputs to hypothalamic neurons controlling reproduction and fertility. *Cell*, *123*(4), 669–682. https://doi.org/10.1016/j.cell.2005.08.039

Yu, Y., Burton, S. D., Tripathy, S. J., & Urban, N. N. (2015). Postnatal development attunes olfactory bulb mitral cells to high frequency signaling. *Journal of Neurophysiology*, *013490*, jn.00315.2015. https://doi.org/10.1152/jn.00315.2015

Zagotta, W. N., Olivier, N. B., Black, K. D., Young, E. C., Olson, R., & Gouaux, E. (2003).

Structural basis for modulation and agonist specificity of HCN pacemaker channels. *Nature*, *425*(6954), 200–205. https://doi.org/10.1038/nature01922

Zemankovics, R., Káli, S., Paulsen, O., Freund, T. F., & Hájos, N. (2010). Differences in subthreshold resonance of hippocampal pyramidal cells and interneurons: the role of h-current and passive membrane characteristics. *The Journal of Physiology*, *588*(Pt 12), 2109–2132. https://doi.org/10.1113/jphysiol.2009.185975

Zhang, X., & Meeks, J. P. (2020). Paradoxically Sparse Chemosensory Tuning in Broadly Integrating External Granule Cells in the Mouse Accessory Olfactory Bulb. *The Journal of Neuroscience*, *40*(27), 5247–5263. https://doi.org/10.1523/JNEUROSCI.2238-19.2020

Zhao, C., Deng, W., & Gage, F. H. (2008). Mechanisms and functional implications of adult neurogenesis. *Cell*, *132*(4), 645–660. https://doi.org/10.1016/j.cell.2008.01.033

Zhou, F.-W., Dong, H.-W., & Ennis, M. (2016). Activation of β-noradrenergic receptors enhances rhythmic bursting in mouse olfactory bulb external tufted cells. *Journal of Neurophysiology*, *116*(6), 2604–2614. https://doi.org/10.1152/jn.00034.2016

Zhou, S., & Yu, Y. (2018). Synaptic E-I balance underlies efficient neural coding. *Frontiers in Neuroscience*, *12*(FEB), 1–11. https://doi.org/10.3389/fnins.2018.00046

Zimnik, N. C., Treadway, T., Smith, R. S., & Araneda, R. C. (2013). α(1A)-Adrenergic regulation of inhibition in the olfactory bulb. *The Journal of Physiology*, *591*(Pt 7), 1631–1643. https://doi.org/10.1113/jphysiol.2012.248591